Distribution Agreement

In presenting this thesis or dissertation as a partial fulfillment of the requirements for an advanced degree from Emory University, I hereby grant to Emory University and its agents the non-exclusive license to archive, make accessible, and display my thesis or dissertation in whole or in part in all forms of media, now or hereafter known, including display on the world wide web. I understand that I may select some access restrictions as part of the online submission of this thesis or dissertation. I retain all ownership rights to the copyright of the thesis or dissertation. I also retain the right to use in future works (such as articles or books) all or part of this thesis or dissertation.

Signature:

_____ _____

Carolyn Krisel Beam Date

Characterization of the *Drosophila* growth-regulatory genes *gang of four*, *archipelago* and *erupted*

By

Carolyn Krisel Beam
Doctor of Philosophy

Graduate Division of Biological and Biomedical Science
Genetics and Molecular Biology

_____
Kenneth H. Moberg, Ph.D.
Advisor

_____
Ping Chen, Ph.D.
Committee Member

_____
Andreas Fritz, Ph.D.
Committee Member

_____
Andrew Neish, M.D.
Committee Member

_____
Barry Yedvobnick, Ph.D.
Committee Member

Accepted:

_____
Lisa A. Tedesco, Ph.D.
Dean of the James T. Laney School of Graduate Studies

_____
Date

Characterization of the *Drosophila* growth-regulatory genes *gang of four*, *archipelago* and *erupted*

By

Carolyn Krisel Beam
B.S., Wake Forest University, 2004

Advisor: Kenneth H. Moberg, Ph.D.

An abstract of
A dissertation submitted to the Faculty of the
James T. Laney School of Graduate Studies of Emory University
in partial fulfillment of the requirements for the degree of
Doctor of Philosophy
Graduate Division of Biological and Biomedical Science
Genetics and Molecular Biology
2009

Abstract

Characterization of the *Drosophila* growth-regulatory genes *gang of four*, *archipelago* and *erupted*

By Carolyn Krisel Beam

The reproducible size and shape of an organism relies on a balance of genetically controlled signaling pathways that regulate tissue growth. While patterned activation of these pathways shapes developing tissues, deregulation of these same mechanisms can contribute to hyperplastic diseases like cancer. Because pathways regulating cell size and cell number are highly conserved, we chose to study the basic processes of growth control in the fruit fly, *Drosophila melanogaster*.

This dissertation presents work on three *Drosophia* growth-regulatory genes—*gang of four*, *archipelago*, and *erupted*. Though each gene was identified in a forward genetic screen for mutations causing tissue overgrowth, each has unique properties. These findings show that *gang of four* behaves genetically as gain-of-function for an RNA binding protein, *bru-3*, and affects growth and patterning via multiple signaling pathways. Likewise, mutations in human *archipelago* are associated with T-cell acute lymphoblastic leukemia, and elevated Notch signaling causes phenotypes in *archipelago* mutant tissue in the fly reminiscent of those in the mouse T-cell lineage, thus uncovering a conserved system in which to directly address clinically relevant aspects of *archipelago* biology. Finally, we show that *erupted* mutations deregulate signaling through the JAK-STAT pathway. The human ortholog of *erupted*, *Tsg101*, is involved in human cancers, but its roles in cellular transformation are unclear; therefore, further elucidation of *erupted* molecular mechanisms can also directly impact human disease. Collectively, I have identified conserved aspects of three recently isolated growth regulators, significantly advancing our fundamental understanding of growth control in a multicellular organism.

Characterization of the *Drosophila* growth-regulatory genes *gang of four*, *archipelago* and *erupted*

By

Carolyn Krisel Beam
B.S., Wake Forest University, 2004

Advisor: Kenneth H. Moberg, Ph.D.

A dissertation submitted to the Faculty of the
James T. Laney School of Graduate Studies of Emory University
in partial fulfillment of the requirements for the degree of
Doctor of Philosophy
Graduate Division of Biological and Biomedical Science
Genetics and Molecular Biology
2009

Acknowledgements

In the spirit of collaboration and scientific advancement, I thank my colleagues in the fly community for gifts of stocks and reagents: M.M. Gilbert, A. Vrailas-Mortimer, D. Marenda, R. Jones, S. Sanyal, K. Saigo, B. Yedvobnick, H. Richardson, K. Irvine, I.K. Hariharan, F. Schweisguth, H. Bellen, J. Belote, R. Duronio, N. Dyson, W. Du, D. Bilder, E. Bach, S. Noselli, E. Knust, J. Castelli-Gair Hombria, and N. Reich. I thank A. Locke and M. Zwick for genomic sequencing and S. Burdick for technical support. Finally, I thank members of the Moberg, Sanyal, and Fridovich-Keil laboratories, the Emory Fly Group, and my thesis committee—Ping, Andreas, Andy, and Barry—for valuable discussion and comment over the years. CKB was supported by an NIH Training Grant; KHM was supported by NIH grant GM079242.

On a personal note, I especially thank my mentor, Ken, who taught me not only how to do science but also how to be a scientist. From his lab, I will take away the true essence of Monod's assertion: "What is true for *E. coli* is true for the elephant."

I thank the current and former members of the Moberg Lab, in addition to those who have drifted through over the years… In particular, Nate taught me that protocols are much easier in practice than they appear on paper, and Melissa taught me that doing science right is better than doing science quickly. Jeremy, Brian, Sarah and ChangHui added a renewed life to the lab when one needs it the most—around year three. To a future Moberg Lab member, Jacob, thank you for being my ever steady and always reliable study partner, co-captain, and, for the last few months, reason for a roof over my head.

Last, but not least, I am so very thankful for my family (Krisels and Beams, alike) for their unconditional love and support. Whether helping to construct science fair posters, providing transportation to my presentations, or allowing me to culture aquatic worms in my bedroom, my parents are the reason I have earned the title, doctor. And, of course, I could not have made it to November 12, 2009 if it were not for my husband, David, without whom life just wouldn't be as enjoyable and with whom I realize that a marathon is the perfect metaphor for just about any of life's challenges. Here's to a life-long pursuit of science and religion—I dedicate this work to you.

Table of Contents

Index of Figures

Index of Tables

Chapter I: Introduction

I.A. Purpose

Regulation of tissue growth is the fundamental means by which developing organisms achieve a characteristic shape and size. Therefore, by studying genetic lesions that alter tissue growth in the *Drosophila* eye, our goal is to understand more about these pathways and to identify the signaling networks that function together to control the growth process.

I present here three projects at various stages of progression. While each project is quite distinct, they share a common origin—a genetic screen for overgrowth mutants. The objective of my first project presented in Chapter II is to identify and characterize the gene represented by the novel complementation group, *gang of four* (*gfr*), with the aim linking *gfr*'s growth and patterning effects in a common genetic pathway. By studying this uncharacterized gene, we hope to shed light on a previously unrecognized aspect of growth control. My second project, presented in Chapter III, is focused on the role of Notch activity in *archipelago* (*ago*) mutant growth and differentiation phenotypes. This project began with the combined observations that *ago* inactivation increased Notch activity but did not simultaneously elevate endogenous Notch protein. Because both human *ago* and Notch signaling are strongly associated with T-cell acute lymphoblastic leukemia, characterizing the interactions between *ago* and *Notch* has significant clinical implications. Finally, the project presented in Chapter IV follows-up on the observation that the cell-autonomous overgrowth of *erupted* (*ept*) mutant eye tissue requires a full genetic dosage of *stat92E*. While it was previously accepted that elevated JAK-STAT pathway activity is, at least in part, responsible for the non-autonomous overproliferation of wild-type cells in the *ept* mosaic eye, it is not known whether signaling through the

JAK-STAT pathway contributes to the overgrowth of *ept* mutant cells themselves. Since the *ept* human ortholog, *Tsg101*, has been implicated in human cancers, yet its tumor-suppressive properties remain uncertain, determining the roles of *ept* in the eye epithelium provides us the unique opportunity to directly inform tumor biology. In this chapter, I will first introduce all of the components underlying the biology in these three projects before presenting the results.

Our overall purpose is to use *Drosophila* as a model in which to more fully elucidate the genetic integration of cell growth, division, differentiation, and apoptosis during development. The known pathways controlling growth during fly eye development are highly conserved in metazoans and are reiteratively utilized in diverse developmental programs. Therefore, I anticipate that my work investigating the recently identified growth-regulatory genes *gfr*, *ago*, and *ept* will contribute to models for these genes in human disease.

I.B. Coordination of growth and patterning in development

The reproducible size and shape of an organism relies on a delicate balance of pathways regulating tissue growth. Metazoan development is therefore predicated upon genetically controlled signaling pathways that drive cell growth, cell division, cell death, and cell fate determination with strict spatial and temporal precision. Patterned activation of these pathways shapes developing tissues; however, deregulation of the same mechanisms that control normal growth can contribute to hyperplastic diseases like cancer.

To understand how these processes are disrupted in cancer, we must first understand how normal cells communicate and respond to signals during development. Studies in the fruit fly *Drosophila melanogaster* have not only provided insight into the regulation of metazoan development but have also contributed significantly toward understanding the basic cell biology of tumorigenesis—in particular, links among cell growth, proliferation, and apoptosis (reviewed in Brumby and Richardson, 2005). In fact, the similarities between fly and human tumors, such as loss of cell differentiation and increased cell motility and invasiveness, historically lead to the widespread use of *Drosophila* as a cancer model in many laboratories (reviewed in Gateff, 1978). Today, it is becoming increasingly evident that tumor suppressor genes first identified in the fly can cause tumor susceptibility in mice and are mutated in human cancers (e.g., Spruck et al., 2002; St John et al., 1999). Since human cancer reflects the collaboration of genetic alterations in multiple genes (Hanahan and Weinberg, 2000), the fly offers a simpler model system in which to mimic some of the steps of mammalian tumorigenesis in a developing tissue (Brumby and Richardson, 2005).

We use the *Drosophila* eye to study the coordination of growth and patterning during development. A relatively small number of highly conserved pathways are used reiteravely throughout development to regulate cell size and cell number in the fly eye. These pathways include signaling through Insulin/PI3-kinase, Tsc/TOR, Myc, Ras/MAPK, Cyclin D/cdk4, and the recently described Hippo pathway (Figure I.1) (reviewed in Hariharan and Bilder, 2006; Neufeld and Hariharan, 2002). Insulin/PI3K, Tsc/TOR, and Myc have known roles in regulating tissue growth in *Drosophila* by affecting cell size, whereas perturbation of Ras/MAPK, CycD/cdk4, or Hippo signaling coordinately increase both growth and division, resulting in increased cell proliferation. Mutations in genes affecting some of these pathways will be described further below.

I.1. Pathways regulating growth in the *Drosophila* eye.

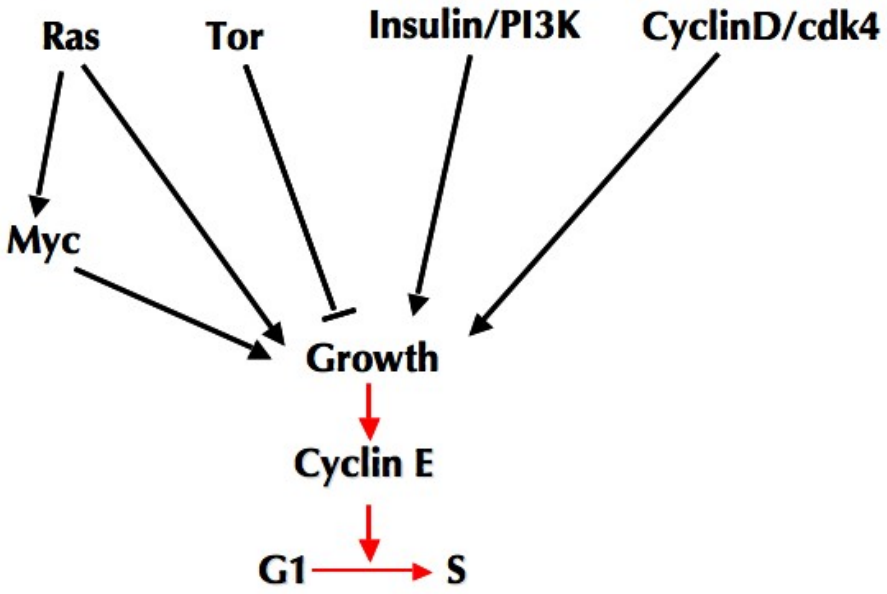

Insulin/PI3-kinase, Tsc/TOR, Myc, Ras/MAPK, and Cyclin D/cdk4 are the main pathways regulating growth of the developing *Drosophila* eye. As indicated here, cell growth is epistatic to cell division.

I.C. The Model: *Drosophila* eye development

The *Drosophila* eye provides an ideal system in which to characterize genes acting within pathways to regulate tissue growth and patterning in the context of a developing organ. Fly eye development has been extensively characterized, and the precise, sterotypical patterning of the eye makes it a sensitive amplifier of mutations in genes with even minor effects on cell proliferation or specification. Because the eye is not required for viability, essential genes can be examined in this tissue without killing the animal.

The adult eye is composed of 750-800 repeating lens units called ommatidia that are arranged in an invariant pattern (Ready et al., 1976). Eye development occurs in a monolayer, columnar cell epithelium, the imaginal disc. During embryonic development, approximately twenty cells are set aside to eventually form the adult eye and antenna (Garcia-Bellido and Merriam, 1969). These imaginal disc cells undergo random proliferation during the first and second larval instars. During the mid-third instar, a wave of differentiation called the morphogenetic furrow (MF) sweeps across the eye disc from posterior to anterior (Ready et al., 1976; Tomlinson and Ready, 1987; Wolff and Ready, 1991), essentially splitting the disc into three regions of cellular mitotic activity—unpatterned, asynchronous proliferation in front of (anterior to) the MF; early G1 phase cell cycle arrest within the MF (Finley et al., 1996); and a final synchronous round of cell division behind (posterior to) the furrow known as the Second Mitotic Wave (Baker and Yu, 2001; Ready et al., 1976; Wolff and Ready, 1991) (Figure I.2). These events begin retinal pattern formation. Generation of the cells necessary to specify the photoreceptors, cone cells, pigment cells, and bristle precursor cells occurs prior to entering the pupal

stage, where these cells will further differentiate into a structured lattice of cell clusters that will become the ommatidia.

Cell fate assignments are completed in pupal eye development. Very few cells proliferate in the pupal stage. The bristle sensory organ precursor (SOP) cell is the only mitotically active cell type detected during this time; it divides twice during the mid-pupal phase (~16-24 h after pupal formation) to generate the four cells of the bristle complex, two of which degenerate late in development (Perry, 1968). The total number of cells generated during eye development is close to 20,000, approximately 2,000 of which remain unspecified and are eliminated by apoptosis (Wolff and Ready, 1991; Wolff and Ready, 1993). This cell death is the final step in patterning the precise array of the fly eye. Each ommatidium is a stereotyped assembly of 8 neuronal photoreceptors, 4 cone cells, and 2 primary pigment cells. Neighboring ommatidia are arranged in a hexagonal lattice formed by 6 shared secondary pigment cells with a tertiary pigment cell and a bristle cell complex each at alternating verticies (Figure I.3). The final size of the adult eye is determined by changes in cell morphology and post-mitotic growth during pupal stage (for review of pupal retina development, see Cagan and Ready, 1989).

Such precision in growth, division, and patterning during *Drosophila* eye development clearly illustrates why we use the fly as a system for gene discovery in order to better understand how these developmental processes are regulated.

Figure I.2. Three phases of mitotic activity in the larval eye imaginal disc.

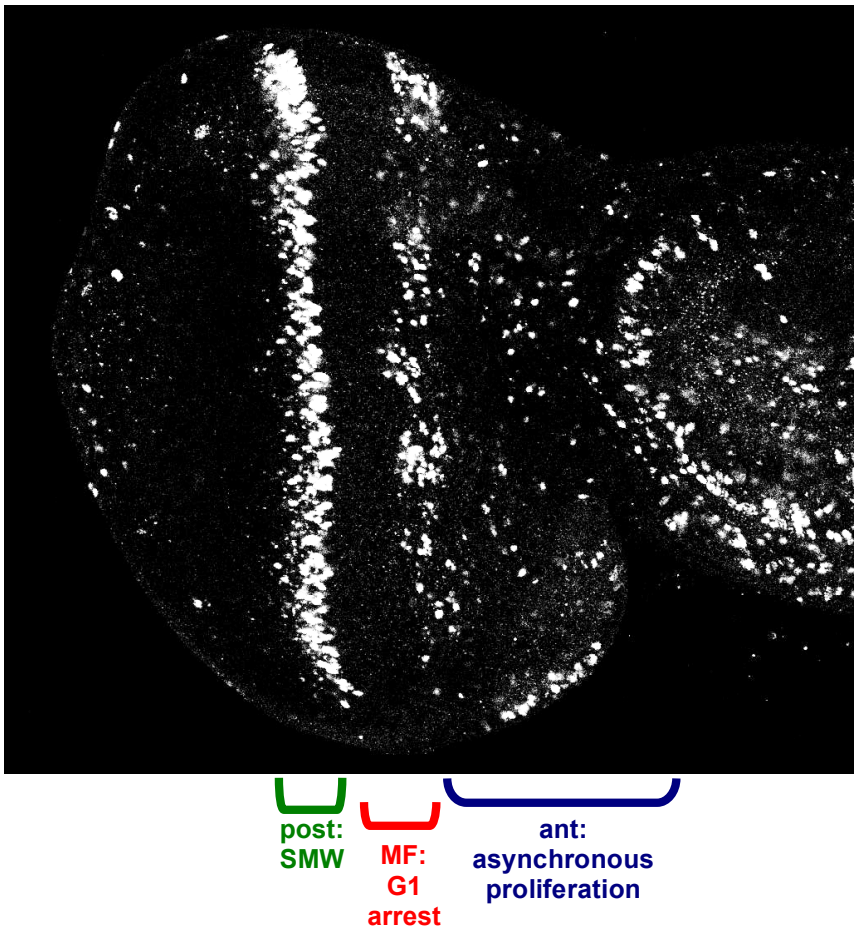

BrdU incorporation marking S-phases in the third instar larval eye imaginal disc. Phases of mitotic activity are indicated (see text). ant, anterior; MF, morphogenetic furrow; post, posterior. (Confocal image courtesy of M. M. Gilbert)

Figure I.3. Structure of the ommatidium.

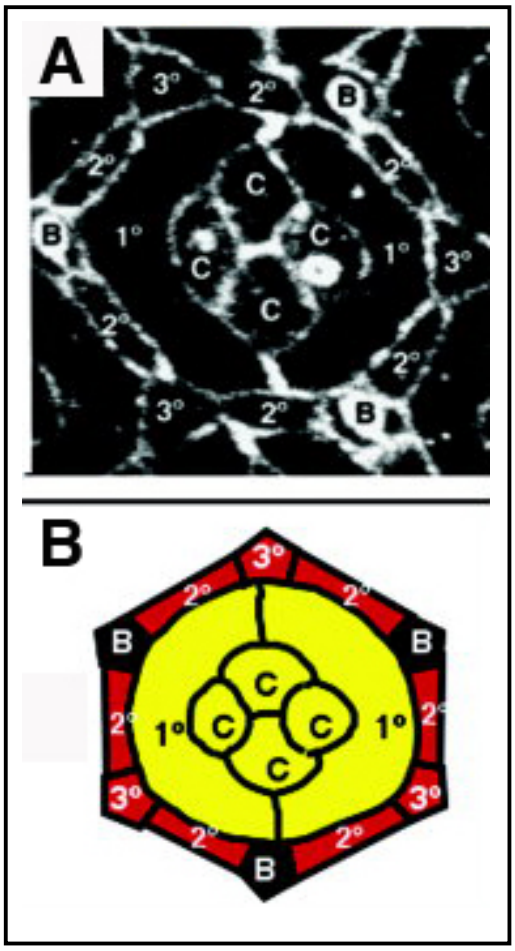

(A) A single ommatidium from a pupal eye imaginal disc stained with an antibody to outline the cells. Four cone cells, C, located in the center are flanked by two primary pigment cells, 1^{o}; secondary pigment cells, 2^{o}, form the sides, and tertiary pigment cells, 3^{o}, and bristles, B, are located at alternating verticies to create a hexagonal shape. (B) Schematic rendering of pupal ommatidium in (A). (Adapted from Voas and Rebay, 2004)

I.D. The Screen: Identification of novel growth-regulatory genes

To identify genes that regulate cell growth or cell number during *Drosophila* eye development, a genetic mosaic screen was previously conducted to isolate recessive mutations that allow homozygous mutant cells to overgrow relative to their wild-type neighbors (e.g., Harvey et al., 2003; Moberg et al., 2001; Tapon et al., 2002; Tapon et al., 2001; Tseng et al., 2007). The screen utilized ethyl methanesulfonate (EMS) chemical mutagenesis and the *eyelessFLP*/*FRT* system of mitotic recombination to generate populations of homozygous mutant tissue (marked white) and homozygous wild-type tissue (marked red) in the eyes of otherwise heterozygous flies (Golic and Lindquist, 1989) (Figure I.4). This mitotic recombination, or 'FLPing,' occurs between *FRT* sites during embryonic development in the 20 cells set aside to become the adult eye and antenna. Competition throughout development between the mutant and wild-type cell populations determines the proportions of red and white tissue in the adult eye. Generating clones of the parental *FRT* chromosome results in an approximately equal proportion of red and white tissue, thus forming the basis of the screen. Because reduced tissue growth can result from mutations in a wide variety of genes, including housekeeping genes, the majority of flies scored had normally patterned eyes containing more red than white tissue (KHM, pers. comm.). Alternatively, tissue overgrowth almost always results from mutations in genes that function in specific pathways to regulate tissue growth and organ size. Therefore, flies were retained in which the adult eye was composed of more white, mutant tissue than red, wild-type tissue, indicating that the mutant cells have a proliferative and/or growth advantage; these mutations were placed into complementation groups. Hence, this screen is affectionately referred to as the

'W>R' screen. The premise of the screen was verified by the identification of multiple orthologs of several known human tumor suppressor genes, including the Notch regulator *fringe* and a negative regulator of Ras signaling, *Gap1* (KHM pers. comm.).

Two main classes of overgrowth mutants were isolated in the screen: hyperplastic and neoplastic. Mutations that result in hyperplastic growth promote overgrowth of the imaginal disc tissue such that the epithelium retains its general structure and, typically, the ability to terminally differentiate; mutations with hyperplastic phenotypes indeed appeared as more white, mutant tissue relative to red, wild-type tissue in the original screen. Alleles of hyperplastic growth-suppressors such as the tuberous sclerosis genes, *Tsc1* and *Tsc2*, and the PI3K inhibitor *pten* increase both cell number and cell size, resulting in overgrowth of the entire eye (Gao et al., 2000; Goberdhan et al., 1999; Huang et al., 1999; Tapon et al., 2001). Mutations in components of the Hippo pathway, including *salvador* and *hippo*, also result in hyperplastic organ overgrowth but due to increased rates of growth combined with defects in apoptosis (Harvey et al., 2003; Tapon et al., 2002). Likewise, mutations in genes such as *capicua* and *archipelago* drive a balanced increase in rates of division and growth, producing enlarged clones composed of normally sized cells without affecting the overall size of the mosaic eye (Moberg et al., 2001; Tseng et al., 2007) (Figure I.5). A second class of mutations identified in the screen increased the overall size of the eye, but the eye was composed almost entirely of red, wild-type tissue rather than mutant tissue, indicating that although the mutant cells themselves have a growth disadvantage, these cells nonautonomously promote overgrowth of the wild-type cells in the same tissue. Alleles of *erupted* were identified for having this phenotype (Moberg et al., 2005). The growth advantage conferred by such

mutations is only revealed when the wild-type cells are eliminated, creating an imaginal disc composed entirely of mutant cells. In this latter scenario, the mutant cells promote cell-autonomous overgrowth of the imaginal disc tissue with disrupted epithelial structure, an inability to terminally differentiate, and invasive characteristics. These context-dependent phenotypes are summarized in Figure I.6 (reviewed in Gilbert and Moberg, 2006). Such characteristics are reminiscent of malignant human tumors; hence, these genes are called neoplastic tumor suppressors. Neoplastic tumor suppressor genes (nTSGs) include alleles of genes involved in epithelial polarity, such as *discs large* (*dlg*) and *scribble*, in addition to alleles of genes involved in endocytosis, such as *avalanche* (*avl*), *Rab5*, *erupted*, and *vps25* (reviewed in Hariharan and Bilder, 2006). The subsequent chapters will discuss work to further characterize alleles of novel growth-regulatory genes identified in this screen—*gang of four*, *archipelago*, and *erupted*.

Figure I.4. The *eyelessFLP/FRT* system of mitotic recombination.

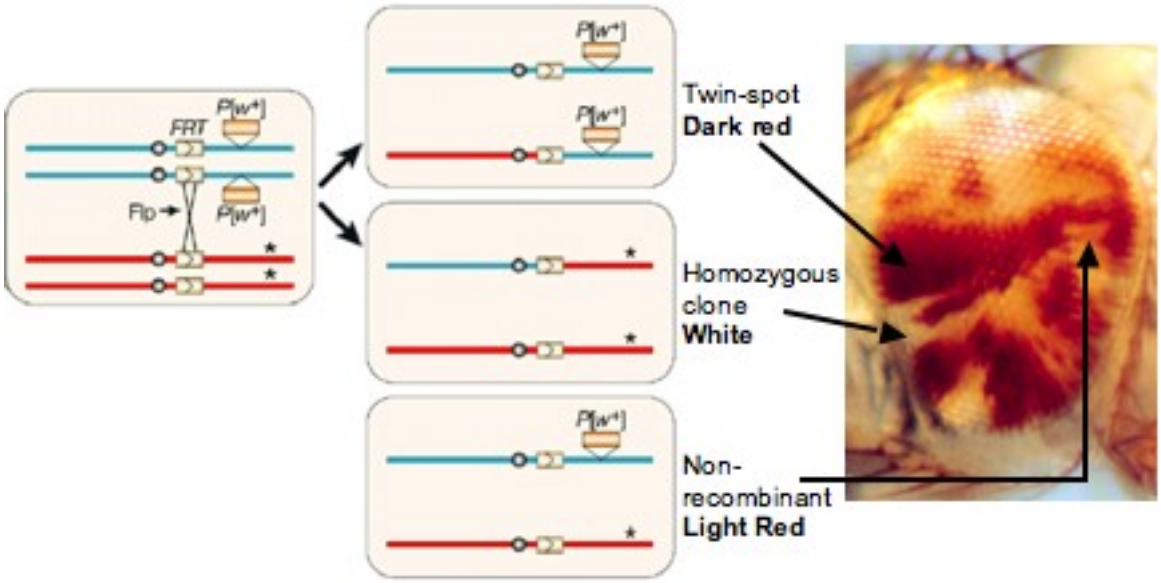

By placing *FLP* recombinase under the control of the *eyeless* enhancer, FLP/FRT-mediated recombination can be used to generate homozygous mutant clones in the eyes of flies that are otherwise heterozygous. The non-mutant chromosome is marked by a *mini-white* transgene (w^+); wild-type twin-spots appear dark red in the adult eye due to the presence of two w^+ copies. The asterisk indicates a mutation; homozygous mutant tissue appears white in the adult eye due to lack of w^+ transgene. Non-recombinant, 'unFLPed' tissue appears light red due to one w^+ copy. (Adapted from St Johnston, 2002)

Figure I.5. Hyperplastic growth suppressors affect core pathways.

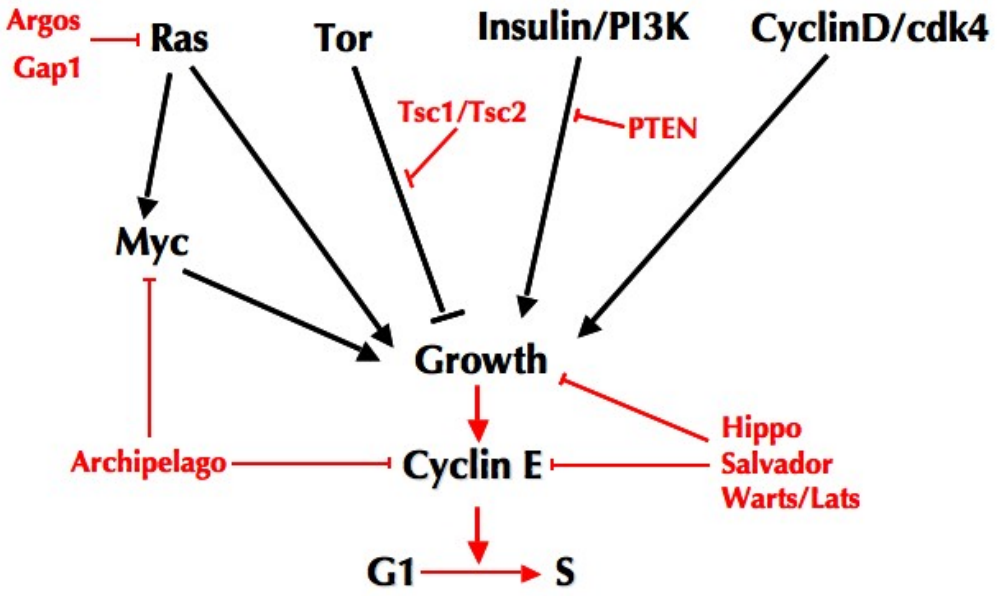

Hyperplastic growth suppressors identified in the 'W>R' screen (indicated in red) and their effects on the core growth pathways (indicated in black) in the *Drosophila* eye (Harvey et al., 2003; Moberg et al., 2001; Moberg et al., 2004; Tapon et al., 2002; Tapon et al., 2001).

Figure I.6. Context-dependent phenotypes of neoplastic tumor suppressor genes.

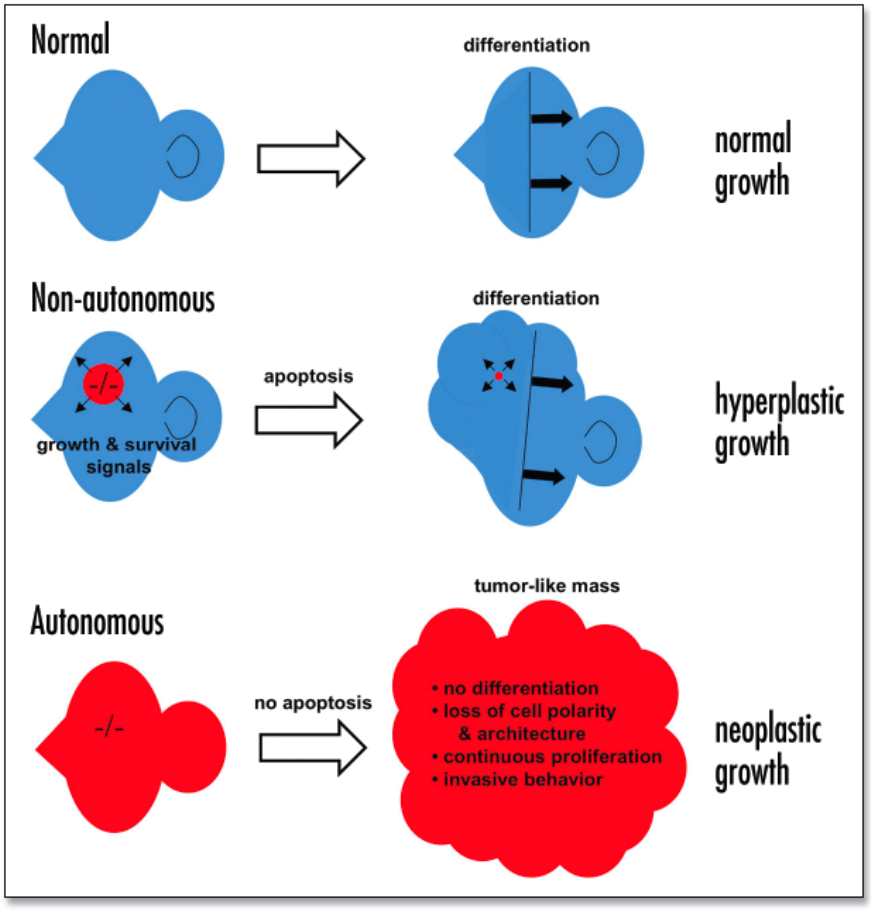

Top (normal): The morphogenetic furrow (black line) sweeps anteriorly across a wild-type eye imaginal disc, prompting cells to exit the cell cycle and leading to an appropriately sized larval eye. Middle (non-autonomous): Clones of mutant cells (-/-) in a genetically mosaic eye disc are eliminated by apoptosis, but cause hyperplasia of surrounding wild-type tissue. Bottom (autonomous): An eye composed entirely of mutant cells overgrows into a large, tumor-like mass in which cells fail to differentiate, continuously proliferate, lose apical-basal polarity, and exhibit invasive behavior. Blue, wild-type tissue; red, *ept* mutant tissue. (Courtesy of Gilbert and Moberg, 2006)

I.E. *gang of four*

The *gang of four* (*gfr*) gene has not been previously characterized. It was named because a lethal complementation group consisting of four alleles was originally isolated in the screen. A fifth allele, gfr^{x}, was independently isolated for its ability to synergize with a block in cell death to produce clonal overgrowth (MMG and KHM, unpublished). Mutations in *gfr* confer a subtle, yet reproducible, growth advantage: adult eyes mosaic for *gfr* show an increased representation of *gfr* mutant tissue (white) over wild-type tissue (red) (Figure I.7). Ommatidia within these clones can contain either multiplication or loss of interommatidial bristles, and the *gfr* mutant pupal retina has general patterning defects, including changes in cell number and organization (see Chapter II). Using the fly eye as a model of *gfr* function, I have identified several pathways that may act to mediate the growth and patterning defects of mutations in *gfr*, including signaling through MAPK cascades and activation of the Notch receptor.

Although multiple alleles of the *gfr* locus were recovered in the original screen, these alleles do not all appear to behave as simple recessive, loss-of-function lesions. Deletions spanning the region to which *gfr* alleles map (70A-B) fully complement *gfr* mutant chromosomes, and three of the four alleles tested overexpress the closely linked gene *bruno-3* (*bru-3*). The molecular lesions representing the *gfr* alleles are unknown, but genetic evidence indicates that these alleles behave as gain-of-function lesions and that overexpression of *bru-3* is central to *gfr* mutant phenotypes.

I.E1. *bru-3*

Drosophila bru-3 encodes an mRNA binding protein and translational repressor that binds to EDEN (embryo deadenylation element) sequences in target mRNAs and is orthologous to *Xenopus* EDEN-BP and human CUG-BP (Delaunay et al., 2004). Bru-3, EDEN-BP, and CUG-BP all contain RNA recognition motifs (RRMs) and a more recently described divergent linker region (linker-specific motif, lsm) thought to confer specificity for target mRNA recognition (Delaunay et al., 2004) (Figure 1.8). Although the Bru-3 paralogs Bruno and Bru-2 have been long recognized, neither binds EDEN sequence elements (Delaunay et al., 2004), and little is known specifically about Bru-3. Human CUG-BP was first shown to act as a splicing regulatory factor involved in myotonic dystrophy disease and is now recognized for its roles in translational regulation and deadenylation (Paillard et al., 2003; Philips et al., 1998; Timchenko et al., 2001), whereas the only reported function for EDEN-BP is as a translational repressor through deadenylation (Paillard et al., 1998). Although EDEN-BP is named for its posttranscriptional control of maternally loaded mRNAs, its deadenylation properties are not limited to embryonic development (Gautier-Courteille et al., 2004). Known EDEN-BP target mRNAs include cell cycle regulators and Su(H), a Notch pathway component (Graindorge et al., 2008), and EDEN-BP and CUG-BP both bind the c-Jun mRNA (Paillard et al., 2002). Likewise, a role for Bru-3 in growth control was recently identified: overexpression of *bru-3* promotes hyperproliferation of hemocytes and enlarged lymph glands (Stofanko et al., 2008). Therefore, even if the *gfr* complementation group is not allelic to *bru-3*, it is clear that *bru-3* overexpression contributes to *gfr*'s mutant phenotypes (see also Chapter II).

I.E2. MAPK Pathways

gfr has dual roles in both growth and patterning, and while these alleles elicit phenotypes via effects on multiple pathways, including Notch and potentially Hippo, MAPK signaling is central to *gfr*'s molecular mechanisms. Multicellular organisms have three well-characterized subfamilies of MAPKs (mitogen-activated protein kinases) that are used reiteratively during development to integrate signals controlling processes such as proliferation, differentiation, survival, and migration (Craig et al., 2008; Wagner and Nebreda, 2009). These MAPKs include ERKs (extracellular signal-related kinases), JNKs (Jun N-terminal kinases), and p38 kinases. The ERKs respond predominantly to growth factors and hormones and are activated in a Ras-dependent manner, whereas the p38 and JNKs respond to different environmental stresses and are activated preferentially downstream of Rac1 and Cdc42 small G proteins (reviewed in Canman and Kastan, 1996). MAPK activity is controlled by phosphorylation and is therefore determined by a balance of MAPK kinase and MAPK phosphatase activities. *gfr* mutations interact most strongly with components of the ERK (Rolled, Rl) and JNK (Basket, Bsk) MAPK cascades.

Ras/ERK signaling is involved in almost every aspect of fly eye development and has known roles in both proliferation and differentiation (Sundaram, 2005; Voas and Rebay, 2004). In *Drosophila*, Ras acts primarily within a cannonical RTK (receptor tyrosine kinase)-Ras-ERK pathway (Figure I.9). Binding of ligand to RTK (e.g., EGFR) causes receptor dimerization and subsequent recruitment of factors necessary to activate the small GTPase, Ras. Ras-GTP sets the MAPK cascade into motion by activating the MAPK kinase kinase (MAPKKK), Raf. Raf phorphorylates the MAPKK, MEK, which in

turn, dually phosphorylates ERK, prompting its nuclear translocation and activation of numerous targets that affect gene expression, including the Ets-domain and dJun transcription factors (reviewed in Kockel et al., 1997; Sundaram, 2005).

Although JNKs were originally identified as stress response proteins (Minden et al., 1994), *Drosophila* JNK is activated in response to various environmental and developmental cues that initiate the MAPK cascade via small GTPases (reviewed in Kockel et al., 2001). This signal is transduced to the JNKK, Hep, which in turn, dually phosphorylates JNK/Bsk, prompting its nuclear translocation and subsequent phosphorylation of the AP-1 transcription factor homologs, dJun and dFos (Figure I.10). AP-1 drives the transcription of at least two identified target genes, *puckered* and *dpp*. *Drosophila puckered* (*puc*) encodes a dual specificity JNK-specific phosphatase that is both a transcriptional target and negative regulator of the pathway (Martin-Blanco et al., 1998). In the *Drosophila* eye imaginal disc, JNK activity is typically pro-apoptotic: activation of JNK induces cell death, resulting in an eye ablation phenotype (Takatsu et al., 2000), and JNK is also involved in both radiation-induced and developmentally regulated cell death (McEwen and Peifer, 2005). However, JNK activity can switch from pro-apoptotic to pro-growth either in the presence of activated Ras (Igaki et al., 2006) or in collaboration with a block in cell death (McEwen and Peifer, 2005), indicating that the JNK pathway has both oncogenic and tumor-suppressive roles depending on cellular context.

Figure I.7. The *gfr* mosaic eye.

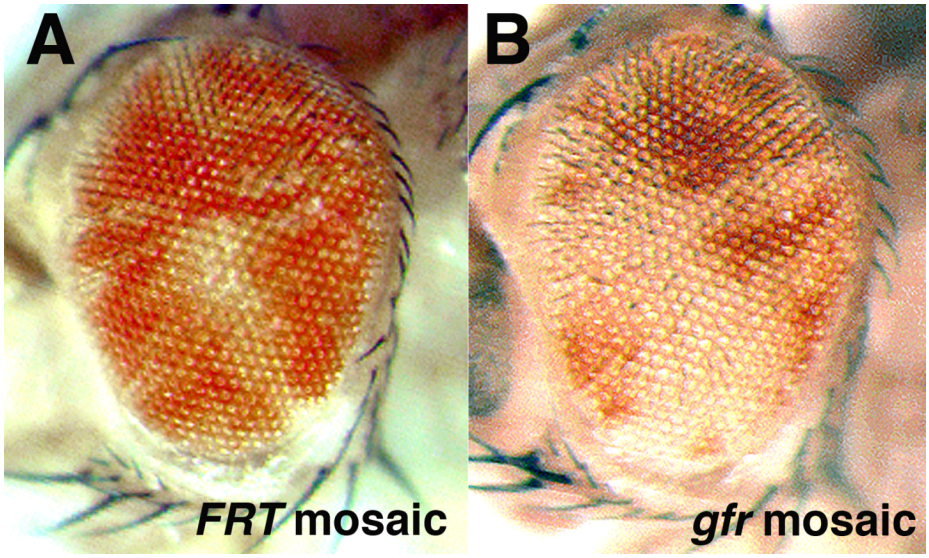

Adult eyes mosaic for the parental *FRT* chromosome (A) or *gfr* (B). Relative to the *FRT* control, the *gfr* mosaic eye has an over-representation of white, mutant tissue.

Figure I.8. Bru-3 is orthologous to EDEN-BP and CUG-BP.

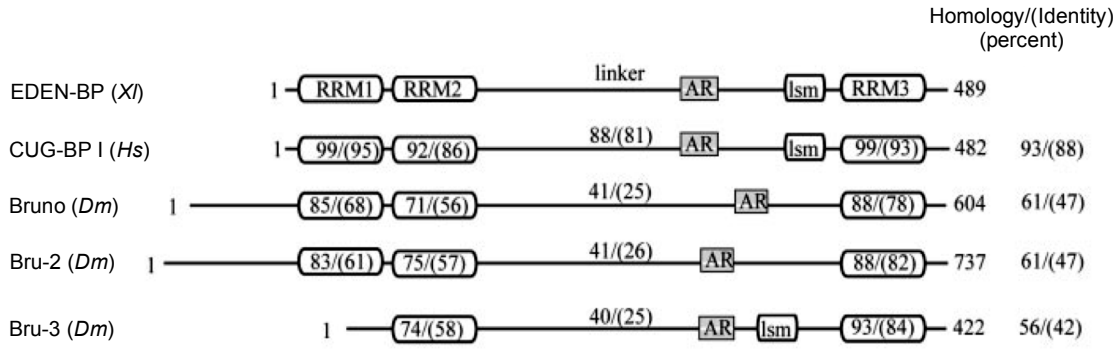

Schematic representation of the conserved domains of the most closely related proteins to EDEN-BP (*Xenopus laevis*) in *Homo sapiens* (CUG-BP) and *Drosophila melanogaster* (Bruno, Bru-2, Bru-3). Boxes represent characteristic domains (RRM, RNA recognition motif; AR, alanine-rich region; lsm, linker-specific motif). (Adapted from Delaunay et al., 2004)

Figure I.9. ERK Signaling.

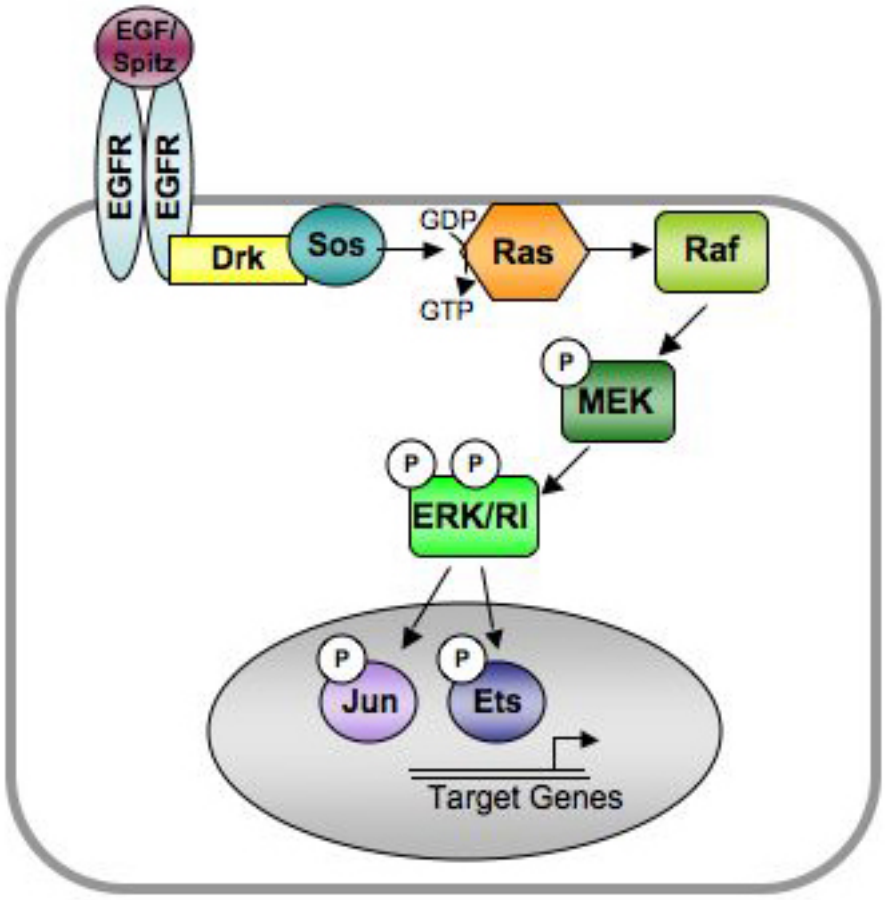

The RTK/Ras/ERK pathway is shown here using *Drosophila* epidermal growth factor receptor (EGFR) as the representative receptor tyrosine kinase (RTK). Upon ligand (EGF/Spitz) binding and receptor activation, the adaptor Drk recruits the guanine exchange factor Sos, allowing it to activate the GTPase Ras. Activated Ras facilitates activation of the MAPKKK Raf, setting off the MAPK cascade. Activated ERK/Rl translocates to the nucleus where it phosphorylates transcription factors, such as Ets-domain proteins and dJun, to regulate target gene expression (see text). (Adapted from Sundaram, 2005; Voas and Rebay, 2004)

Figure I.10. JNK Signaling.

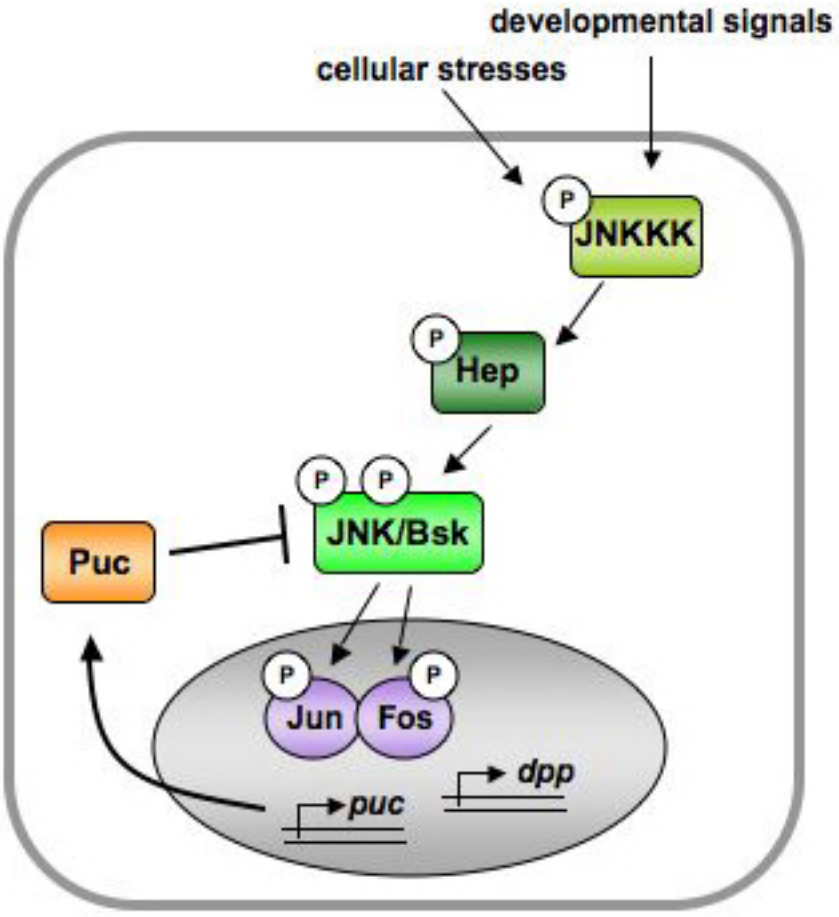

The core components of the JNK pathway are shown here. The MAPK cascade is typically activated downstream of Rac1 and Cdc42 small G proteins (not shown) in response to various environmental and developmental signals. Note that the transcriptional target *puckered* (*puc*) feedsback to dephosphorylate and negatively regulate JNK/Bsk activity (see text). (Adapted from Kockel et al., 2001)

I.F. *archipelago*

Mutations in *archipelago* (*ago*, also known as *Fbw7*, *sel-10*, *cdc4*) were identified in the original screen because *ago* mutant cells conferred a dramatic growth advantage relative to wild-type cells in the mosaic eye (Figure I.11). The *ago* locus encodes an F-box/WD-repeat (tryptophan/aspartic acid) protein which functions as the substrate-specificity factor for an SCF (Skp/Cullin/F-box) type E3 ubiquitin ligase (Moberg et al., 2001). Ago interacts with the ubiquitination machinery via its F-box domain, and the seven tandem WD repeats form a ß-propellar structure through which Ago binds specific substrates, recruiting them into the assembled ubiquitin ligase for polyubiquitination and subsequent proteosomal destruction (Figure I.12). Known Ago substrates in in *Drosophila* include the G1/S cell cycle regulator Cyclin E (CycE) and the fly ortholog of the c-Myc proto-oncogene, dMyc (Moberg et al., 2001; Moberg et al., 2004). *ago* mutant tissues show elevated levels of these proteins, leading to ectopic cell divisions and increased tissue growth, respectively. These functions are conserved in vertebrate *ago* homologs: mouse and human Fbw7 have also been shown to regulate levels of CycE (Koepp et al., 2001; Strohmaier et al., 2001) and c-Myc (Welcker et al., 2004). In addition to this mitotic role, Ago also regulates hypoxia-sensitivity and post-mitotic morphogenesis of the embryonic tracheal system via degradation of the Trachealess transcription factor (Mortimer and Moberg, 2007; Mortimer and Moberg, 2009).

However, Fbw7 has been implicated in the turnover of several additional proteins, including Notch, Presenilin, c-Jun, SREBP, and mTor kinase (reviewed in Welcker and Clurman, 2008; Mao et al., 2008). Thus, loss of one gene has the potential to disrupt the function of several proto-oncogenes at simultaneously. Indeed, mutational inactivation of

ago/*Fbw7* not only drives overgrowth in *Drosophila* tissues but also causes tumors in mouse models (Mao et al., 2004; Maser et al., 2007; Onoyama et al., 2007) and is associated with a variety of human cancers, including T-cell acute lymphoblastic leukemia (T-ALL) and tumors of the prostate, colon, endometrium, and pancreas (reviewed in Welcker and Clurman, 2008). Therefore, gaining further insight into the roles of individual Ago/Fbw7 substrates may be lead to a better understanding of the tumor-suppressive functions of *ago/Fbw7*.

I.F1. The Notch Signaling Pathway

The intracellular domain of the Notch receptor has been implicated as an Fbw7/Sel-10 substrate in mammalian and *C. elegans* systems, respectively (Gupta-Rossi et al., 2001; Hubbard et al., 1997; Oberg et al., 2001; Wu et al., 2001); however, the interactions between fly Notch and Ago have not yet been characterized. Notch signaling regulates numerous cellular processes, including cell fate specification, proliferation, and apoptosis (Artavanis-Tsakonas et al., 1999), and aberrent pathway activation is associated with T-ALL (Demarest et al., 2008). Whereas mammals have four *Notch* genes, *Drosophila* has only one, thus providing a simpler model for pathway characterization. This evolutionarily conserved transmembrane receptor was first characterized in *Drosophila* and named for its loss-of-function wing notching phenotype (Artavanis-Tsakonas et al., 1983). Pathway signaling occurs when a DSL (Delta/Serrate/LAG-2) ligand on an adjacent cell binds to Notch (Figure I.13). Ligand-receptor interaction induces proteolytic cleavages of Notch. Intramembrane cleavage mediated by the Presenilin-dependent gamma-secretase complex results in translocation of the C-terminal Notch intracellular

domain (N^{ICD}) to the nucleus. Although conventional models of Notch signaling indicate that the gamma-secretase cleavage event occurs on the cell membrane, the gamma-secretase complex has been detected on both the cell membrane as well as in endocytic compartments (Gupta-Rossi et al., 2004), and recent work suggests the cleavage can happen in either location (reviewed in Tien et al., 2009). However, gamma-secretase cleavage of Notch is much reduced when trafficking to the early endosomes in impaired, indicating that endocytosis of the Notch receptor is crucial for optimal signaling (Vaccari et al., 2008). Indeed, endocytic sorting of Notch mediates a key decision between its activation and lysosomal degradation (reviewed in Bray, 2006; Le Borgne, 2006). In the event of activation and N^{ICD} release, nuclear N^{ICD} recruits the coactivator Mastermind, allowing the CSL (CBF1/RBPJk in mammals, Suppressor of Hairless (Su(H)) in flies, and LAG-1 in worms) transcription factor to activate target gene expression. Signaling is terminated upon N^{ICD} polyubiquitin and proteolytic degradation (for a recent review of Notch signaling, see Tien et al., 2009).

Figure I.11. The *ago* mosaic eye.

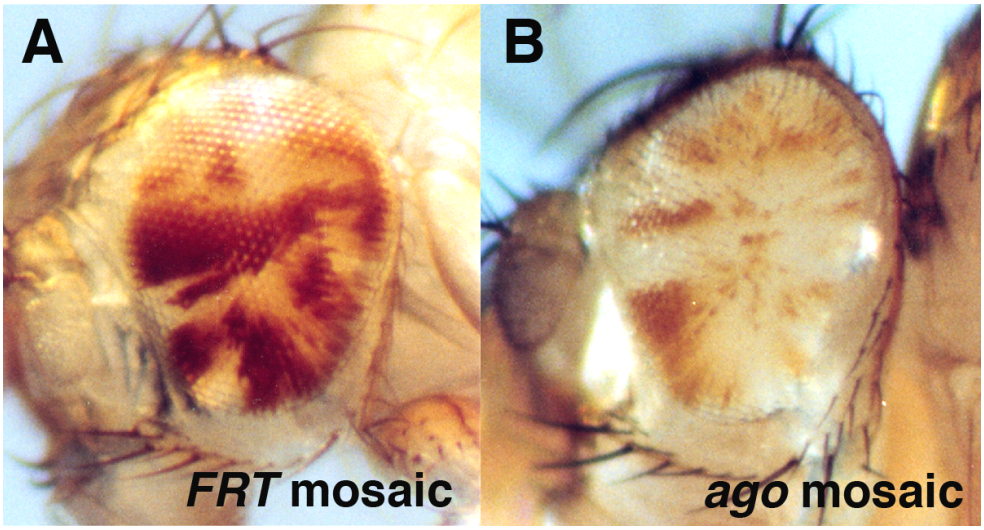

Adult eyes mosaic for the parental *FRT* chromosome (A) or *ago* (B). Relative to the *FRT* control, the *ago* mosaic eye has an over-representation of white, mutant tissue (Moberg et al., 2001).

Figure I.12. The SCF-Ago Complex.

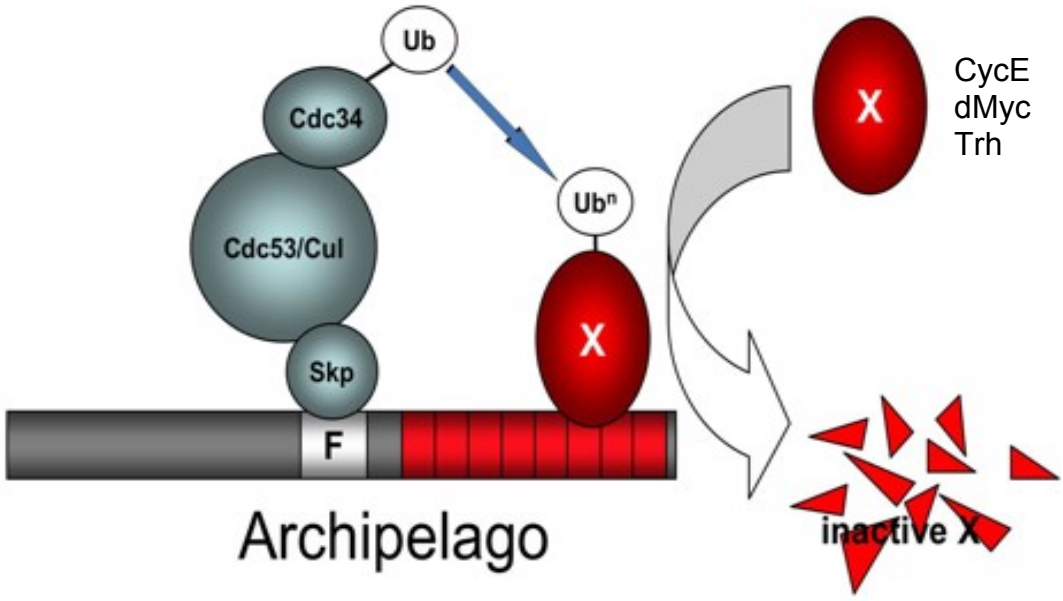

Archipelago binds to the ubiquitination machinery via its F-box domain and recruits substrates into the SCF complex via its WD-repeats. To date, known SCF^{Ago} substrates in *Drosophila* include Cyclin E (Moberg et al., 2001), dMyc (Moberg et al., 2004), and Trachealess (Mortimer and Moberg, 2007).

Figure I.13. The Notch Signaling Pathway.

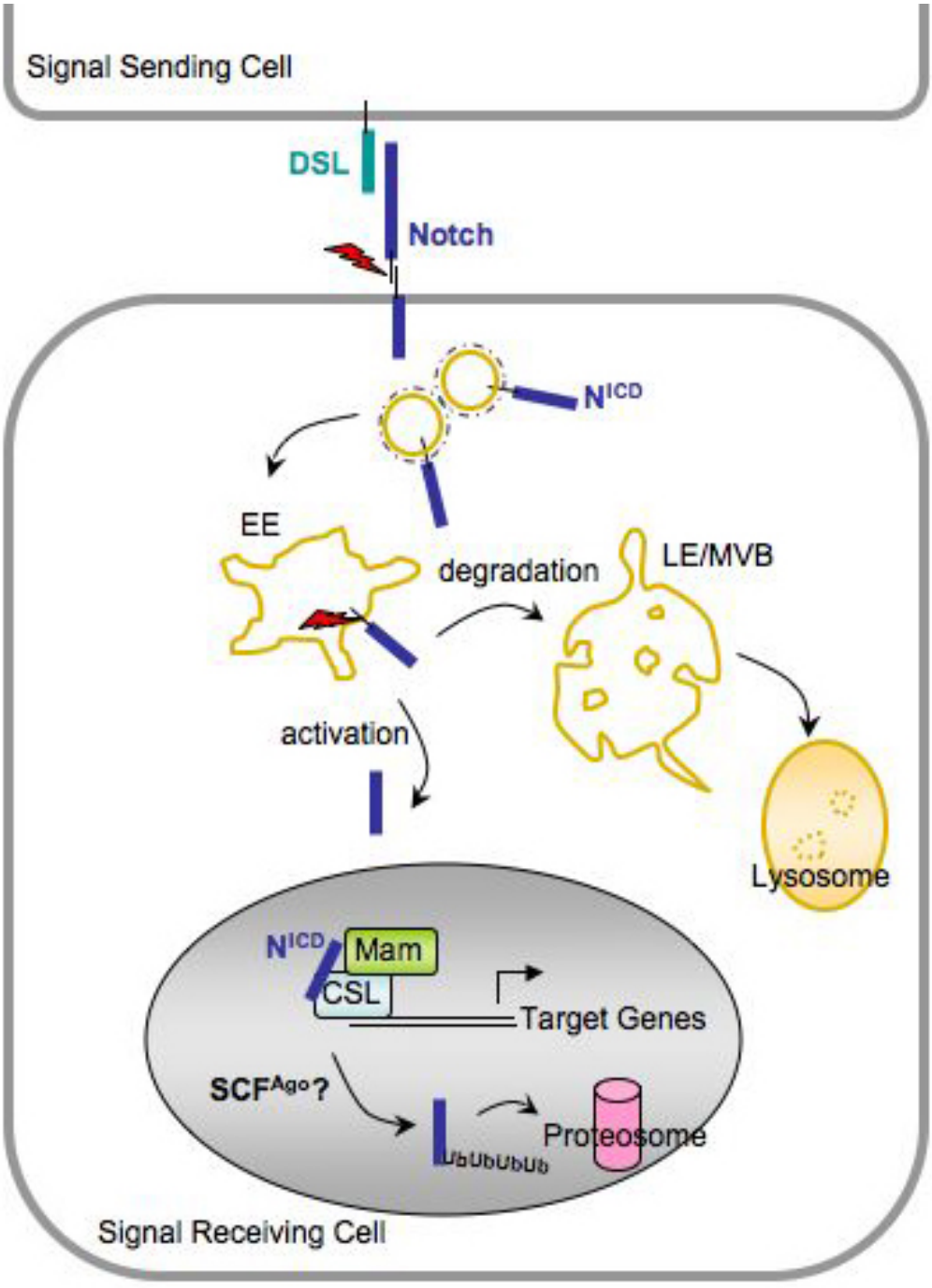

Schematic representation of the Notch pathway. Notch (dark blue) interacts with the DSL (Delta/Serrate/LAG-2) ligands (teal) resulting in a series of proteolytic events (red). The first proteolytic cleavage occurs at the plasma membrane and is mediated by the ADAM protease; the second cleavage is mediated by the gamma-secretase complex and allows for N^{ICD} nuclear translocation. In the nucleus, N^{ICD} recruits the co-activator Mam (Mastermind, green) and promotes transcription of CSL (CBF1/Su(H)/LAG-1, light blue) target genes. Notch signaling is terminated upon polyubiquitination and proteosomal degradation of the N^{ICD}; SCF-Ago is thought to control this process (see text). (Adapted from Bray, 2006; Tien et al., 2009; Vaccari et al., 2008)

I.G. *erupted*

The *Drosophila* gene *erupted* (*ept*) encodes an ortholog of human Tumor Susceptibility Gene-101 (TSG101) and yeast Vps23p, which function as part of the ESCRT (endosomal sorting complex required for transport)-I complex to sort monoubiquitinated transmembrane receptors from the early endosome to the multi-vesicular body (MVB) for ultimate lysosomal degradation (Bishop and Woodman, 2001; Katzmann et al., 2001; Stuffers et al., 2008) (Figure I.14). *vps23* was one of at least 15 class E *vps* (vacuolar protein sorting) mutants first identified in yeast for having enlarged early endosomes that accumulate ubiquitinated proteins; these *vps* genes form the structural components of the ESCRTs (reviewed in Katzmann et al., 2002). Because ESCRT function is required for MVB formation, like their yeast counterparts, mutations in any one component of the ESCRT complexes lead to defects in endolysosomal sorting (reviewed in Herz and Bergmann, 2009). While the *vps* genes are highly conserved from yeast to mammals, until recently, the phenotypic consequences disrupted *vps* gene function in multicellular organisms have been unclear.

Alleles of *ept* were identified in the original screen because although the mosaic eye was composed almost entirely of red, wild-type tissue, the overall size of the eye was larger (Figure I.15). Initial characterization of this effect by Moberg *et al*. showed that activated Notch is trapped in *ept* mutant endosomes (Moberg et al., 2005). Ectopic expression of the Notch target gene *unpaired* (*upd*) promotes JAK-STAT pathway activation and subsequent nonautonomous overgrowth of surrounding wild-type tissue. Additionally, localization of the apical-polarity determinant protein Crumbs is altered in *ept* mutant eye disc cells. Although *ept* mutant tissue elicits hyperplastic overgrowth of

adjacent wild-type cells, the *ept*$^{-/-}$ cells themselves divide signifcantly more slowly and are eliminated by cell competition in the presence of wild-type cells. The autonomous overgrowth of *ept* mutant cells is therefore only revealed when either cell death is blocked or the wild-type cells are eliminated, creating an imaginal disc composed entirely of mutant cells. Under these conditions, the tissue transforms to adopt neoplastic characteristics, including loss of apical-basal polarity, loss of epithelial character, failure to stop proliferating, lack of differentiation, and invasive behavior. Therefore, *ept* controls growth in two ways: (1) mutant clones of *ept* promote the nonautonomous growth of surrounding tissue, and (2) eye discs composed almost entirely of *ept* mutant tissue fail to exit the cell cycle and continue to grow during an extended larval stage, becoming tumorous masses (see Chapter IV).

Mutations in *ept* link proliferation control and epithelial polarity, and defective sorting of the transmembrane proteins Notch and Crumbs is central to both the autonomous and nonautonomous consequences of *ept* loss (Gilbert et al., 2009; Moberg et al., 2005). To date, several signaling receptors other than Notch have been shown to accumulate in endosomes in ESCRT mutants, including the Notch ligand Delta, EGFR, the Hedgehog receptors Patched and Smoothened, and the Dpp/TGF-ß receptor Thickveins (reviewed in Herz and Bergmann, 2009). Therefore, other receptors and transmembrane proteins sorted through the ESCRT pathway remain to be identified in order to more fully characterize the autonomous growth properties of *ept* mutant cells.

Mammalian TSG101 was first identified because *Tsg101* knock-down enabled fibroblasts to form colonies on soft agar and produce tumors in nude mice (Li and Cohen, 1996). Although mutations in *Tsg101* have been linked to human cancers (Li et al.,

1997), knock-out studies in mice have been inconclusive (Wagner et al., 2003), and tumor-suppressive properties of *Tsg101* remain controversal. However, if inactivating *Tsg101* mutations behave similarly to loss-of-function *ept*, then it is likely that tumor cells harboring *Tsg101* mutations die at the expense of promoting overproliferation of surrounding stromal cells. Because human cancer involves the cooperation among mutations in several genes (Hanahan and Weinberg, 2000), additional genetic alterations that block apoptosis may be necessary to collaborate with *Tsg101* loss and induce tumorigenesis.

I.G1. The JAK-STAT Pathway

Signaling through the JAK-STAT pathway plays a critical role in *ept* mutant phenotypes. The Janus kinase-Signal transducer and activator of transcription (JAK-STAT) pathway is an evolutionarily conserved signaling cascasde that plays essential roles in numerous biological processes in vertebrates and invertebrates, including immunity, hematopoiesis, and proliferation (reviewed in Levy and Darnell, 2002). Whereas mammalian systems have four JAKs and seven STATs, *Drosophila* has a single JAK (Hopscotch, Hop, Binari and Perrimon, 1994) and a single STAT (Stat92E, Hou et al., 1996; Yan et al., 1996). The JAK-STAT pathway is initiated upon binding of the extracellular, cytokine-like ligand Unpaired (Upd, Harrison et al., 1998) to the Domeless (Dome, Brown et al., 2001) transmembrane receptor, causing receptor dimerization (Figure I.16). The receptor-associated JAK molecules then phosphorylate each other and the Dome cytoplasmic tail. Cytosolic Stat92E is recruited to these phosphorylated receptor sites and is in turn tyrosine phosphorylated by the JAK proteins (Yan et al., 1996). Activated Stat92E

molecules dimerize and accumulate in the nucleus where they induce transcription of target genes (reviewed in Li, 2008). Because the fly pathway shares biological functions with its mammalian counterpart, it is important to understand mechanisms that regulate JAK-STAT signaling, and the single-copy genes in *Drosophila* simplify interpretation of pathway function.

Figure I.14. ESCRT complexes sort proteins from EE to MVB.

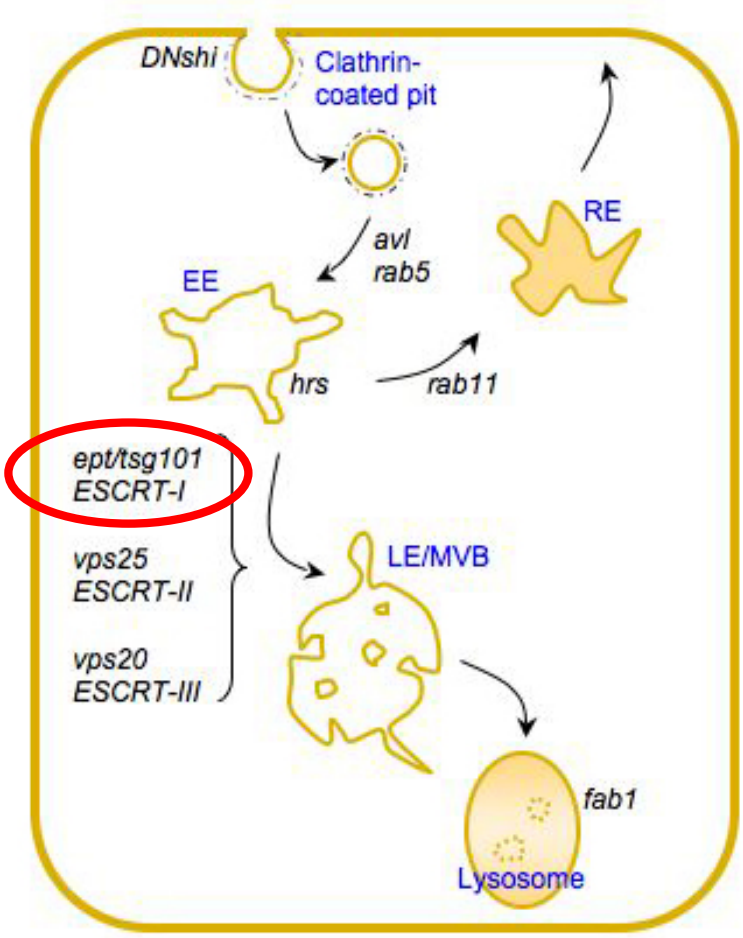

Diagram illustrates core components of the endolysosomal pathway. Endosomal compartments are labeled in blue; genes involved at each step of the pathway are indicated in black. *erupted* (*ept*) is a component of the ESCRT-I complex. *DNshi*, dominant-negative shibire; *avl*, avalanche; *hrs*, hepatocyte growth factor regulated tyrosine kinase substrate; EE, early endosome; RE, recycline endosome; LE/MVB, late endosome/multi-vesicular body. (Adapted from Hariharan and Bilder, 2006; Vaccari et al., 2008)

Figure I.15. The *ept* mosaic eye.

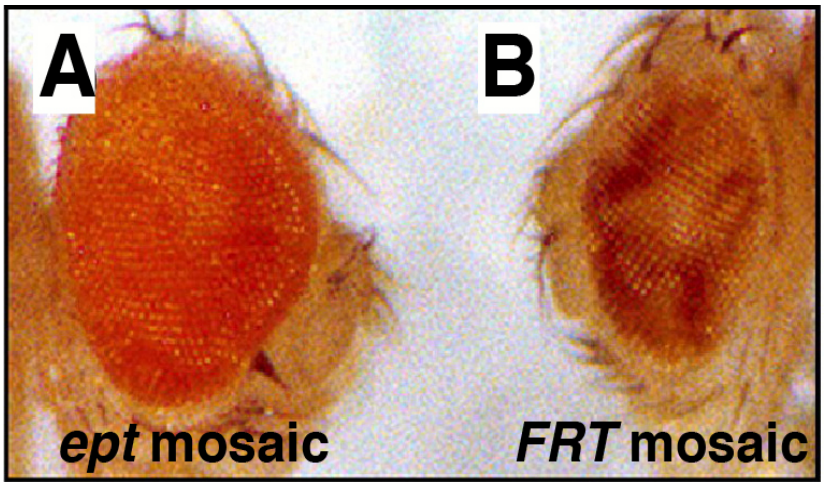

Adult eyes mosaic for *ept* (A) or the parental *FRT* chromosome (B). Relative to the *FRT* control, the *ept* mosaic eye is composed of mostly red, wild-type tissue (Moberg et al., 2005).

Figure I.16. The JAK-STAT Pathway.

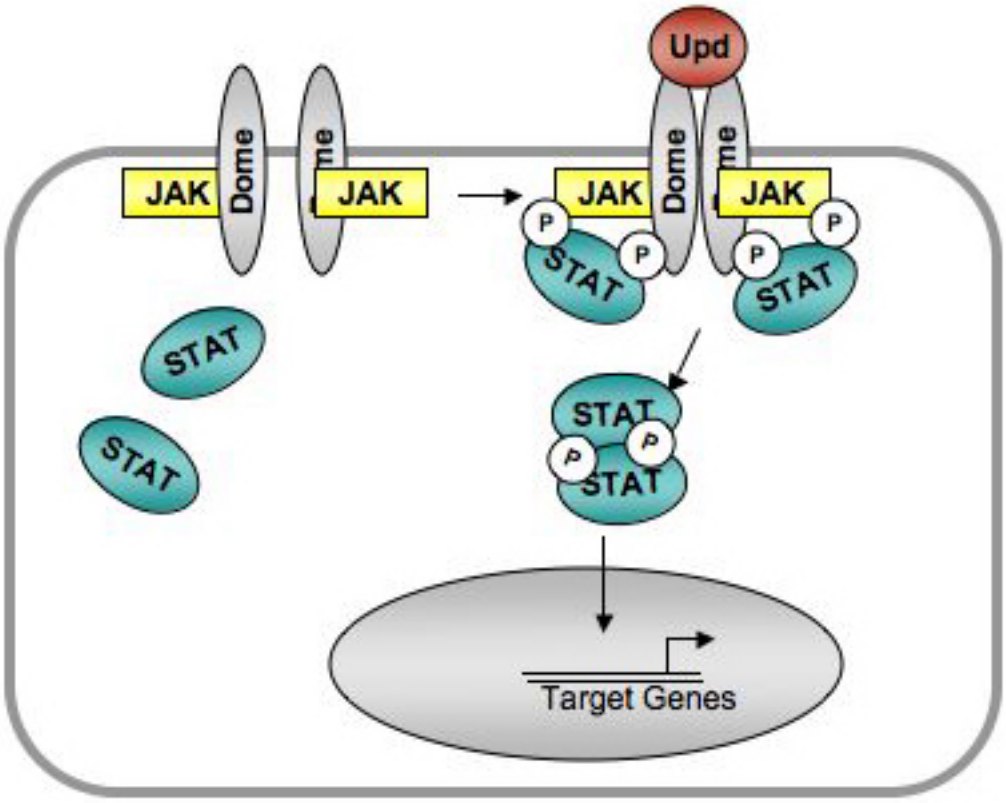

Schematic representation of the JAK-STAT pathway. Binding of the extracellular receptor, Upd (Unpaired, red), to the Dome (Domeless) transmembrane receptor (gray) activates the kinase activity of associated JAKs (yellow). The phosphorylated receptor/JAK complex acts as a docking site for cytosolic STATs (Stat92E, teal), which are recruited and phosphorylated. P-STAT dimerizes, translocates to the nucleus, and binds DNA to induce target genes expression (see text). (Adapted from Arbouzova and Zeidler, 2006)

I.H. REFERENCES

Arbouzova, N. I. and Zeidler, M. P. (2006). JAK/STAT signalling in Drosophila: insights into conserved regulatory and cellular functions. *Development* **133**, 2605-16.

Artavanis-Tsakonas, S., Muskavitch, M. A. and Yedvobnick, B. (1983). Molecular cloning of Notch, a locus affecting neurogenesis in Drosophila melanogaster. *Proc Natl Acad Sci U S A* **80**, 1977-81.

Artavanis-Tsakonas, S., Rand, M. D. and Lake, R. J. (1999). Notch signaling: cell fate control and signal integration in development. *Science* **284**, 770-6.

Baker, N. E. and Yu, S. Y. (2001). The EGF receptor defines domains of cell cycle progression and survival to regulate cell number in the developing Drosophila eye. *Cell* **104**, 699-708.

Binari, R. and Perrimon, N. (1994). Stripe-specific regulation of pair-rule genes by hopscotch, a putative Jak family tyrosine kinase in Drosophila. *Genes Dev* **8**, 300-12.

Bishop, N. and Woodman, P. (2001). TSG101/mammalian VPS23 and mammalian VPS28 interact directly and are recruited to VPS4-induced endosomes. *J Biol Chem* **276**, 11735-42.

Bray, S. J. (2006). Notch signalling: a simple pathway becomes complex. *Nat Rev Mol Cell Biol* **7**, 678-89.

Brown, S., Hu, N. and Hombria, J. C. (2001). Identification of the first invertebrate interleukin JAK/STAT receptor, the Drosophila gene domeless. *Curr Biol* **11**, 1700-5.

Brumby, A. M. and Richardson, H. E. (2005). Using Drosophila melanogaster to map human cancer pathways. *Nat Rev Cancer* **5**, 626-39.

Cagan, R. L. and Ready, D. F. (1989). The emergence of order in the Drosophila pupal retina. *Dev Biol* **136**, 346-62.

Canman, C. E. and Kastan, M. B. (1996). Signal transduction. Three paths to stress relief. *Nature* **384**, 213-4.

Craig, E. A., Stevens, M. V., Vaillancourt, R. R. and Camenisch, T. D. (2008). MAP3Ks as central regulators of cell fate during development. *Dev Dyn* **237**, 3102-14.

Delaunay, J., Le Mee, G., Ezzeddine, N., Labesse, G., Terzian, C., Capri, M. and Ait-Ahmed, O. (2004). The Drosophila Bruno paralogue Bru-3 specifically binds the EDEN translational repression element. *Nucleic Acids Res* **32**, 3070-82.

Demarest, R. M., Ratti, F. and Capobianco, A. J. (2008). It's T-ALL about Notch. *Oncogene* **27**, 5082-91.

Finley, R. L., Jr., Thomas, B. J., Zipursky, S. L. and Brent, R. (1996). Isolation of Drosophila cyclin D, a protein expressed in the morphogenetic furrow before entry into S phase. *Proc Natl Acad Sci U S A* **93**, 3011-5.

Gao, X., Neufeld, T. P. and Pan, D. (2000). Drosophila PTEN regulates cell growth and proliferation through PI3K-dependent and -independent pathways. *Dev Biol* **221**, 404-18.

Garcia-Bellido, A. and Merriam, J. R. (1969). Cell lineage of the imaginal discs in Drosophila gynandromorphs. *J Exp Zool* **170**, 61-75.

Gateff, E. (1978). Malignant neoplasms of genetic origin in Drosophila melanogaster. *Science* **200**, 1448-59.

Gautier-Courteille, C., Le Clainche, C., Barreau, C., Audic, Y., Graindorge, A., Maniey, D., Osborne, H. B. and Paillard, L. (2004). EDEN-BP-dependent post-transcriptional regulation of gene expression in Xenopus somitic segmentation. *Development* **131**, 6107-17.

Gilbert, M. M. and Moberg, K. H. (2006). ESCRTing cell proliferation off the beaten path: lessons from the drosophila eye. *Cell Cycle* **5**, 283-7.

Gilbert, M. M., Robinson, B. S. and Moberg, K. H. (2009). Functional interactions between the erupted/tsg101 growth suppressor gene and the DaPKC and rbf1 genes in Drosophila imaginal disc tumors. *PLoS One* **4**, e7039.

Goberdhan, D. C., Paricio, N., Goodman, E. C., Mlodzik, M. and Wilson, C. (1999). Drosophila tumor suppressor PTEN controls cell size and number by antagonizing the Chico/PI3-kinase signaling pathway. *Genes Dev* **13**, 3244-58.

Golic, K. G. and Lindquist, S. (1989). The FLP recombinase of yeast catalyzes site-specific recombination in the Drosophila genome. *Cell* **59**, 499-509.

Graindorge, A., Le Tonqueze, O., Thuret, R., Pollet, N., Osborne, H. B. and Audic, Y. (2008). Identification of CUG-BP1/EDEN-BP target mRNAs in Xenopus tropicalis. *Nucleic Acids Res* **36**, 1861-70.

Gupta-Rossi, N., Le Bail, O., Gonen, H., Brou, C., Logeat, F., Six, E., Ciechanover, A. and Israel, A. (2001). Functional interaction between SEL-10, an F-box protein, and the nuclear form of activated Notch1 receptor. *J Biol Chem* **276**, 34371-8.

Gupta-Rossi, N., Six, E., LeBail, O., Logeat, F., Chastagner, P., Olry, A., Israel, A. and Brou, C. (2004). Monoubiquitination and endocytosis direct gamma-secretase cleavage of activated Notch receptor. *J Cell Biol* **166**, 73-83.

Hanahan, D. and Weinberg, R. A. (2000). The hallmarks of cancer. *Cell* **100**, 57-70.

Hariharan, I. K. and Bilder, D. (2006). Regulation of imaginal disc growth by tumor-suppressor genes in Drosophila. *Annu Rev Genet* **40**, 335-61.

Harrison, D. A., McCoon, P. E., Binari, R., Gilman, M. and Perrimon, N. (1998). Drosophila unpaired encodes a secreted protein that activates the JAK signaling pathway. *Genes Dev* **12**, 3252-63.

Harvey, K. F., Pfleger, C. M. and Hariharan, I. K. (2003). The Drosophila Mst ortholog, hippo, restricts growth and cell proliferation and promotes apoptosis. *Cell* **114**, 457-67.

Herz, H. M. and Bergmann, A. (2009). Genetic analysis of ESCRT function in Drosophila: a tumour model for human Tsg101. *Biochem Soc Trans* **37**, 204-7.

Hou, X. S., Melnick, M. B. and Perrimon, N. (1996). Marelle acts downstream of the Drosophila HOP/JAK kinase and encodes a protein similar to the mammalian STATs. *Cell* **84**, 411-9.

Huang, H., Potter, C. J., Tao, W., Li, D. M., Brogiolo, W., Hafen, E., Sun, H. and Xu, T. (1999). PTEN affects cell size, cell proliferation and apoptosis during Drosophila eye development. *Development* **126**, 5365-72.

Hubbard, E. J., Wu, G., Kitajewski, J. and Greenwald, I. (1997). sel-10, a negative regulator of lin-12 activity in Caenorhabditis elegans, encodes a member of the CDC4 family of proteins. *Genes Dev* **11**, 3182-93.

Igaki, T., Pagliarini, R. A. and Xu, T. (2006). Loss of cell polarity drives tumor growth and invasion through JNK activation in Drosophila. *Curr Biol* **16**, 1139-46.

Katzmann, D. J., Babst, M. and Emr, S. D. (2001). Ubiquitin-dependent sorting into the multivesicular body pathway requires the function of a conserved endosomal protein sorting complex, ESCRT-I. *Cell* **106**, 145-55.

Katzmann, D. J., Odorizzi, G. and Emr, S. D. (2002). Receptor downregulation and multivesicular-body sorting. *Nat Rev Mol Cell Biol* **3**, 893-905.

Kockel, L., Homsy, J. G. and Bohmann, D. (2001). Drosophila AP-1: lessons from an invertebrate. *Oncogene* **20**, 2347-64.

Kockel, L., Zeitlinger, J., Staszewski, L. M., Mlodzik, M. and Bohmann, D. (1997). Jun in Drosophila development: redundant and nonredundant functions and regulation by two MAPK signal transduction pathways. *Genes Dev* **11**, 1748-58.

Koepp, D. M., Schaefer, L. K., Ye, X., Keyomarsi, K., Chu, C., Harper, J. W. and Elledge, S. J. (2001). Phosphorylation-dependent ubiquitination of cyclin E by the SCFFbw7 ubiquitin ligase. *Science* **294**, 173-7.

Le Borgne, R. (2006). Regulation of Notch signalling by endocytosis and endosomal sorting. *Curr Opin Cell Biol* **18**, 213-22.

Levy, D. E. and Darnell, J. E., Jr. (2002). Stats: transcriptional control and biological impact. *Nat Rev Mol Cell Biol* **3**, 651-62.

Li, L. and Cohen, S. N. (1996). Tsg101: a novel tumor susceptibility gene isolated by controlled homozygous functional knockout of allelic loci in mammalian cells. *Cell* **85**, 319-29.

Li, L., Li, X., Francke, U. and Cohen, S. N. (1997). The TSG101 tumor susceptibility gene is located in chromosome 11 band p15 and is mutated in human breast cancer. *Cell* **88**, 143-54.

Li, W. X. (2008). Canonical and non-canonical JAK-STAT signaling. *Trends Cell Biol* **18**, 545-51.

Mao, J. H., Kim, I. J., Wu, D., Climent, J., Kang, H. C., DelRosario, R. and Balmain, A. (2008). FBXW7 targets mTOR for degradation and cooperates with PTEN in tumor suppression. *Science* **321**, 1499-502.

Mao, J. H., Perez-Losada, J., Wu, D., Delrosario, R., Tsunematsu, R., Nakayama, K. I., Brown, K., Bryson, S. and Balmain, A. (2004). Fbxw7/Cdc4 is a p53-dependent, haploinsufficient tumour suppressor gene. *Nature* **432**, 775-9.

Martin-Blanco, E., Gampel, A., Ring, J., Virdee, K., Kirov, N., Tolkovsky, A. M. and Martinez-Arias, A. (1998). puckered encodes a phosphatase that mediates a feedback loop regulating JNK activity during dorsal closure in Drosophila. *Genes Dev* **12**, 557-70.

Maser, R. S., Choudhury, B., Campbell, P. J., Feng, B., Wong, K. K., Protopopov, A., O'Neil, J., Gutierrez, A., Ivanova, E., Perna, I. et al. (2007). Chromosomally unstable mouse tumours have genomic alterations similar to diverse human cancers. *Nature* **447**, 966-71.

McEwen, D. G. and Peifer, M. (2005). Puckered, a Drosophila MAPK phosphatase, ensures cell viability by antagonizing JNK-induced apoptosis. *Development* **132**, 3935-46.

Minden, A., Lin, A., Smeal, T., Derijard, B., Cobb, M., Davis, R. and Karin, M. (1994). c-Jun N-terminal phosphorylation correlates with activation of the JNK subgroup but not the ERK subgroup of mitogen-activated protein kinases. *Mol Cell Biol* **14**, 6683-8.

Moberg, K. H., Bell, D. W., Wahrer, D. C., Haber, D. A. and Hariharan, I. K. (2001). Archipelago regulates Cyclin E levels in Drosophila and is mutated in human cancer cell lines. *Nature* **413**, 311-6.

Moberg, K. H., Mukherjee, A., Veraksa, A., Artavanis-Tsakonas, S. and Hariharan, I. K. (2004). The Drosophila F box protein archipelago regulates dMyc protein levels in vivo. *Curr Biol* **14**, 965-74.

Moberg, K. H., Schelble, S., Burdick, S. K. and Hariharan, I. K. (2005). Mutations in erupted, the Drosophila ortholog of mammalian tumor susceptibility gene 101, elicit non-cell-autonomous overgrowth. *Dev Cell* **9**, 699-710.

Mortimer, N. T. and Moberg, K. H. (2007). The Drosophila F-box protein Archipelago controls levels of the Trachealess transcription factor in the embryonic tracheal system. *Dev Biol* **312**, 560-71.

Mortimer, N. T. and Moberg, K. H. (2009). Regulation of Drosophila embryonic tracheogenesis by dVHL and hypoxia. *Dev Biol* **329**, 294-305.

Neufeld, T. and Hariharan, I. K. (2002). Regulation of Growth and Cell Proliferation during Eye Development. In *Drosophila Eye Development*, vol. 37 (ed. K. Moses), pp. 107-133. New York: Springer.

Oberg, C., Li, J., Pauley, A., Wolf, E., Gurney, M. and Lendahl, U. (2001). The Notch intracellular domain is ubiquitinated and negatively regulated by the mammalian Sel-10 homolog. *J Biol Chem* **276**, 35847-53.

Onoyama, I., Tsunematsu, R., Matsumoto, A., Kimura, T., de Alboran, I. M., Nakayama, K. and Nakayama, K. I. (2007). Conditional inactivation of Fbxw7 impairs cell-cycle exit during T cell differentiation and results in lymphomatogenesis. *J Exp Med* **204**, 2875-88.

Paillard, L., Legagneux, V. and Beverley Osborne, H. (2003). A functional deadenylation assay identifies human CUG-BP as a deadenylation factor. *Biol Cell* **95**, 107-13.

Paillard, L., Legagneux, V., Maniey, D. and Osborne, H. B. (2002). c-Jun ARE targets mRNA deadenylation by an EDEN-BP (embryo deadenylation element-binding protein)-dependent pathway. *J Biol Chem* **277**, 3232-5.

Paillard, L., Omilli, F., Legagneux, V., Bassez, T., Maniey, D. and Osborne, H. B. (1998). EDEN and EDEN-BP, a cis element and an associated factor that mediate sequence-specific mRNA deadenylation in Xenopus embryos. *EMBO J* **17**, 278-87.

Perry, M. M. (1968). Further studies on the development of the eye of Drosophila melanogaster. II: The inter-ommatidial bristles. *J. Morphol.* **124**, 249-262.

Philips, A. V., Timchenko, L. T. and Cooper, T. A. (1998). Disruption of splicing regulated by a CUG-binding protein in myotonic dystrophy. *Science* **280**, 737-41.

Ready, D. F., Hanson, T. E. and Benzer, S. (1976). Development of the Drosophila retina, a neurocrystalline lattice. *Dev Biol* **53**, 217-40.

Spruck, C. H., Strohmaier, H., Sangfelt, O., Muller, H. M., Hubalek, M., Muller-Holzner, E., Marth, C., Widschwendter, M. and Reed, S. I. (2002). hCDC4 gene mutations in endometrial cancer. *Cancer Res* **62**, 4535-9.

St John, M. A., Tao, W., Fei, X., Fukumoto, R., Carcangiu, M. L., Brownstein, D. G., Parlow, A. F., McGrath, J. and Xu, T. (1999). Mice deficient of Lats1 develop soft-tissue sarcomas, ovarian tumours and pituitary dysfunction. *Nat Genet* **21**, 182-6.

St Johnston, D. (2002). The art and design of genetic screens: Drosophila melanogaster. *Nat Rev Genet* **3**, 176-88.

Stofanko, M., Kwon, S. Y. and Badenhorst, P. (2008). A misexpression screen to identify regulators of Drosophila larval hemocyte development. *Genetics* **180**, 253-67.

Strohmaier, H., Spruck, C. H., Kaiser, P., Won, K. A., Sangfelt, O. and Reed, S. I. (2001). Human F-box protein hCdc4 targets cyclin E for proteolysis and is mutated in a breast cancer cell line. *Nature* **413**, 316-22.

Stuffers, S., Brech, A. and Stenmark, H. (2008). ESCRT proteins in physiology and disease. *Exp Cell Res*.

Sundaram, M. V. (2005). The love-hate relationship between Ras and Notch. *Genes Dev* **19**, 1825-39.

Takatsu, Y., Nakamura, M., Stapleton, M., Danos, M. C., Matsumoto, K., O'Connor, M. B., Shibuya, H. and Ueno, N. (2000). TAK1 participates in c-Jun N-terminal kinase signaling during Drosophila development. *Mol Cell Biol* **20**, 3015-26.

Tapon, N., Harvey, K. F., Bell, D. W., Wahrer, D. C. R., Schiripo, T. A., Haber, D. A. and Hariharan, I. K. (2002). salvador Promotes Both Cell Cycle Exit and Apoptosis in Drosophila and Is Mutated in Human Cancer Cell Lines. *Cell* **110**, 467-478.

Tapon, N., Ito, N., Dickson, B. J., Treisman, J. E. and Hariharan, I. K. (2001). The Drosophila tuberous sclerosis complex gene homologs restrict cell growth and cell proliferation. *Cell* **105**, 345-55.

Tien, A. C., Rajan, A. and Bellen, H. J. (2009). A Notch updated. *J Cell Biol* **184**, 621-9.

Timchenko, N. A., Iakova, P., Cai, Z. J., Smith, J. R. and Timchenko, L. T. (2001). Molecular basis for impaired muscle differentiation in myotonic dystrophy. *Mol Cell Biol* **21**, 6927-38.

Tomlinson, A. and Ready, D. F. (1987). Neuronal differentiation in the Drosophila ommatidium. *Devel. Biol.* **120**, 366-376.

Tseng, A. S., Tapon, N., Kanda, H., Cigizoglu, S., Edelmann, L., Pellock, B., White, K. and Hariharan, I. K. (2007). Capicua regulates cell proliferation downstream of the receptor tyrosine kinase/ras signaling pathway. *Curr Biol* **17**, 728-33.

Vaccari, T., Lu, H., Kanwar, R., Fortini, M. E. and Bilder, D. (2008). Endosomal entry regulates Notch receptor activation in Drosophila melanogaster. *J Cell Biol* **180**, 755-62.

Voas, M. G. and Rebay, I. (2004). Signal integration during development: insights from the Drosophila eye. *Dev Dyn* **229**, 162-75.

Wagner, E. F. and Nebreda, A. R. (2009). Signal integration by JNK and p38 MAPK pathways in cancer development. *Nat Rev Cancer* **9**, 537-49.

Wagner, K. U., Krempler, A., Qi, Y., Park, K., Henry, M. D., Triplett, A. A., Riedlinger, G., Rucker, I. E. and Hennighausen, L. (2003). Tsg101 is essential for cell growth, proliferation, and cell survival of embryonic and adult tissues. *Mol Cell Biol* **23**, 150-62.

Welcker, M. and Clurman, B. E. (2008). FBW7 ubiquitin ligase: a tumour suppressor at the crossroads of cell division, growth and differentiation. *Nat Rev Cancer* **8**, 83-93.

Welcker, M., Orian, A., Grim, J. A., Eisenman, R. N. and Clurman, B. E. (2004). A nucleolar isoform of the Fbw7 ubiquitin ligase regulates c-Myc and cell size. *Curr Biol* **14**, 1852-7.

Wolff, T. and Ready, D. F. (1991). The beginning of pattern formation in the Drosophila compound eye: the morphogenetic furrow and the second mitotic wave. *Development* **113**, 841-850.

Wolff, T. and Ready, D. F. (1993). Pattern formation in the *Drosophila* retina. In *The Development of Drosophila melanogaster*, vol. II (ed. M. Bate and A. Martinez Arias), pp. 1277-1325. Plainview, New York: Cold Spring Harbor Laboratory Press.

Wu, G., Lyapina, S., Das, I., Li, J., Gurney, M., Pauley, A., Chui, I., Deshaies, R. J. and Kitajewski, J. (2001). SEL-10 is an inhibitor of notch signaling that targets notch for ubiquitin-mediated protein degradation. *Mol Cell Biol* **21**, 7403-15.

Yan, R., Small, S., Desplan, C., Dearolf, C. R. and Darnell, J. E., Jr. (1996). Identification of a Stat gene that functions in Drosophila development. *Cell* **84**, 421-30.

Chapter II: The *gang of four* gene regulates growth and patterning of the developing *Drosophila* eye[1]

[1] Beam and Moberg, 2009; in review for publication at *Genetics*.

II.A. ABSTRACT

We report here the identification of a novel complementation group in the fruit fly *Drosophila melanogaster* named *gang of four* (*gfr*). Mutations in *gfr* disrupt patterns of cell differentiation in the eye and increase eye size through a proliferative mechanism that can be enhanced by a block in apoptosis. *gfr* mutant cells show several features of deregulated Ras/MAP kinase activity, including reduced expression of the Capicua growth suppressing transcription factor and synthetic lethality with alleles of the Jun N-terminal kinase phosphatase *puckered*. *gfr* alleles also upreguate Notch activity in the eye. Thus, *gfr* alleles appear to elicit growth and patterning phenotypes via effects on multiple signaling pathways. The *gfr* alleles behave as gain-of-function lesions and overexpress the gene, *bruno-3* (*bru-3*), which is located within the genomic region to which the *gfr* lesions map. Genetic reduction of *bru-3* suppresses phenotypes caused by *gfr* alleles, and like *gfr* alleles, overexpression of *bru-3* depresses levels of Cic protein, indicating that overexpression of *bru-3* is central to *gfr* mutant phenotypes.

II.B. INTRODUCTION

Genetic screens in the fruit fly *Drosophila melanogaster* have identified many genes that are required to restrict the growth (i.e., mass) of developing tissues (reviewed in Hariharan and Bilder, 2006; Pan, 2007). Some of these genes exclusively control the process of mass accumulation by changes in cell number or cell size. However, since a small number of signaling pathways are used reiteratively during metazoan development to control different processes, it is perhaps not surprising that others of these growth mutants exhibit more complex patterning phenotypes indicative of roles in multiple developmental pathways. Indeed, most developing *Drosophila* organs are patterned by a combination of signals from factors such as Hedgehog, Wingless, Notch, Decapentaplegic (Dpp), and Epidermal Growth Factor (EGF) (reviewed in Baker, 2007), yet it is also well established that mutations that affect these pathways can produce ectopic tissue growth in *Drosophila* (e.g., Dominguez and de Celis, 1998) and drive cancers in humans (reviewed in Edwards, 1999).

Here we report the isolation of a complementation group called *gang of four* (*gfr*) that displays effects on multiple cell biological processes, including tissue growth and retinal patterning. *gfr* alleles were identified in an *eyFLP;FRT* mosaic screen in the *Drosophila* eye for mutations that confer a clonal growth advantage relative to wild-type tissue (Harvey et al., 2003; Moberg et al., 2001; Tapon et al., 2002; Tapon et al., 2001; Tseng et al., 2007). The *gfr* gene also controls the overall size of the adult head and the specification of certain retinal cell types in the developing eye. Genetic and molecular data argue that this growth advantage arises by an increased rate of growth rather than a decrease in cell death and that the gene acts on Notch and JNK/ERK MAP kinase

(MAPK) signaling pathways—pathways that play dual roles in cell fate and cell proliferation control (reviewed in (Craig et al., 2008; Maillard and Pear, 2003; Wagner and Nebreda, 2009). *gfr* alleles interact very strongly with alleles of the JNK phosphatase *puckered* (*puc*), and *gfr* mutant cells show several features of deregulated ERK activity, including reduced expression of the Capicua (Cic) growth suppressor (Tseng et al., 2007). A subset of *gfr* growth and patterning phenotypes may thus arise due to a requirement for the gene as a MAPK regulator. Finally, although multiple alleles of the *gfr* locus were recovered in the original screen, these alleles do not appear to behave as simple recessive, loss-of-function lesions. Deletions spanning the region to which *gfr* alleles map fully complement *gfr* mutant chromosomes. *gfr* alleles also overexpress the *bruno-3* (*bru-3*) gene, which maps to the same genetic interval as the *gfr* lesions and encodes an RNA-binding protein that can bind to the EDEN translational repression sequence (Delaunay et al., 2004) and drive over-proliferation of cells in the hemocyte lineage (Stofanko et al., 2008). Genetic reduction of *bru-3* suppresses phenotypes caused by *gfr* alleles, and like *gfr* alleles, overexpression of *bru-3* depresses levels of Cic protein. In sum, these data suggest that *gfr* alleles behave as gain-of-function lesions and that overexpression of *bru-3* is central to *gfr* mutant phenotypes.

II.C. RESULTS

II.C1. Isolation of the *gang of four* complementation group

To identify genes that regulate cell growth or cell number during development of the *Drosophila melanogaster* eye, the *eyFLP;FRT* system of mitotic recombination was used to screen for mutations that allow homozygous mutant cells to overgrow relative to their wild-type neighbors (e.g., Harvey et al., 2003; Moberg et al., 2001; Tapon et al., 2002; Tapon et al., 2001; Tseng et al., 2007). Flies whose eyes were composed of more mutant than wild-type tissue were retained and placed into complementation groups. In addition to alleles of genes such as *Tsc1*, *salvador*, and *hippo*, clones of which result in overgrowth of the entire eye (reviewed in Hariharan and Bilder, 2006), mutations in genes such as *archipelago* and *capicua*, which produce clonal overgrowth without overt organ hyperplasia, were also identified (Moberg et al., 2001; Tseng et al., 2007). Four mutations of the latter type were found to represent a single complementation group that was named *gang of four* (*gfr*). A fifth allele, gfr^{x}, was independently isolated by its ability to synergize with a block in cell death to produce clonal overgrowth (K.H. Moberg and M.M. Gilbert, unpublished; see below). Each allele is recessive lethal over itself and *in trans* to other *gfr* alleles; some *gfr/gfr* animals die as L1 larvae, indicating that the *gfr* alleles lead to late embryonic/early larval death.

II.C2. Mapping of the *gfr* locus[2]

The genetic configuration of the original *eyFLP;FRT* screen indicates that the *gfr* locus is located on the left arm of chromosome 3. Deficienty mapping with the 3L Bloomington kit, plus additional Exelixis and DrosDel deficiencies that spanned some gaps in coverage, failed to identify a deficiency that uncovers the lethality associated with the *gfr* alleles. We therefore hypothesized that because the *gfr* alleles behave as recessive lethals, then the lesions must lie within a chromosomal region not yet covered by the many deficiencies tested. Close examination of the deficiency maps indeed revealed several remaining gaps in coverage (red arrows, Figure II.1). Consequently, we employed alternative approaches to map the *gfr* lesions. In each mapping scheme, we verified the presence of the *gfr* mutation by complementation with an independent allele to avoid mapping errors due to second-site mutations.

To narrow down the putative gap in deficiency coverage containing *gfr*, our first approach was to choose two dominant markers that divided chromosome arm 3L into thirds and to create a genetic map with respect to these markers. Meiotic mapping was performed between gfr^3 and the dominant markers *Roughened* (*R*; located at 62B7, 1.86 Mb; FlyBase) and *Lyra* (*Ly*; located at 70A8, 13.39 Mb; FlyBase) (Figure II.1). Multiple gfr^3,*R* chromosomes were recovered from a pool of potential recombinants; however, no gfr^3,*Ly* chromosomes were recovered in over 50 chromosomes scored, indicating that *gfr* maps proximal to *R* and is closely linked to *Ly*, a gain-of-function allele of *sens* (Nolo et al., 2000). All five *gfr* alleles complement a large deficiency that removes the *Ly* region,

---

[2] This mapping section was added for the purposes of the dissertation and was not included in the submitted manuscript.

Df(3L)ED4502 (13.2-13.95 Mb), and also complement several loss-of-function alleles of *sens*. Notably, a gap in deficiency coverage is close to the *Ly* region; this gap is between 69E2 and 70A2 (13.0-13.2 Mb), spans approximately 200 kb, and contains about 30 predicted genes. Therefore, lethal alleles in this region were tested for complementation with *gfr* alleles; however, none failed to complement, prompting additional rounds of mapping in the region.

Meiotic recombination mapping with molecularly defined *P*-element insertions densely located within the previously mentioned gap in deficiency coverage (69E2-70A2), in addition to other *P* elements located along the length of chromosome 3L, was performed in accordance with the crossing scheme previously described by Zhai *et al.* 2003 (Figure II.2; Zhai et al., 2003). Briefly, gfr^1 was crossed individually to several w^+-marked *P*-element insertion strains. gfr^1/P F_1 females were crossed to males heterozygous for another *gfr* allele and a *hs-hid* balancer (Moore et al., 1998). This cross was heat-shocked at 37°C for 1.5 hour 5 days after setting up the cross to kill off progeny carrying the balancer. Surviving F_2 progeny were scored for eye color: red-eyed progeny are gfr^2/P nonrecombinants, and white-eyed progeny are the result of recombination between gfr^1 and the *P* insertion. The percentage of white-eyed flies in the F_2 progeny represents the recombination distance in cM between the gfr^1 lesion and the *P* insertion. By this method, gfr^1 is most tightly linked to two *P* elements flanking *Ly*: *KG01069* (located at 70A4, 13.23 Mb; FlyBase) and *BG00690* (located at 70A8, 13.48 Mb; Figure II.3 and Table II.3I.1). After scoring approximately 4500 recombinant chromosomes from P/gfr^1 females, we mapped the lethality of gfr^1 to 0.39 cM (18 recombinants; 4593 scored) from *KG01069* and 0.82 cM (36 recombinants; 4412 scored) from *BG00690* (see Table II.1).

This mapping strategy confirmed the original hypothesis that the *gfr* lesions are closely linked to the chromosomal region containing *Ly*; however, it does not reveal whether they lay proximal or distal to these transposon insertion sites.

To address this question of directionality, we next used site-specific male-recombination mapping as previously described by Chen et al. 1998 (Figure II.4; Chen et al., 1998). To map a mutation using *P*-element-induced male recombination, two visible markers flanking the selected mapping *P* elements are first put *in cis* to your mutation of interest. In this case, *R* and *Stubble* (*Sb*; located on 3R) were recombined onto a chromosome with a *gfr* mutation. This *R,gfr*^{3}*,Sb* chromosome was then put *in trans* to a chromosome containing the mapping *P* element in male flies; a transposase source (*Delta2-3*) is also provided on another chromosome. A male-recombination event at the location of the *P* element results in the cosegration of the *gfr* mutation with either *R* or *Sb*, depending on the relative position of the *gfr* lesion and the chosen *P* element. For example, if *gfr* lethality cosegregates with *R*, it can be inferred that the *gfr* lesion is distal to the chosen *P*; however, if *gfr* lethality cosegregates with *Sb*, *gfr* is proximal to the indicated *P*. We only inferred a location relative to each *P* element if recombinants of both classes (*R* and *Sb*) were recovered and scored for complementation against another *gfr* allele. By this technique, *gfr*^{3} lethality maps proximal to both *KG01069* and *BG00690* (Table II.2). These recombination data are in conflict with the meiotic recombination genetic map created with the two *P* insertions relative to the *gfr*^{1} allele. Indeed, after collecting male-recombination data for additional *P* insertions, *gfr*^{3} was found to map proximal to the *P* elements *EY08487* and *l(3)05871*, which are located at 70C2 (13.65 Mb; Table II.2). The single *Sb* recombinant isolated for *EY21145* suggests that *gfr*^{3} may

even be located proximal to 13.86 Mb (see Table II.2). Attempts at using this male *P*-mapping strategy for the gfr^{1} allele were not successful. Collectively, gfr^{3} appears to map rather proximal to the genetic map created for gfr^{1} (see above). Because gfr^{3} behaves differently from alleles *1*, *2*, and *x* in several molecular assays (data not shown), this allele will not be considered in further analyses.

In sum, extensive meiotic mapping places the lethality associated with gfr^{1} closely linked to a fairly small genomic interval at 70A-B. Though all *gfr* alleles are lethal *in trans* to each other, they are viable with no obvious defects *in trans* to the molecularly defined *Df(3L)ED4502* (13.2-13.95 Mb), which spans the putative *gfr* region on 3L, and are also viable *in trans* to all available lethal alleles in this region. As *Df(3L)ED4502* fails to complement all other tested lethal alleles in the region (data not shown), the lack of an interaction between *Df(3L)ED4502* and the *gfr* alleles is not likely due to incomplete coverage of the region but instead to a failure of *gfr* alleles to behave as simple recessive, loss-of-function lesions (see below).

Figure II.1. Gaps in coverage of the 3L Bloomington deficiency kit.

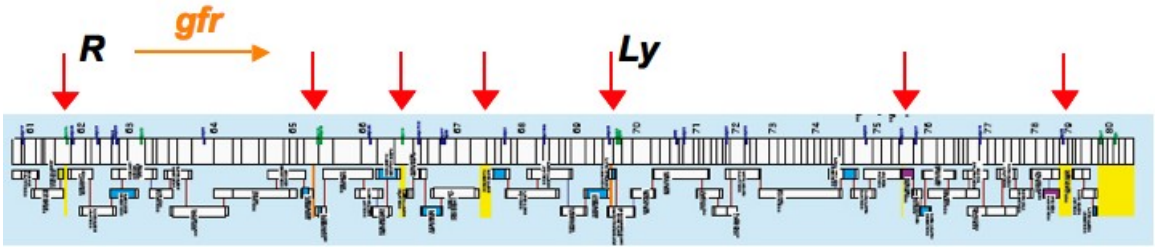

Schematic of the 3L Bloomington deficiency kit; gaps in coverage are highlighted in yellow and identified with red arrows. Meiotic recombination mapping with two dominant markers, *R* and *Ly* (their relative chromosomal locations shown), indicated that the *gfr* locus was proximal to *R* (illustrated in orange) and closely linked to *Ly* (see text). (Adapted from http://flystocks.bio.indiana.edu/)

Figure II.2. Strategy for *P*-element meiotic recombination mapping.

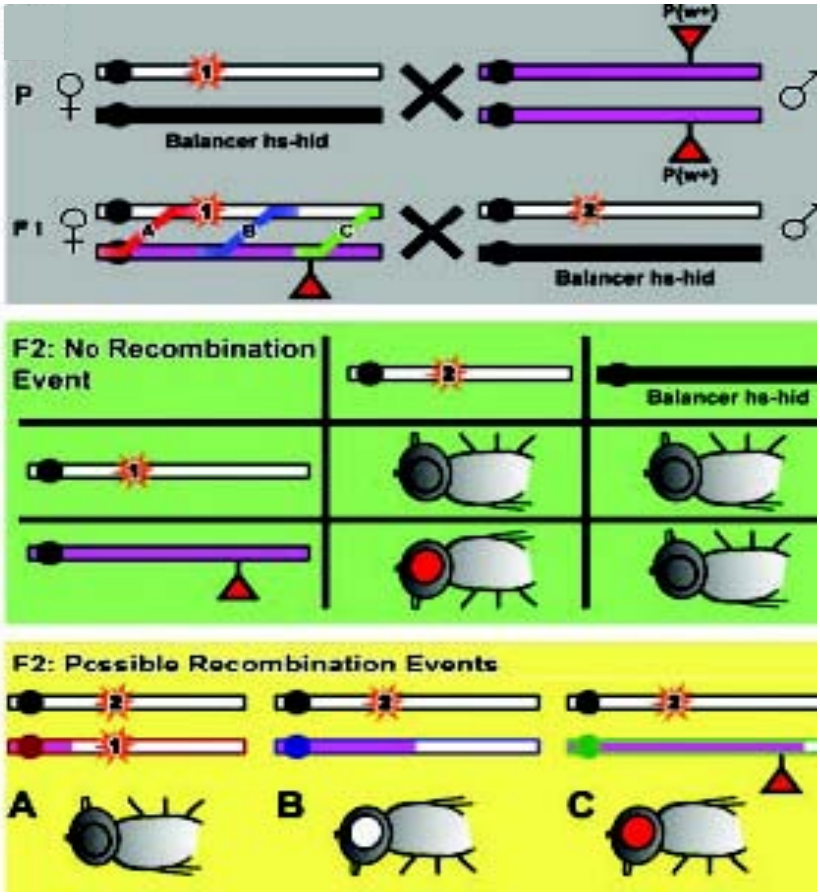

Crossing scheme of *P*-element mapping. Mutant chromosomes indicated by open bars, *P* element-containing chromoromes are in purple, and balancer chromosomes are in black. The mutation sites (red stars) are marked with either 1 or 2 to indicate the different alleles; location of *P* insertion indicated by red triangle. Note that all flies are in a w^- background, meaning the *P* elements are the only source of w^+. Shown in the gray box are *P* and F_1 crosses. Shown in the green box are the nonrecombinant offspring. Shown in the yellow box are the possible recombination events, which are color coded and labeled A, B, and C, corresponding to the F_1 female (in gray box) where the three types of recombination events are marked accordingly (see text). (Courtesy of Zhai et al., 2003)

Figure II.3. Summary of *P*-element mapping results for *gfr*^{1}.

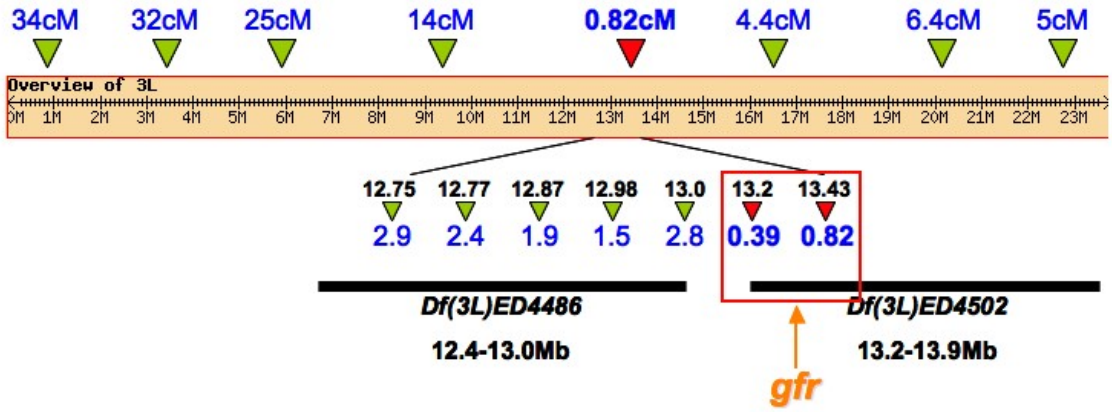

Illustration of mapping results for *P*-element meiotic recombination mapping. Molecular scale of chromosomal 3L shown in tan box. Triangles represent *P*-element insertions used for mapping. Molecular chromosomal locations (in megabases, Mb) of *P* elements and deficiencies (black bars) shown with black numbers; calculated genetic distance (in centimorgans, cM) between individual *P* elements and *gfr* shown with blue numbers. Predicted location of *gfr* locus indiated in orange (see text and Table II.1).

Table II.1. Summary of *P*-element mapping results for *gfr*^{1}.

P-element	Molecular Position (Mb)	# Recom-binants	Total Scored	Recombination Distance (cM)
KG02776	0.085	548	1589	34.49
KG09489	3.441	383	1170	32.74
KG00023	5.935	256	991	25.83
KG02042	9.260	167	1167	14.31
EY07351	12.752	178	6203	2.87
EY04154	12.772	167	7047	2.37
KG00330	12.871	55	2932	1.88
EY01866	12.982	71	4804	1.48
KG07481	13.017	179	6300	2.84
KG01069	13.237	18	4593	0.39
BG00690	13.486	36	4412	0.82
BG01582	16.400	124	2844	4.36
BG02493	20.148	79	1239	6.38
BG01780	22.755	50	1002	4.99

Information regarding meiotic recombination events between *gfr*^{1} and each indicated *P* element. Recombination distance (cM) = (# Recombinants / Total Scored) x 100.

Figure II.4. *P* element-mediated male recombination mapping.

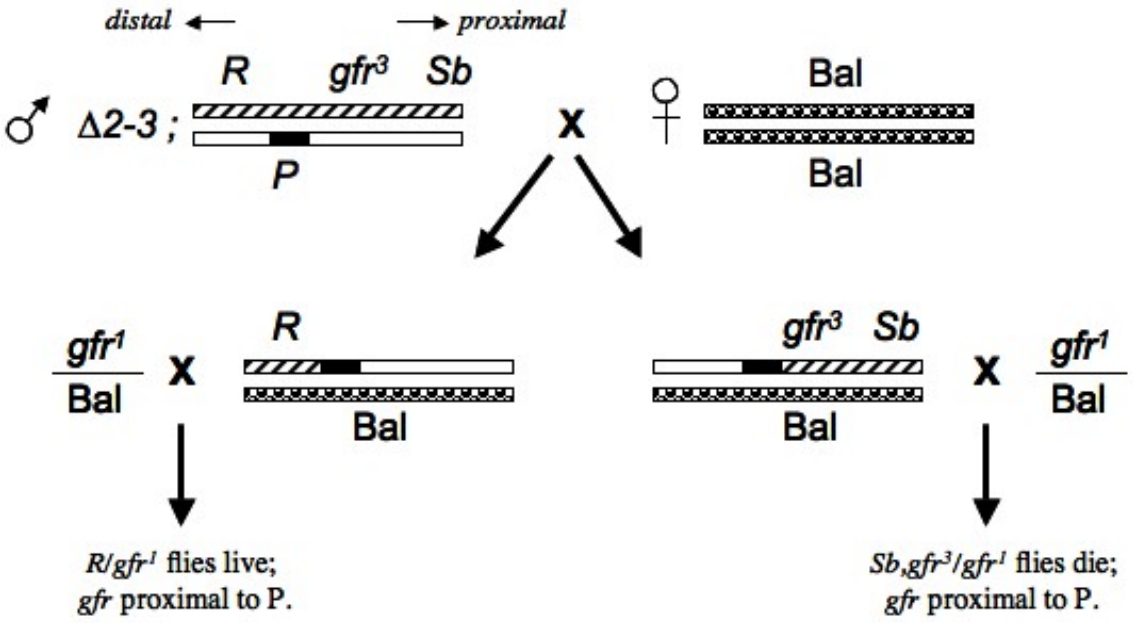

Crossing scheme for *P* element-mediated male recombination mapping. *P* element-containing chromosomes indicated by open bars, mutant chromosomes marked by striped bars, and balancer chromosomes are patterned bars. As showns, a *gfr* allele is placed *in cis* to two dominant markers, *R* and *Sb*, and *in trans* to a *P*. In the presence of *Delta2-3* (Δ*2-3*) transposase, recombination events are induced at the ends of the *P* element in male flies. In the next generation, most flies are of the parental phenotype; recombinants are identified by the presence of only *R* or *Sb*. Each recombinant is tested for complementation against another *gfr* allele. In this example, gfr^3 maps proximal to the location of the *P*-element insertion (black rectangle) because its lethality cosegregates with *Sb* (see text). (Adapted from Chen et al., 1998)

Table II.2. Summary of male *P* mapping for *gfr*^{3}.

P-element	Molecular Position (Mb)	# Recombinants; C/FTC/U				Total Scored	Interpretation: proximal/distal?
		R		Sb			
		Male	Female	Male	Female		
KG01069	13.27	1; C	1; U	1; 1 FTC	0; U	3427	proximal
KG04150	13.44	1; C	0; U	2; 2 FTC	0; U	2423	proximal
stv[00543]	13.47	1; C	0; U	4; 3 FTC, 1 U	3; U	3363	proximal
BG01691	13.54	0; U	1; U	3; 2 FTC, 1 U	1; U	2070	
l(3)05871	13.65	1; C	0; U	1; 1 FTC	2; U	1323	proximal
EY08487	13.65	0; U	0; U	5; 4 FTC, 1 U	6; U	2643	
EY21145	13.86	0; U	0; U	1; 1 FTC	2; U	2329	

Information regarding *P* element-induced male recombination events between *gfr*^{3} and each indicated *P*. Interpretation of *gfr* location relative to each *P* insertion site is indicated only when recombinants of both classes were scored for complementation against another *gfr* allele. R, *Roughened*; Sb, *Stubble*; C, complement; FTC, failure to complement; U, undetermined.

II.C3. *gfr* alleles regulate growth in the developing eye

Adult *gfr* mosaic eyes generated using the *eyFLP;FRT* technique show increased representation of *gfr* mutant tissue (white) over control tissue (red) (Figure II.5A-B), and ommatidia within these clones can contain either multiplication or loss of interommatidial bristles (Figure II.5C). To examine how *gfr* mutations might increase clonal growth in the eye, patterns of expression of the major mitotic cyclins, Cyclin A, B, E and D, were analyzed in *gfr* mosaic larval eye discs. Compared with surrounding wild-type tissue, levels of the mitotic regulator Cyclin A are increased in *gfr* clones in the asynchronously dividing cells anterior to the morphogenetic furrow (MF); Cyclin A also perdures past the point of wild-type expression in mutant clones posterior to the MF (Figure II.6A-A", B-B"; yellow arrows denote examples of elevated CycA in *gfr* clones). A similar, although more mild, version of this effect is observed with Cyclin B (Figure II.6C-C"). Expression of the S-phase inducer Cyclin E is elevated in *gfr* clones within the MF and also perdures just posterior to the MF; clones anterior to the MF contain a higher density of Cyclin E-positive cells compared with surrounding wild-type tissue (Figure II.6D-D"). Patterns of Cyclin D were not substantially altered in *gfr* clones (data not shown). Compared with the parental chromosome (Figure II.7A,D), *gfr* mutant clones show relatively normal patterns of S-phase as visualized by BrdU incorporation in the larval and 24-hour pupal eye (Figure II.7B-B', C-C") and of mitosis as assessed by staining with anti-phospho-Histone H3 (Figure II.7E-E'). Thus, despite their effects on cyclin expression, *gfr* alleles have relatively little effect on patterns of division and mitosis. This is confirmed by flow cytometric data showing that the size and cell cycle phasing of *gfr* mutant cells are very similar to that of wild-type cells at this stage (data

not shown). Because Cyclin expression is most strongly elevated anterior to the MF and we see no dramatic effects on BrdU and phospho-H3, it is likely that *gfr* mutations increase cell proliferation among the already randomly dividing cells prior to furrow progression.

Figure II.5. *gfr* mutations confer a clonal growth advantage in the adult eye.

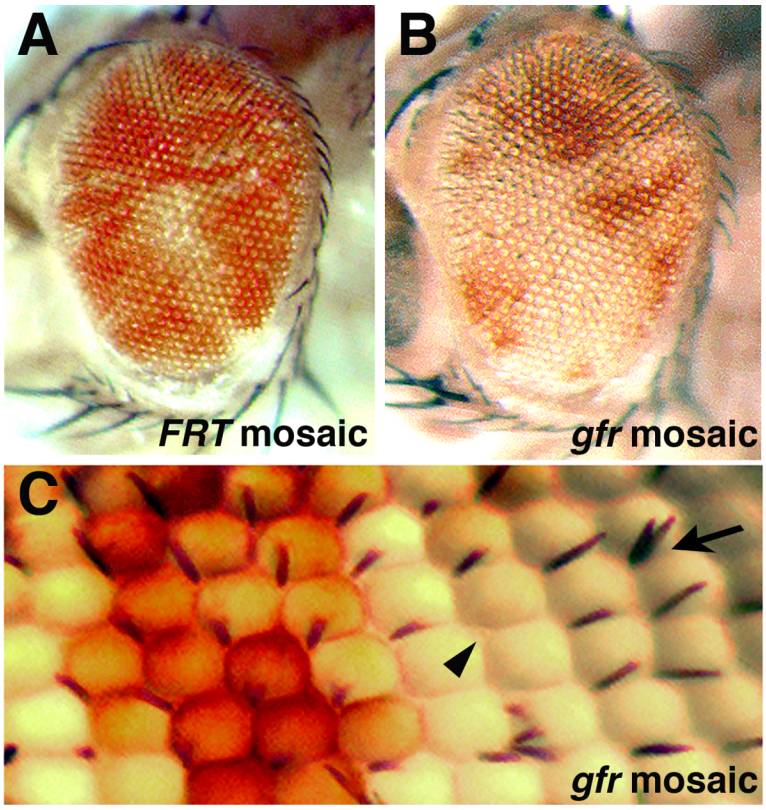

Light microscopic images of adult eyes mosaic for the parental *FRT* chromosome (A) or *gfr* (B). Red pigment marks wild-type cells; white tissue is homozygous for *FRT* (A) or *gfr* (B, C). Note that the *gfr* mosaic eye has a greater white:red ratio compared with the *FRT* mosaic eye. (C) Zoomed image of *gfr* clone to show loss (arrow) and multiplication (arrowhead) of interommatidial bristles.

Figure II.6. *gfr* mutant tissue has increased levels of Cyclins A, B, and E.

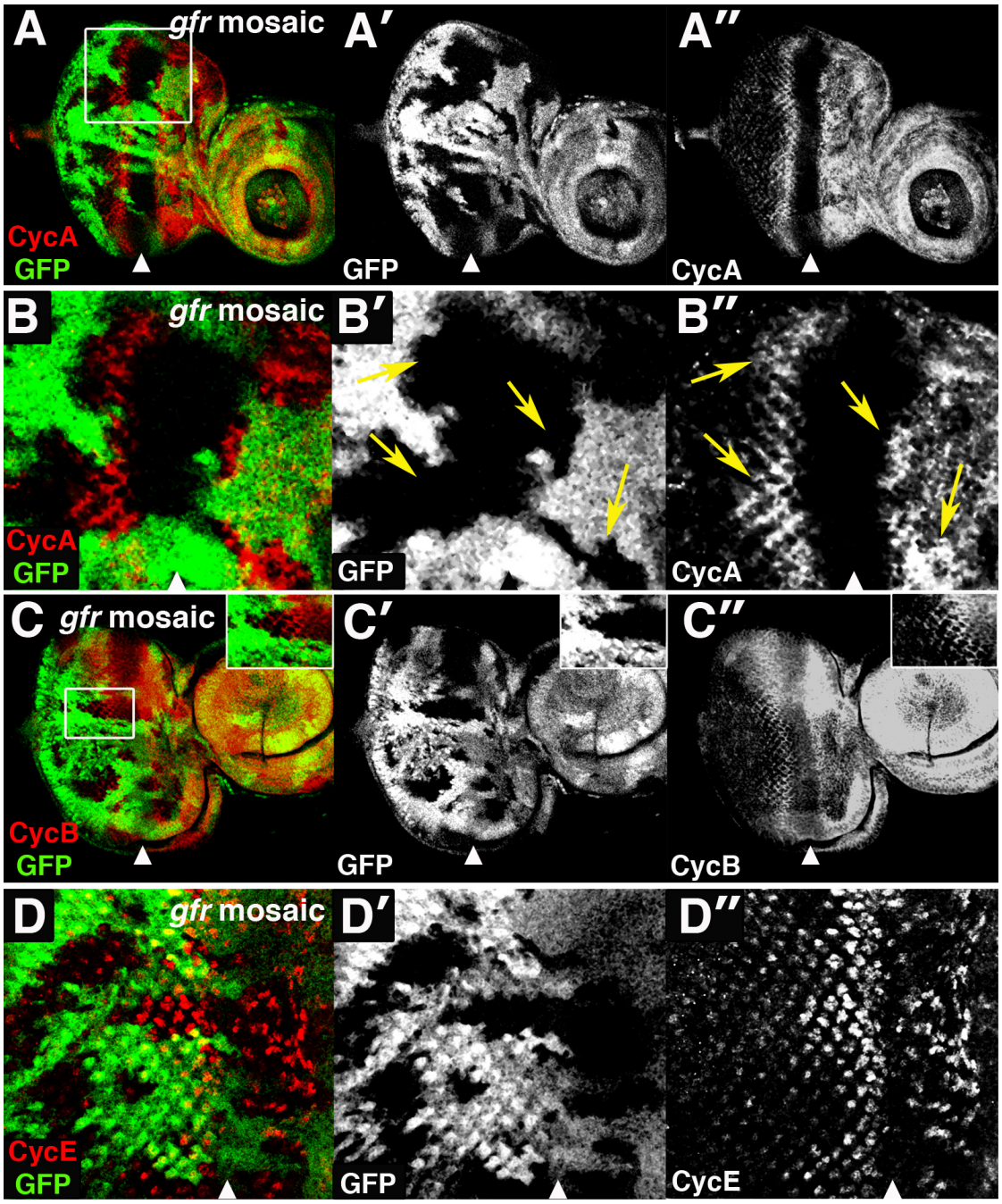

Merged confocal sections of *gfr*^{1} clones marked by the absence of GFP (green) and stained for Cyclin A (A-A", B-B"), Cyclin B (C-C"), or Cyclin E (D-D") in red. (A-A", B-B") Cyclin A is strongly increased in *gfr* clones anterior to the MF and trails in clones posterior to the MF. B-B" is zoom of boxed area in A. (C-C") Cyclin B is mildly increased in clones just posterior to the MF; inset is zoom of boxed area in C. (D-D") Zoomed confocal image showing trailing Cyclin E expression in *gfr* clones posterior to the MF and an increased density of Cyclin E-positive cells anterior to the MF. Arrowheads mark position of the MF. In this an all following images, posterior is to the left.

Figure II.7. Patterns of cell division and mitosis are largely unaltered in *gfr* cells.

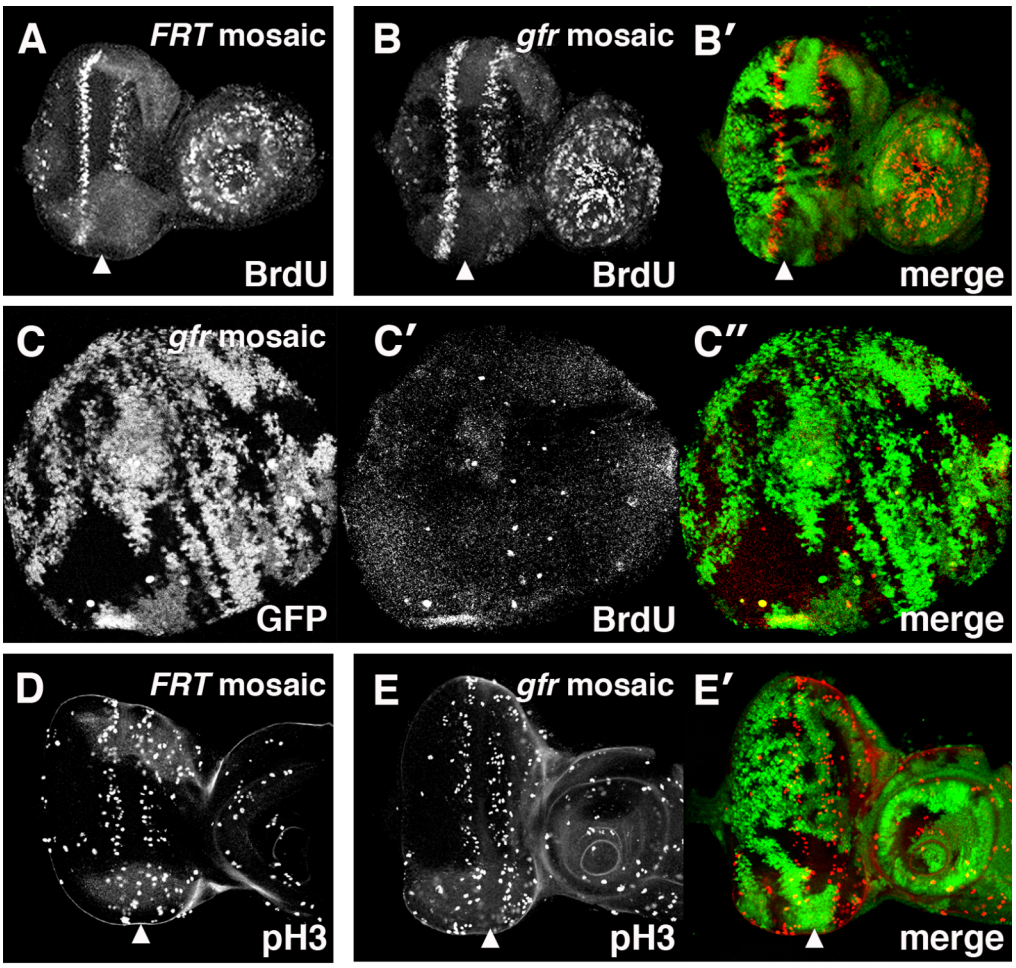

(A) Wild-type pattern of BrdU (white) in third instar eye disc mosaic for the parental *FRT* chromosome (clonal boundaries not shown). BrdU (red) incorporation to mark S-phase cells in third instar larval eye discs (B-B') and 24-hour pupal eye discs (C-C") mosaic for *gfr* mutant cells marked by the absence of GFP (green). (D) Wild-type pattern of phospho-Histone H3 (white) in third instar eye disc mosaic for the parental *FRT* chromosome (clonal boundaries not shown). (E-E') phospho-Histone H3 (red) staining to mark mitoses in third instar larval eye disc mosaic for *gfr* mutant cells marked by the absence of GFP (green). Arrowheads indicate position of the MF.

II.C4. *gfr* alleles affect patterining of the developing eye

The adult bristle defects in *gfr* mutant eye clones indicate that *gfr* mutations affect the generation or survival of cells that make up the mature bristle complex. The four cells of the mature bristle complex are clonally derived from a single precursor and are specified by a Notch-dependent process during early pupal development (reviewed in Doroquez and Rebay, 2006). Analysis of Senseless, which marks sensory organ precursor cells (Frankfort et al., 2001), at 24 hours after pupariation formation (APF) and BarH1, which marks primary pigment cells and a subset of bristle cells (Higashijima et al., 1992), at 48 hours APF, shows a disruption of the normal organization of bristle complexes in *gfr* clones: in wild-type tissue, bristle precursors are arranged into an linear array, whereas in *gfr* mutant tissue, this pattern is disrupted by changes in both the number and location of Sens- and BarH1-positive cells (Figure II.8A-A", B-B"). Visualizing cell outlines in the mid-pupal eye with anti-Discs large (Dlg) reveals that the bristle complexes and tertiary pigment cells are no longer located at alternating vertices, and the hexagonal lattice created by secondary pigment cells is disrupted (Figure II.8B-B'). Visualizing BarH1 more apically also reveals a disruption in both ommatidial rotation and the number of primary pigment cells: in wild-type tissue, primary pigment cells are found at the top and bottom of each ommatidium creating a linear pattern over the disc, whereas the primary pigment cells in *gfr* mutant ommatidia are often missing or in inappropriate locations around the ommatidium (Figure II.8C, C"). Moreover, many of the *gfr* mutant ommatidia have fewer than the wild-type complement of four cone cells. (Figure II.8C, C').

The absence of cone cells in *gfr* clones could be an indirect consequence of the apoptotic cell death of properly specified cell types or a more direct effect of *gfr*

mutations on the specification or recruitment of these cells into the retina. To distinguish between these two possibilities, cell outlines and bristle cell complexes were visualized in *gfr* mutant clones 48 hours APF in a background in which cell death is blocked by simultaneous loss of the *Df(3L)H99* genomic deletion, which removes the pro-apoptotic genes *rpr*, *grm* and *hid* (White et al., 1994). If *gfr* mutations lead to the death of properly specified cells, then the cell fate and patterning defects observed in *gfr* clones should be rescued in *gfr,H99* double mutant clones. However, blocking cell death did not rescue the reduced number of cone cells or the disrupted ommatidial patterning in *gfr* clones (Figure II.8D-D'). The *H99* deficiency also does not rescue bristle complex number or organization as visualized by anti-BarH1 staining (Figure II.8D"). Similar data were obtained using the *UAS-p35* transgene to block cell death (data not shown). Thus, mutations in *gfr* alter cell number and patterning in the developing eye by a cell death-independent mechanism.

Figure II.8. Patterning of the pupal retina is disrupted in *gfr* clones.

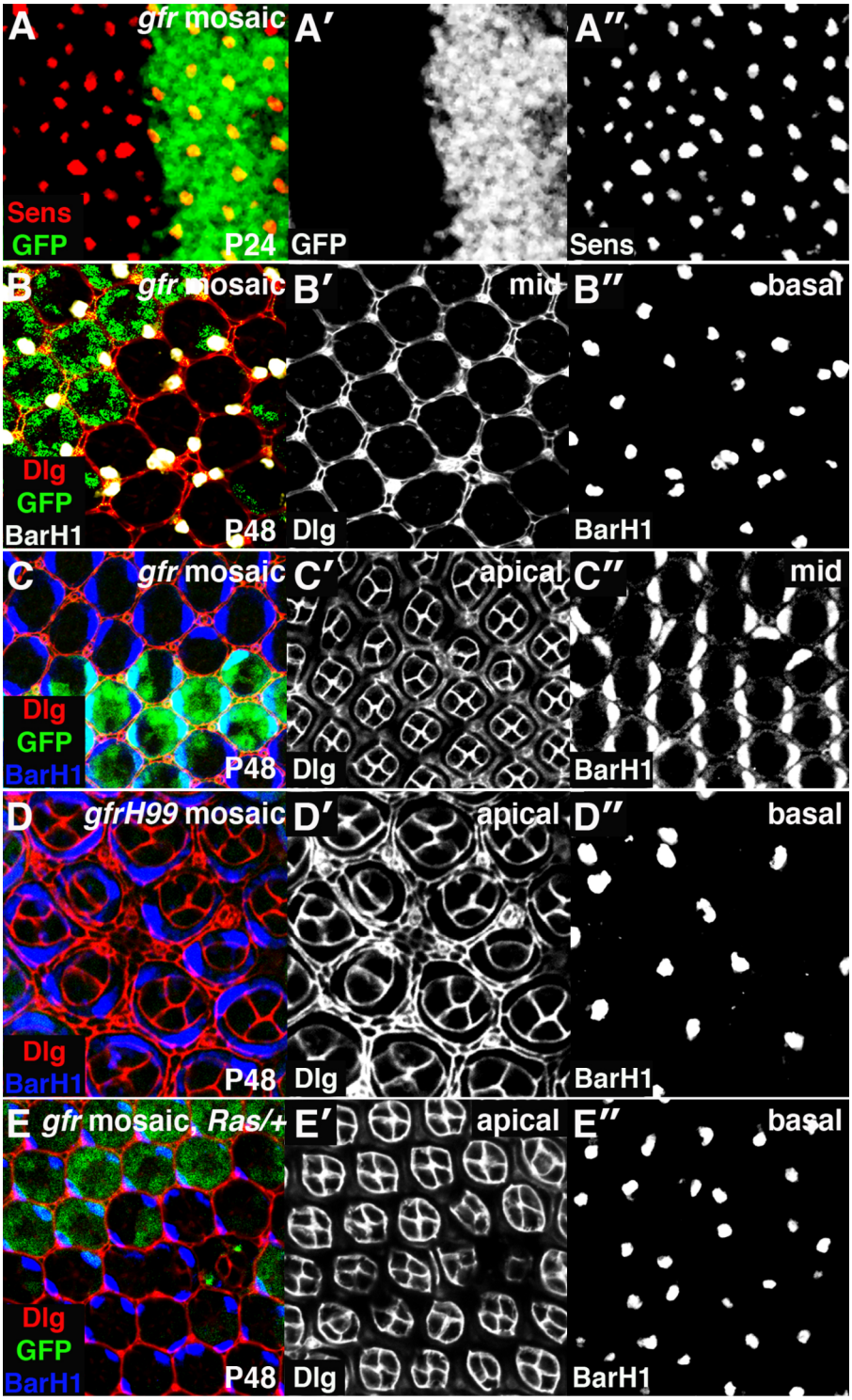

(A-C") Merged confocal sections of *gfr*^{1} clones marked by the absence of GFP (green). (A-A") 24-hour mosaic pupal eye disc stained for Sensless (red). (B-B") 48-hour mosaic pupal eye disc stained for Dlg (red; cell outlines) and BarH1 (white; bristle cells). Note disrupted ommatidial lattice in *gfr* clone in B' and bristle loss and multiplication in B". (C-C") 48-hour mosaic pupal eye disc stained with Dlg (red; cell outlines in C, cone cells in C') and BarH1 (blue; primary pigment cells). Note decreased cone cell number in C'; disrupted ommatidial rotation and primary pigment cell number in C". (D-D") Dlg (red; cell outlines and cone cells) and BarH1 (blue; primary pigment cells in D, bristle cells in D") stainings in *gfr*^{x}*H99* 48-hour pupal eye disc clone. (E-E") Dlg (red; cell outlines in E and cone cells in E') and BarH1 (blue; primary pigment cells in E, bristle cells in E") stainings in *gfr*^{1}*,FRT80B/FRT80B,ubiGFP:Ras85D*^{e2f}/+ 48-hour pupal eye disc. Note that the same patterning defects observed in *gfr* mid-pupal eye clones (B-C") are still present when cell death is blocked (D-D") or *Ras85D* dosage is decreased (E-E"). Each row represents one field of view; apical, mid, and basal denote the plane of the confocal section within each field of view.

II.C5. *gfr* mutations confer a proliferative advantage and synergize with a block in cell death

Based on forward scatter profiles of *gfr* cells in larval eye discs (data not shown) and the relative size of Dlg-positive apical profiles in *gfr* and control areas of pupal eye discs (e.g. Fig 3B', 3C'), *gfr* mutant cells are not significantly different in size from normal cells. The apparent growth advantage conferred by the *gfr* alleles might therefore result from increased cell proliferation, decreased cell death, or a combination of these processes. To test in more detail if *gfr* alleles affect these processes, we first determined whether loss of *gfr* could alter organ size. This was accomplished by using the *eyFLP;FRT* system in combination with the cell-lethal *Minute* (*M*) mutation $RpL14^{1}$ (Saeboe-Larssen et al., 1997) to generate eyes and head cuticle composed almost entirely of *gfr* mutant tissue (e.g, as in Nicholson et al., 2009). The heads of *gfr/M(3)* adult female flies are consistently larger than control *FRT80B/M(3)* heads generated from the *FRT80B* parental chromosome (Figure II.9A-B); simultaneously making the head mutant for *gfr* and blocking death with *Df(3L)H99* promotes an even greater organ overgrowth (Figure II.9C). Quantification of the *en face* two-dimensional eye area normalized to an invariant body metric (size of wing compartment bounded by L3 and L4 veins and posterior cross-vein) showed that homozygosity for the gfr^{1}, gfr^{2} or gfr^{x} alleles led to a statistically significant increase in eye size of approximately 10% relative to *FRT80B* (gfr^{1}=0.45 ± 0.01, gfr^{2}=0.43 ± 0.01, gfr^{x}=0.43 ± 0.01 vs *FRT80B*=0.39 ± 0.01; $P<0.001$; Figure II.10F). Combining a *gfr* allele with the *H99* deletion indeed produced an increase in adult eye size: gfr^{X}*,H99/M(3)* eyes are an additional 9% larger than gfr^{x}*/M(3)* eyes (0.47 ± 0.02 vs. 0.43 ± 0.01, respectively; $P<0.001$; Figure II.10B, C, G) and 15% larger than

H99/M(3) control eyes (*P<0.001*; Figure II.10F). This synergistic effect between *gfr* and a block in cell death suggests that a proliferative mechanism underlies the growth advantage of *gfr* mutant cells. Likewise, *gfr* alleles have no effect on rates of developmental cell death in larval or pupal eye discs (data not shown). Thus, the data collectively support the hypothesis that *gfr* alleles promote growth and differentiation phenotypes via a primarily proliferative mechanism.

Figure II.9. Mutations in *gfr* increase organ size and synergize with a block in cell death.

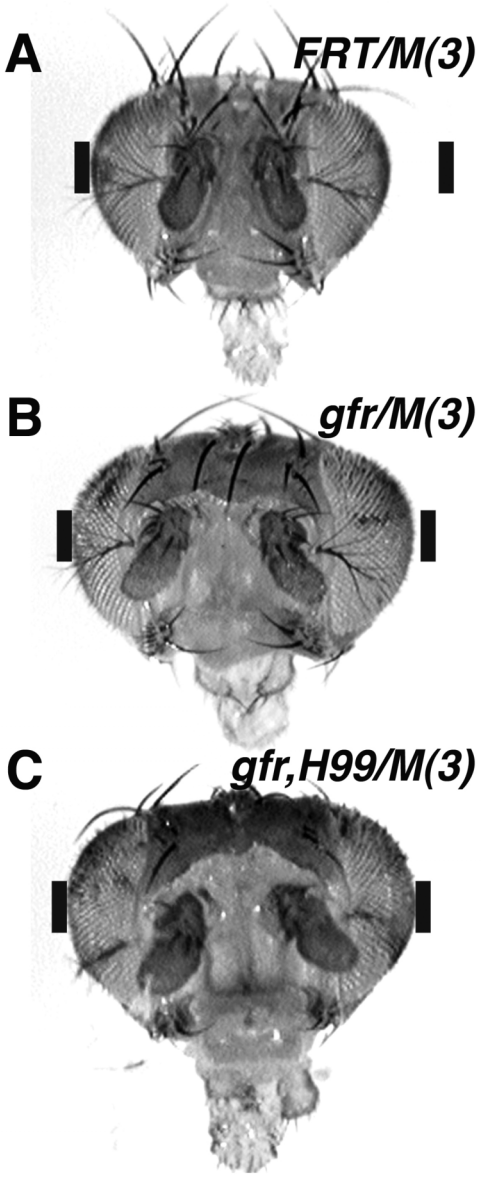

Composite image of (A) *FRT80B/M(3)*, (B) *gfr^{x}/M(3)*, and (C) *gfr^{x}Df(3L)H99/M(3)* adult female heads. Black brackets in panels A-C are standardized to the width of the *gfr^{x}Df(3L)H99/M(3)* head in panel C in order to show additive effects of the *gfr* and *Df(3L)H99* mutations on head size.

Figure II.10. Modification of *gfr* eye size by growth regulators and signaling components.

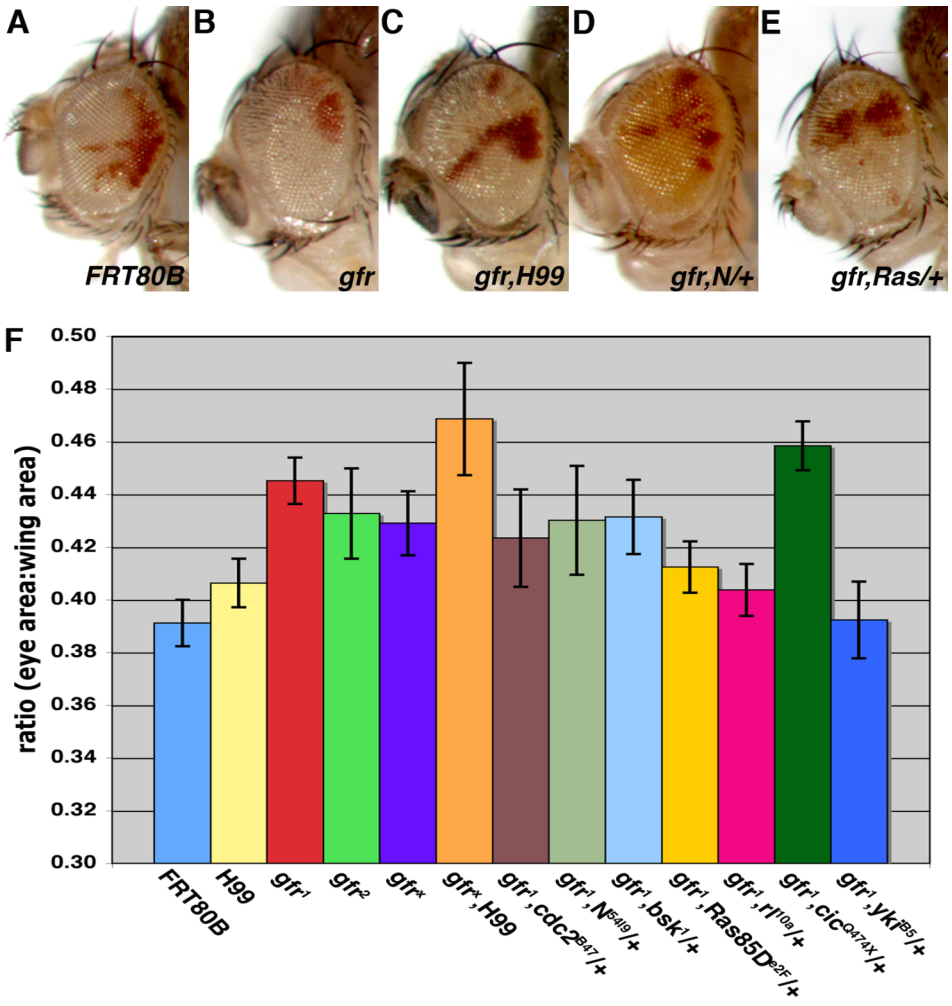

Light microscopic images of (A) *FRT80B/M(3)*, (B) $gfr^{1}/M(3)$, (C) $gfr^{x}Df(3L)H99/M(3)$, (D) $N^{54/9}/+;gfr^{1}/M(3)$, and (E) $gfr^{1},FRT80B:Ras85D^{e2f}/M(3)$ adult female eyes. Note the eyes in B-D are larger than A; the eye in E is comparable in size to A. (F) Graphic summary of the effect of the indicated genotypes on *en face* adult female eye size. In each case, eye area was normalized wing area between the L3,L4, and PCV veins of the same fly; average eye area:wing area ratios are plotted. n ≥ 10 for each genotype. Error bars represent 95% confidence intervals.

II.C6. *gfr* alleles have Notch gain-of function phenotypes

To assess the tissue specificity of the *gfr* overgrowth phenotype, we utilized the cell lethal technique in conjunction with the pan wing FLPase transgene *Ubx>Flp* to generate wings composed almost entirely of *gfr* mutant cells. As previously described, this technique uses the *RpL14^{1} Minute (M)* mutation (Saeboe-Larssen et al., 1997) to eliminate *M/M* cells and allow *gfr/gfr* cells to populate the wing disc and adult structures derived from it. *gfr^{1}/M(3)* wings display patterning defects—most notably, the L5 vein does not reach the margin (~70% penetrance, n=10; compare Figure II.11A & 6B)—but unlike *gfr/M(3)* eyes, they are consistently smaller along the proximal-distal axis relative to *FRT80B/M(3)* wings (Figure II.11C, quantification in Figure II.12). The effect of *gfr* alleles on organ size is thus tissue-specific.

The interrupted vein phenotype in *gfr/M(3)* wings resembles wing-vein phenotypes associated with *Abruptex* (*Ax*) alleles, which contain gain-of-function mutations in the extracellular domain of *Notch* that alter its substrate specificity (de Celis and Garcia-Bellido, 1994). To determine if *gfr* and *Notch* interact genetically in wing development, *gfr* alleles were tested for their ability to dominantly modify the characteristic *Notch* loss-of-function wing notching phenotype (Figure II.11E; and as in Dexter, 1914). Compared to the *FRT80B* control, *gfr* alleles dominantly suppress wing notching in *N^{54l9}*/+ adult female flies (*P<0.001*; Figure II.11D-G), suggesting that *gfr* alleles promote *Notch* signaling in the developing wing pouch. In keeping with a focus on the ability of *gfr* to affect eye size, we sought to determine whether elevated *Notch* activity might be a feature of *gfr* mutant cells in the eye. Consistent with the observed interaction between these genes in the wing, activity of the *Notch* reporter *E(spl)mß-CD2*

(de Celis et al., 1998) is increased in *gfr* clones in both posterior (Figure II.11H-H") and anterior (Figure II.11I-I") regions of the larval eye imaginal disc. This effect on pathway activity occurs independently of an effect on overall Notch levels as detected with an antibody that recognizes the Notch intracellular domain (Figure II.11J-J"). Thus, although the ability of *gfr* alleles to increase organ size appears to be context-dependent, *gfr* mutations increase *Notch* activity in both the eye and the wing. While Notch signaling affects both proliferation and patterning in the *Drosophila* eye (reviewed in Baker, 2007), the N^{54l9} allele was unable to dominantly modify either the *gfr* enlarged eye phenotype (see Figure II.10F) or the bristle defects apparent in *gfr* clones on the surface of the adult eye (data not shown), suggesting either that the effect of *gfr* on Notch activity is too strong to be sensitive to halving the genetic dosage of *Notch* or that a Notch-independent pathway contributes to these *gfr* phenotypes.

Figure II.11. ***gfr*** **alleles confer tissue-specific growth advantage but have general Notch gain-of-function phenotypes.**

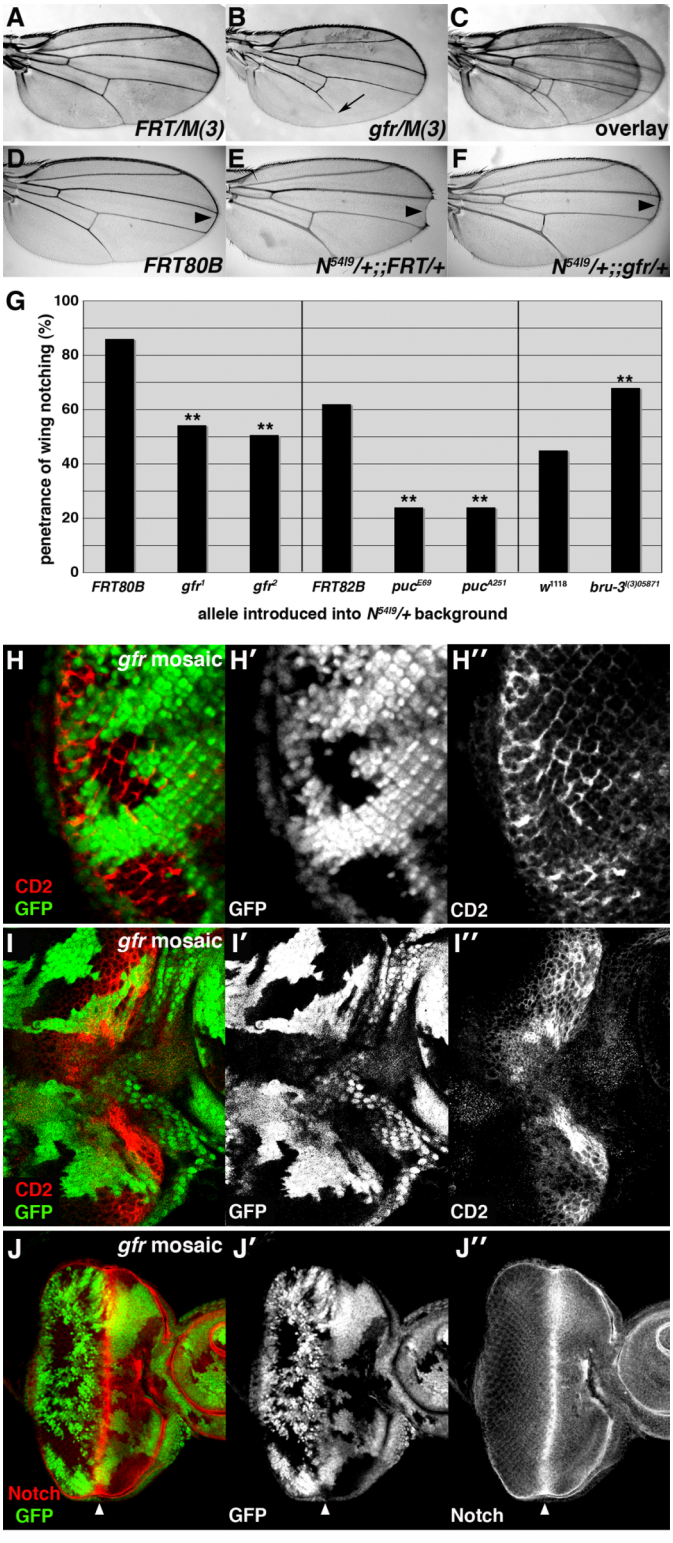

(A-F) Light microscopic images of female adult wings of indicated genotypes. (A-C) *gfr*^{1}*/M(3)* wings (B) have a growth disadvantage relative to *FRT80B/M(3)* wings (A, see overlap in C). (B) The shortened L5 vein (arrow) in *gfr*^{1}*/M(3)* wings phenocopies *Notch* gain-of-function alleles. (D-F) Images of *FRT80B* (D) N^{54l9}*/+;;FRT80B/+* (E) and N^{54l9}*/+;;gfr*^{1}*/+* (F) tracking wing Notching (arrowheads). (G) Quantification of this interaction shows that *gfr* alleles dominantly suppress wing notching in this assay; alleles of *puc* dominantly suppress wing notching in the same manner. *l(3)05871* dominantly enhances wing notching. n ≥ 66 for each genotype; ***P<0.001* relative to *FRT80B, FRT82B*, or w^{1118} in each panel, respectively. (H-J") Merged confocal sections of *gfr*^{1} third instar larval eye disc clones marked by the absence of GFP (green). Activity of the *E(spl)mß-CD2* Notch reporter assessed via levels of CD2 (red) is increased in *gfr* clones both posterior to (H-H") and anterior to (I-I") the MF. (J-J") Levels of the Notch intracellular domain (red) remain unchanged in *gfr* clones; arrowheads mark position of the MF.

Figure II.12. Wings entirely mutant for *gfr* have a growth disadvantage.

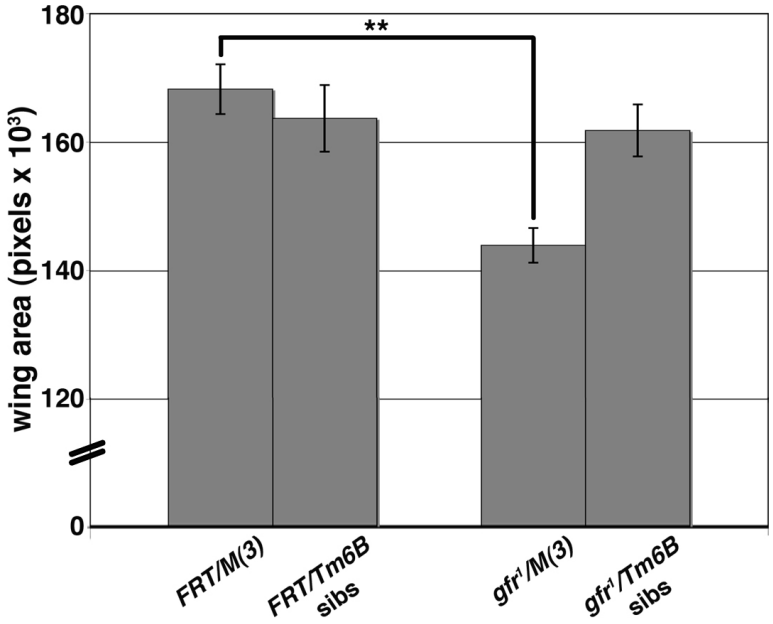

Graphical representation of adult female wing areas (in pixels) of *FRT80B/M(3)*, *FRT80B/Tm6B* sibs, $gfr^{1}/M(3)$, and $gfr^{1}/Tm6B$ sibs. Note that because the *FRT/Tm6B* and $gfr^{1}/Tm6B$ wings are the same size, *FRT80B/M(3)* and $gfr^{1}/M(3)$ wing sizes can be directly compared. Error bars represent 95% confidence intervals. $n \geq 5$ for each genotype; $^{**}P<0.001$. Error bars represent 95% confidence intervals.

II.C7. *gfr* interactions with the *puc* phosphatase

In testing the effect of *gfr* alleles on other pathways that are active in developing discs, we found evidence of a strong genetic interaction between *gfr* and the dual specificity phosphatase *puckered* (*puc*). *puc* acts in an inhibitory feedback loop to antagonize the Jun N-terminal kinase (JNK) pathway, components of which also interact genetically with the *Notch* pathway (e.g., as in Muller et al., 2005). While *puc* or *gfr* heterozygotes are completely viable with no obvious phenotypes, each *gfr* allele is fully lethal *in trans* to either of two different *puc* loss-of-function alleles, puc^{E69} (Martin-Blanco et al., 1998) and puc^{A251} (M. Peifer, pers. comm. to Flybase, 1997), at 25^{o} (0% viability; Table II.3); this lethality was not dependent on the parent-of-origin of *puc* and *gfr* alleles. Because loss of *puc* can increase JNK-dependent apoptosis (McEwen and Peifer, 2005), we tested whether reducing the genetic dosage of *Df(3L)H99* pro-apoptotic genes in the background of *gfr*/*puc trans*-heterozygotes might affect *gfr/puc* lethality. However, the gfr^{x}*,H99* chromosome is still completely lethal *in trans* to either *puc* allele (Table II.3). Thus, *gfr/puc* synthetic lethality is not likely due to a non-specific increase in apoptosis, but instead to a specific role for *gfr* in a *puc*-dependent developmental mechanism.

To characterize the interaction between *puc* and *gfr* further, we tested whether *puc* alleles share properties of *gfr* alleles. Like *gfr*, puc^{E69} and puc^{A251} dominantly suppressed the wing notching observed in N^{54l9}/+ females by approximately 30% ($P<0.001$; Figure II.11G), indicating *gfr* and *puc* normally operate in the same direction in this wing modification assay and supporting further the specificity of the *gfr-puc* genetic interaction. Because *puc* is both a transcriptional target and negative regulator of the JNK pathway, mutations that inactivate *puc* also result in increased *puc* transcription (Martin-

Blanco et al., 1998). To test the hypothesis that *gfr* alleles phenocopy the effect of *puc* alleles on JNK targets, we measured *puc* transcript levels in *gfr* mutant larval eye imaginal discs by quantitative RT-PCR (qPCR). This analysis found a significant 2- to 6-fold increase in *puc* transcription in *gfr* mutant eye discs (Figure II.13A). Thus, *gfr* regulates *puc* transcript abundance in the eye disc. Transcript levels of *dpp*, a second JNK target (Su et al., 1998), are only mildly increased (1.2- to 2.3-fold increase) in the same genetic backgrounds (Figure II.13B). Despite these strong genetic data that link *gfr* to *puc*, a lethal allele of *Drosophila* JNK, bsk^{1} (Riesgo-Escovar et al., 1996), does not dominantly modify the *gfr/M(3)* enlarged eye size (see Figure II.10F). Moreover, *gfr* mutations do not affect phospho-Bsk levels in Western blots of whole eye/antennal discs (Figure II.14A) and do not alter levels or localization of *Drosophila* Jun (dJun/Jra) in mosaic eye discs (Figure II.14B-B"). Thus, although *gfr* behaves genetically as a JNK pathway component, it may regulate this pathway either downstream of or in parallel to Bsk and Jra. Together these data can be interpreted to support a model in which *gfr* alleles elevate JNK pathway activity, and this in turn elevates *puc* expression as part of the established feedback inhibition mechanism; compound heterozygosity for *gfr* and *puc* might then synergistically elevate JNK activity beyond a threshold compatible with viability. However, elevated *puc* transcript levels observed in *gfr* eye discs could also indicate that mutations in *gfr* suppress JNK signaling by increasing *puc* transcript abundance.

Table II.3. Summary of genetic interactions among *gfr*, *puc*, and *bru-3*.

GENOTYPE	VIABILITY (%)	(n)
gfr^{1}/puc^{E69}	**0**	(167)
gfr^{2}/puc^{E69}	**0**	(171)
gfr^{x}/puc^{E69}	**0**	(143)
H99,gfr^{x}/puc^{E69}	**0**	(142)
H99/puc^{E69}	**100**	(275)
gfr^{1}/puc^{A251}	**0**	(91)
gfr^{2}/puc^{A251}	**0**	(79)
gfr^{x}/puc^{A251}	**0**	(75)
H99,gfr^{x}/puc^{A251}	**0**	(62)
cic^{Q474X}/puc^{E69}	**66**	(104)
bru-3$^{l(3)05871}$/Df(3L)Exel6119	**0**	(167)
bru-3$^{l(3)05871}$/puc^{E69}	**100**	(72)
bru-3$^{l(3)05871}$/puc^{A251}	**100**	(47)
bru-3$^{l(3)05871}$/gfr^{1}	**100**	(108)
Df(3L)Exel6119/gfr^{1}	**100**	(92)
gfr^{1}/bru-3$^{l(3)05871}$, puc^{E69} (line A)	**100**	(128)
gfr^{2}/bru-3$^{l(3)05871}$, puc^{E69} (line A)	**100**	(112)
gfr^{x}/bru-3$^{l(3)05871}$, puc^{E69} (line A)	**100**	(103)
gfr^{1}/bru-3$^{l(3)05871}$, puc^{E69} (line B)	**100**	(108)
gfr^{1}/Df(3L)Exel6119, puc^{E69}	**100**	(182)
EY08487/bru-3$^{l(3)05871}$	**90**	(186)
EY08487/Df(3L)Exel6119	**70**	(206)

Information regarding genetic interactions among alleles of *gfr*, *puc*, and *bru-3*. Genotype, percent viability (%), and number scored (n) are presented. Percent viability = (# observed/# expected) x 100.

Figure II.13. Expression of *puc* and *dpp* are elevated in *gfr* mutant tissue.

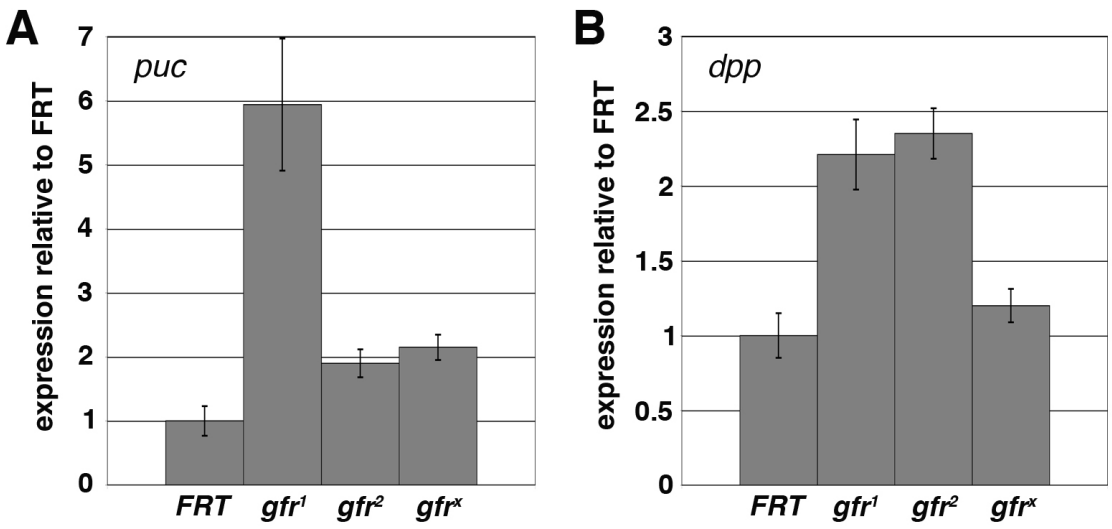

Quantitative real-time PCR analysis of the expression of (A) *puc* and (B) *dpp* mRNAs in *FRT80B/M(3)* control or *gfr/M(3)* third instar eye/antennal discs.

Figure II.14. *gfr* alleles do not affect expression of phospho-JNK or Jra.

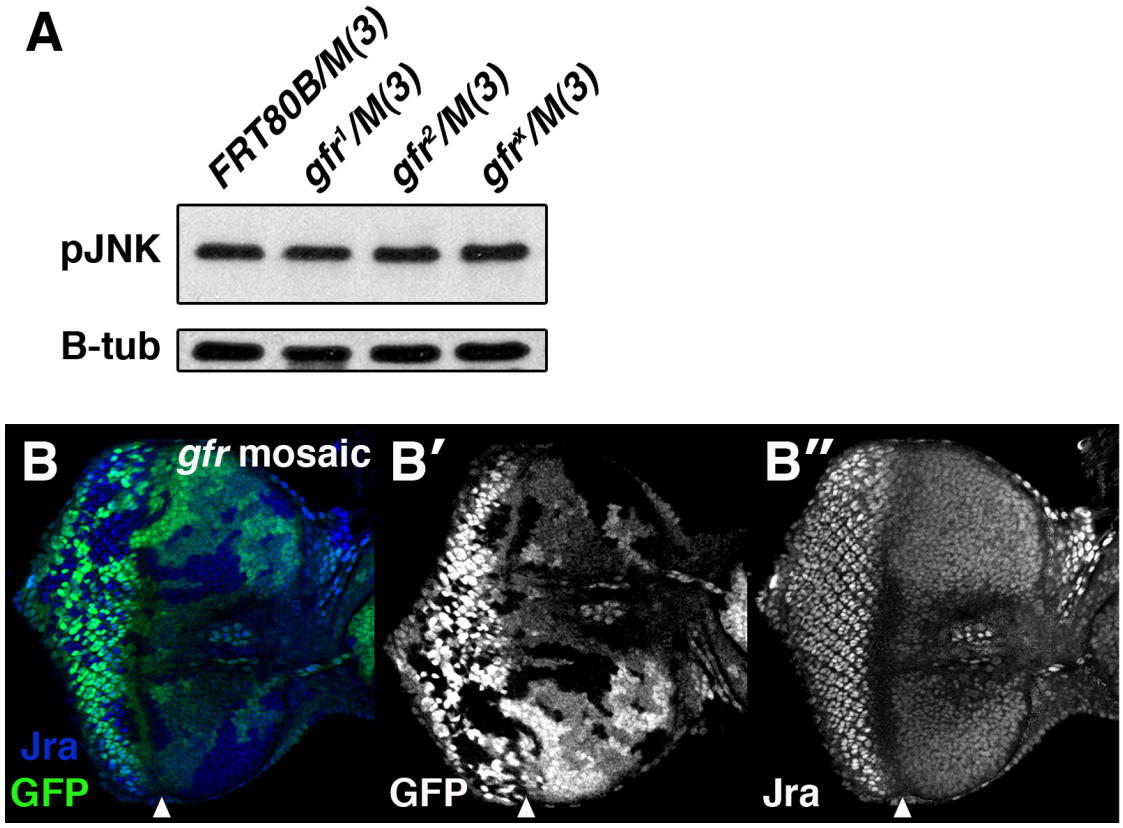

(A) Western blot for phospho-JNK in third instar larval eye/antennal disc lysates of the indicated genotype. 15 pairs of discs loaded per lane; B-tubulin loading control. (B) Merged confocal sections of *gfr*^{1} third instar larval eye disc clones marked by the absence of GFP (green) and stained for Jra (blue). Arrowheads indicate position of the MF.

II.C8. *gfr* alleles decrease Cic levels

JNK signaling controls apoptosis in larval discs (reviewed in Kockel et al., 2001) and is implicated in the localized outgrowth of groups of cells in the larval wing disc (McEwen and Peifer, 2005), but JNK signaling alone is not known to elicit organ-wide hyperplasia. To address the question of how *gfr* alleles cause eyes to become enlarged, we searched for links between *gfr* and several known growth-regulatory pathways. Molecular phenotypes in the eye link *gfr* to the Ras/ERK MAPK module: levels of Capicua (Cic), an HMG-box transcriptional repressor that is destabilized by pro-growth signals from the Ras/ERK MAPK cascade (Jimenez et al., 2000; Tseng et al., 2007), are decreased in *gfr* clones throughout the larval eye imaginal disc (Figure II.15A-A"), and this is particularly evident at the anterior edge of the MF (see yellow arrows; Figure II.15A'-A"). The drop in Cic levels in the eye disc is not accompanied by a change in *cic* transcript levels as detected by qPCR (data not shown). Cic is also decreased in *gfr* clones in the wing imaginal disc (Figure II.16A-A"), suggesting that while the *gfr* growth advantage may be specific to the eye, the molecular consequences of *gfr* mutations may not be. Thus, *gfr* alleles phenocopy Ras/ERK-induced reduction of Cic levels. Interestingly, *cic* alleles were also isolated in an eye-specific *FLP;FRT* screen for overgrowth mutants similar to that which produced the *gfr* complementation group (Tseng et al., 2007). *cic* alleles show a relatively subtle growth phenotype similar to *gfr* but do not affect retinal cell patterning, indicating that while *gfr* may regulate growth via Cic, it must also act upstream of factors involved in retinal patterning.

In view of the genetic link between *gfr* and *puc* and the possibility that the JNK MAPK module might regulate Cic levels in parallel to Ras/ERK, we tested whether

clonal loss of *puc* could also downregulate Cic in eye disc cells. No effect on Cic was observed in puc^{E69} larval eye clones (Figure II.16B-B"). However, we also tested whether *cic* alleles could dominantly influence *puc* viability; indeed, although not nearly as strong as the synthetic lethality observed with *gfr* alleles, the puc^{E69}/cic^{Q474X} *trans*-heterozygous combination shows an approximate 35% reduction in viability (Table II.3).

In consideration of the effect of *gfr* on Cic, we tested whether the *gfr* enlarged eye phenotype was dependent on wild-type dosage of *cic* and two genes predicted to control Cic through the Ras/ERK pathway, *Ras85D* (Brock, 1987) and *rolled* (*rl*; *Drosophila* ERK; Biggs and Zipursky, 1992). While heterozygosity for cic^{Q474X} does not show a strong enhancement *gfr* eye size, $gfr^{1}/M(3)$ eyes generated in backgrounds heterozygous for the alleles $Ras85D^{e2f}$ or rl^{10a} are significantly smaller in size than $gfr^{1}/M(3)$ eyes alone ($P<0.001$; Figure II.10B,E-G). These effects are fairly specific: with the exception of an allele of the Warts/Hippo pathway transcriptional effector *yki,* yki^{B5} (Huang et al., 2005), alleles of *Notch*, *bsk*, and the mitotic cyclin-dependent kinase *cdc2*, do not significantly modify *gfr/M(3)* eye size (Figure II.10F). Additionally, the $Ras85D^{e2f}/+$ genotype was unable to rescue BarHI and Dlg phenotypes in the pupal eye (Figure II.8E-E"). Thus, although activated Ras can result in reduced cone cell numbers (Fortini et al., 1992; Kauffmann et al., 1996), *Ras85D* is more strongly required for the effects of *gfr* alleles on growth than their effects on cellular patterning. In sum, the eye overgrowth produced by *gfr* alleles correlates with reduced levels of Cic and is sensitive to the dose of two genes, *Ras85D* and *rl*, which act within a pathway that promotes clonal overgrowth by repressing Cic levels (Tseng et al., 2007). The significance of the additional effect of the yki^{B5} allele on *gfr* eye size is not clear, but considered with the *puc*, *Notch* and *cic* data, it

may indicate that *gfr* alleles elicit growth and patterning phenotypes via multiple signaling pathways.

Figure II.15. Cic is decreased in the eye due to *gfr* mutation or *bru-3* overexpression.

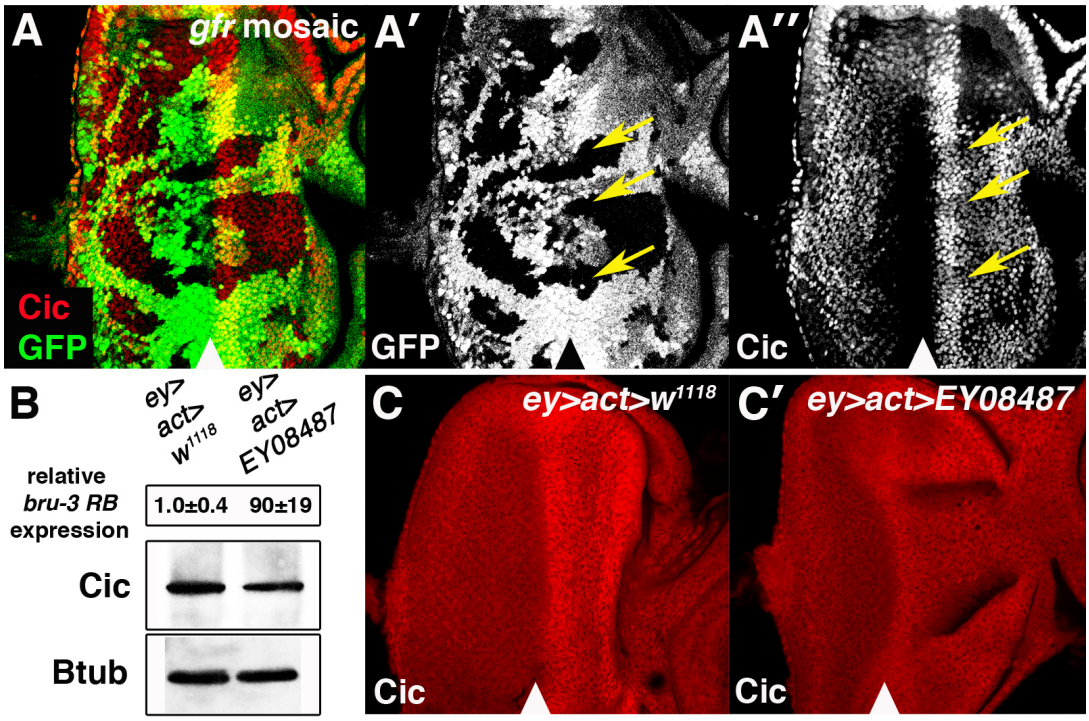

(A-A") Merged confocal sections of *gfr* third instar larval eye disc clones marked by the absence of GFP (green) and stained with Cic (red). (B) Western blot for Cic in third instar larval eye/antennal disc lysates of the indicated genotypes: *eyFLP;act>y*$^{+}$*>gal4-w1118* and *eyFLP;act>y*$^{+}$*>gal4-EY08487*. 15 pairs of discs loaded in each lane; B-tubulin loading control. The relative expression of *bru-3 RB* transcript as measured by qPCR is indicated. (C-C') Merged confocal sections of third instar eye discs stained for Cic (red) of the genotypes immunoblotted in B. Note the level of Cic is reduced in *gfr* clones (GFP-) relative to wild-type twinspots (GFP+; A-A") and in eye discs overexpressing *bru-3* (B, C') relative to control (B, C). Arrowheads indicate position of the MF.

Figure II.16. Cic is decreased in *gfr* wing clones and unchanged in *puc* eye clones.

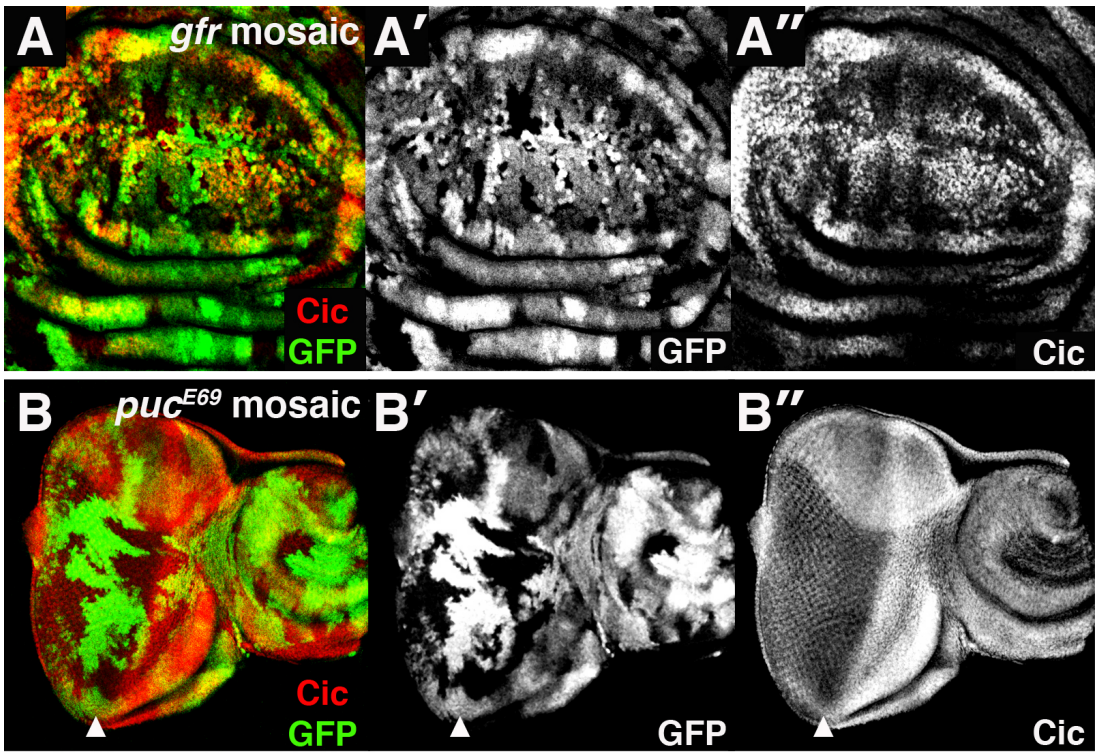

Merged confocal sections of *gfr* third instar larval wing disc clones (A-A") or puc^{E69} third instar larval eye disc clones (B-B") marked by the absence of GFP (green) and stained with Cic (red). Arrowheads indicate position of the MF.

II.C9. *gfr* alleles are gain-of-function for *bru-3*

While cellular and molecular phenotypes associated with *gfr* mutations are quite apparent, the gene representing the *gfr* complementation group is not identified. As previously described (see Section II.C2), gfr^{1} lethality is tightly linked to cytological position 70A-B on chromosome 3L. However, *gfr* alleles do not behave as loss-of-function mutations: they are lethal *in trans* to each other, yet completely viable and without obvious phenotypes *in trans* to several deficiencies and lethal lesions spanning the 70A-B chromosomal region. Direct sequencing of many candidate genes in the region failed to identify any DNA lesions that might cause gain-of-function effects (data not shown). Because the *gfr* alleles may be regulatory in nature, multiple candidate genes near the *P*-elements that are most closely linked to *gfr* lethality (*KG01069* and *BG00690*), including the *CG10133*, *CG17689*, *CG10089*, and *bruno-3* genes, were also tested for changes in expression levels by qPCR. Of these, only *bruno-3* (*bru-3*) expression was changed: both annotated transcripts of the *bru-3* gene, which encodes an RNA-binding protein that can bind to the EDEN translational repression sequence (Delaunay et al., 2004), are overexpressed several fold (2- to 14-fold) relative to levels in eye discs homozygous for the parental *FRT80B* chromosome. This effect on *bru-3* RNA levels is observed in all *gfr* alleles (Figure II.17). As overexpression of *bru-3* has recently been shown to promote hemocyte over-proliferation and enlarged lymph glands (Stofanko et al., 2008), this suggests that excess *bru-3* might contribute to the *gfr* phenotypes.

To further characterize the relationship between the *gfr* complementation group and *bru-3*, we utilized two *bru-3* alleles: *l(3)05871*, a lethal *P*-element insertion immediately upstream of *bru-3*, and *Df(3L)Exel6119*, a deficiency that removes a portion

of the *bru-3* gene but does not overlap with the *l(3)05871 P*-element insertion site (FlyBase). Although not inserted in the gene body, the *bru-3*$^{l(3)05871}$ allele fails to complement *Df(3L)Exel6119* (Table II.3), and acts in a direction opposite to *gfr* alleles with respect to *Notch*: *gfr* alleles are dominant suppressors of N^{54l9}/+ wing notching, but *bru-3*$^{l(3)05871}$ dominantly enhances both the penetrance (68% vs. 45%, respectively; $P<0.001$; Figure II.11G), and expressivity of N^{54l9}/+ wing notching by increasing the percentage of wings having two or more notches (data not shown). *actin-Gal4* driven ubiquitous overexpression of *bru-3* from the UAS-containing *EY08487* element (Bellen et al., 2004) is also lethal (data not shown), suggesting that elevated expression of *bru-3* in the *gfr* background may contribute to the homozygote lethality of *gfr* alleles. Because *bru-3* and *gfr* are tightly linked to the same chromosomal region, *bru-3* alleles cannot be recombined with *gfr* alleles to test whether reducing *bru-3* activity can dominantly rescue *gfr* homozygote lethality (data not shown). Consequently, we tested whether reducing *bru-3* gene dosage with either *bru-3*$^{l(3)05871}$ or *Df(3L)Exel6119* could rescue the *gfr/puc trans*-heterozygote lethality. This lead to a complete rescue of *gfr/puc* lethality (Table II.3) by either *bru-3* allele and in the background of multiple *gfr* alleles; this rescue is also observed in multiple *bru-3,puc* recombinant lines (Table II.3). These data demonstrate that loss-of-function alleles of *bru-3* restore *gfr/puc* viability and that overexpression of *bru-3* in *gfr* alleles is responsible for *gfr/puc* lethality and, by extension, perhaps *gfr/gfr* lethality as well.

Figure II.17. Expression of *bru-3* is elevated in *gfr* mutant eye tissue.

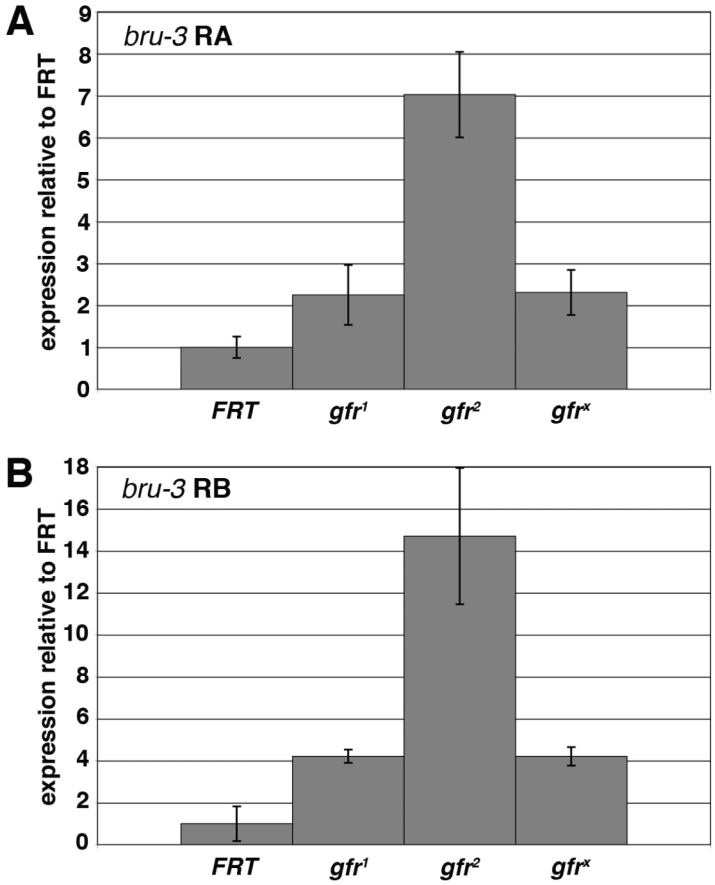

Quantitative real-time PCR analysis of the expression of *bru-3* transcripts RA (A) and RB (B) in *FRT80B/M(3)* control or *gfr/M(3)* third instar eye/antennal discs.

II.C10. *bru-3* regulates Cic and eye size

To test whether overexpression of *bru-3* might phenocopy all or some elements of the *gfr* mutant eye phenotype, the *EY08487 bru-3* UAS-element was initially combined with the *eyeless-Gal4* driver. At all temperatures tested, this failed to increase *bru-3* transcript in larval eye discs as measured by qPCR (data not shown). Consequently, we utilized the "eyFLP-out" technique (Pignoni and Zipursky, 1997) to drive *EY08487* with the *actin>CD2>Gal4* transgene specifically in eye disc cells. By this method, we achieved a 90-fold increase in *bru-3 RB* transcript levels in the eye at 25^{o} (see Figure II.15B). We then tested these *ey>act>EY08487* eye discs for evidence of an effect on Cic protein levels. As observed in *gfr* mutant eye tissue (see Figure II.15 A-A"), overexpression of *bru-3* is also associated with a decrease in the levels of Cic in the larval eye disc as detected both by Western blot (Figure II.15B) and by immunofluorescence (compare Figure II.15C & 9C'). Thus, overexpression of *bru-3* produces an effect on Cic levels that is similar to that of *gfr* alleles. Although overexpressing *bru-3* in this manner was insufficient to increase adult eye size, adult flies homozygous for the *EY08487 bru-3* allele show reduced eye size compared with *EY08487/+* flies ($P<0.001$; Figure II.18). The *EY08487* allele produces reduced viability *in trans* to either *bru-3*$^{l(3)05871}$ or *Df(3L)Exel6119* (Table II.3), suggesting that *EY08487* is a weakly hypomorphic for *bru-3*. While both increased and decreased *bru-3* expression share some phenotypes expected of *gfr* alleles, gain-of-function of the *bru-3* gene product in *gfr* mutant tissue could be a secondary effect of increased activity from *gfr*-affected pathways. In light of the links to *puc* and Cic, we sought to test whether overactivating the JNK or ERK pathways leads to increased *bru-3* transcript levels. qPCR analysis of *bru-3* RNA in *GMR-Gal-4,UAS-hep*^{act}

(Weber et al., 2000) and *UAS-EGFR*^{Elp} (Baker and Rubin, 1989) larval eye discs showed no effect on *bru-3* (Figure II.19), suggesting that overexpression of *bru-3* may be a more primary molecular defect in *gfr* mutant cells.

Figure II.18. Hypomorphic allele of *bru-3* has decreased eye size.

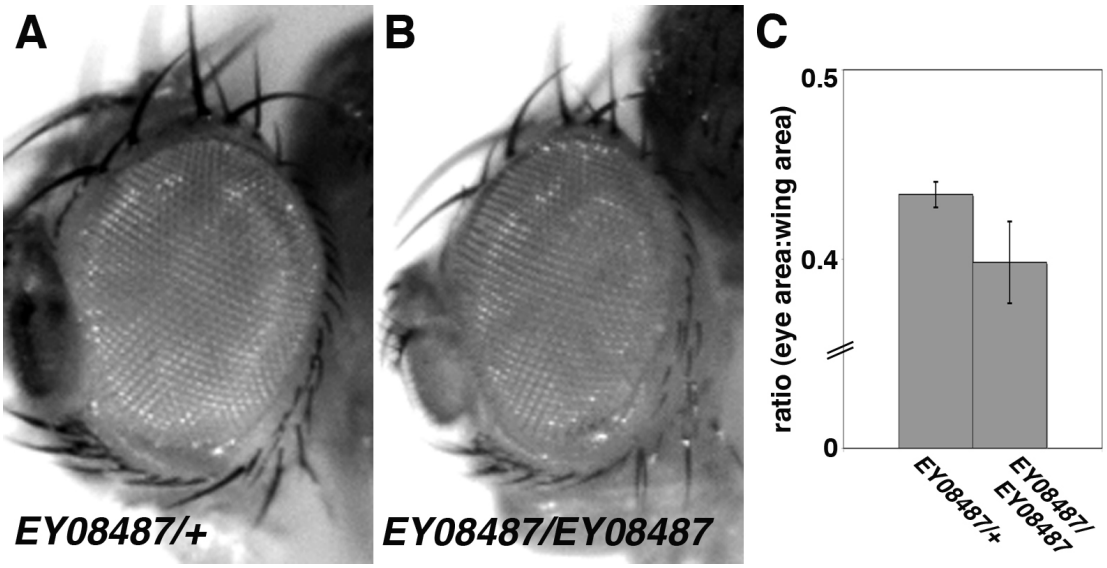

Light microscopic images of (A) *EY08487/+* and (B) *EY08487/EY08487* adult female eyes taken at the same magnification. Note the eye in B is smaller than the eye in A. (C) Graphic summary of the effect of the indicated genotypes on *en face* adult female eye size. In each case, eye area was normalized wing area between the L3,L4, and PCV veins of the same fly; average eye area:wing area ratios are plotted. $n \geq 10$ for each genotype. Error bars represent 95% confidence intervals.

Figure II.19. *bru-3* transcript is not increased due to activated MAPK pathways.

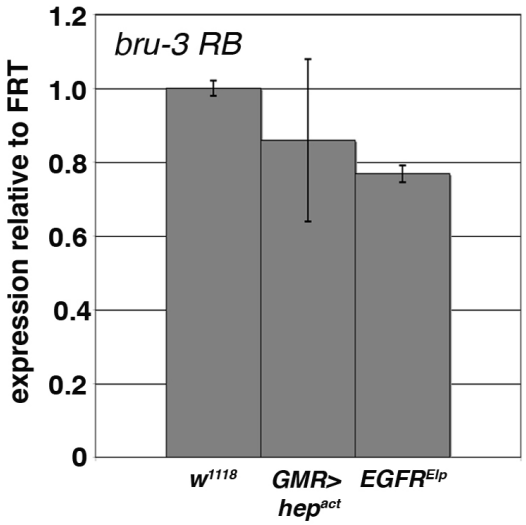

Quantitative real-time PCR analysis of the expression of *bru-3 RB* transcript in w^{1118} control, *GMR-gal4,UAS-hep*^{act}, and *EGFR*^{Elp} third instar eye/antennal discs.

II.D. DISCUSSION

Here we show that mutations in the novel complementation group *gfr* disrupt patterns of cell differentiation in the eye and increase eye size through a proliferative mechanism that can be enhanced by a block in apoptosis. *gfr* alleles display genetic and molecular phenotypes indicative of a regulatory effect on the JNK/ERK and Notch pathways and map to a fairly small genomic interval at 70A-B. This interval contains a gene *bru-3*, which is overexpressed in all *gfr* mutant backgrounds and has been previously identified in a misexpression screen for positive regulators of larval hemocyte proliferation and lymph gland size (Stofanko et al., 2008). In addition to *bru-3*, other loci identified in this screen have known roles in growth control, and several are components of *gfr*-affected pathways; examples include the *bantam* microRNA, which controls proliferation and apoptosis (Brennecke et al., 2003), the *Drosophila* CHK1 kinase homolog *grapes*, the *Drosophila Insulin-like receptor*, which controls cell size and number (Brogiolo et al., 2001), the *Drosophila* Fos homolog *kayak*, and the EGFR ligand *Keren*. *bru-3* encodes an mRNA binding protein and translational repressor that binds to EDEN sequence elements in mRNAs and is orthologous to Xenopus EDEN-BP and human CUG-BP (Delaunay et al., 2004). In mammalian cells, CUG-BP binds the c-Jun mRNA and plays an important role in post-transcriptional control of c-Jun expression (Paillard et al., 2002). Moreover, overexpression of such RNA-binding factors can lead to stabilization of mRNAs containing these target sequences (Fan and Steitz, 1998; Levy et al., 1998; Peng et al., 1998). Thus, *bru-3* overexpression in *gfr* eye disc cells could lead to a stabilization of Jra and subsequent alteration of its downstream transcriptional program. Intriguingly, reducing *bru-3* gene dosage can rescue an embryonic lethal combination of *gfr* and *puc*

alleles, yet ectopic overexpression of *bru-3* is unable to phenocopy the effect of *gfr* alleles on head and eye size. From this, it appears that *bru-3* is necessary for *gfr* mutant phenotypes but may not be sufficient to reproduce them, indicating that other factors are required to drive the full spectrum of *gfr* growth and patterning phenotypes. However, since our system expressed *bru-3* in the eye to levels 90-fold over baseline, it may be that any potential *bru-3* growth phenotypes are masked by the cellular consequences of supra-physiologic levels of Bru-3.

The specific molecular mechanisms by which *gfr* alleles produce excess growth are not known, mainly because the *gfr* lesions remain unidentified. However, certain molecular aspects of the *gfr* phenotype are reminiscent of MAPK pathway components—in particular, the Ras/ERK pathway, which has been shown to promote growth by down-regulating Cic (Tseng et al., 2007). The pattern of Cyclin E expression anterior to the MF resembles what has been reported in *cic* mutant clones, and this correlates with a requirement for wild-type *gfr* to maintain Cic levels in eye cells (see Figure II.15). The genetic dependence of the *gfr* enlarged-eye mutant phenotype on the MAPK components *Ras85D* and *rl* coupled with the synthetic lethality of *gfr* and *puc* alleles further argue that *gfr* alleles elicit a subset of phenotypes via effects on MAPK pathways. Indeed the Cic and *puc* data support a model in which *gfr* acts within one or more MAPK cascades, and that interactions between *gfr* and other pathways (e.g., *Notch* and *yki*) are a consequence of this more primary role. Many *gfr* phenotypes, from decreased cone cells to increased proliferation, could be explained by an increase in Ras/ERK signaling, which has known roles in both proliferation and differentiation in the eye and interacts with many pathways, including *Notch* (Sundaram, 2005). In addition, the *Drosophila* Jun

homolog Jra has well documented roles in the eye downstream of Ras/ERK (Kockel et al., 1997), thereby providing a potential link between decreased Cic levels and the strong genetic interaction between *gfr* and the putative Jra target, *puc*. The synthetic lethality of *gfr* and *puc* alleles is generally only observed between genes that are tightly linked in the same pathway (e.g., *wg* and *dsh*, Theisen et al., 1994), arguing a role for *gfr* in the JNK pathway or another *puc*-specific function. Activation of the JNK pathway in the eye is typically pro-apoptotic (reviewed in Kockel et al., 2001), which is in conflict with the *gfr* overgrowth phenotype. However, it has been shown that in the presence of activated Ras, JNK switches from pro-apoptotic to pro-growth and cooperates with oncogenic Ras to promote tumor growth and metastasis (Igaki et al., 2006). Thus, *gfr* could act to regulate JNK/ERK activity in developing tissues. However, genes directly involved in JNK signaling typically have dorsal closure defects (reviewed in Kockel et al., 2001), and because *gfr/gfr* animals can survive to an early larval stage, a role in dorsal closure, and by extension, a central role as a core JNK pathway component, seems unlikely. Alternately, *gfr* may encode a factor that controls MAPK cascades in a more tissue-specific manner such that *gfr* alleles are insufficient to drive ERK/JNK phenotypes in all cells at all developmental stages.

A major outstanding question remains: what is the *gfr* gene? Meiotic mapping links *gfr* closely to the chromosomal region represented by cytological positions 70A-B; however, direct sequencing of many candidate genes in the region has not uncovered any apparent mutations. Though all *gfr* alleles are lethal *in trans* to each other, they are viable with no obvious defects *in trans* to all available deficiencies and lethal alleles in this region. Thus, the underlying assumption that the *gfr* alleles are caused by recessive, loss-

of-function mutations may be incorrect. *gfr* alleles do not produce dominant morphological phenotypes characteristic of gain-of-function mutations. However, *gfr* heterozygotes do display a dominant genetic phenotype: they are hypersensitized to loss of a single allele of *puc*. That this dominant phenotype can then be suppressed by *bru-3* alleles (*Df(3L)Exel6119* or *l(3)05871*) tends to argue either that *bru-3* is the actual target of the *gfr* mutations or that *bru-3* expression is downstream of the gene affected by *gfr* lesions (Figure II.20). Although this sort of recessive gain-of-function allele is not common, such *gfr* alleles could have been selected for in the *eyFLP* screen due to their pro-growth effects. Several gain-of-function alleles of known *Drosophila* genes, such as *Tufted* and *Bearded* (*Brd*), share some phenotypes with *gfr* mutations, including bristle defects and interactions with the Notch pathway (Lai et al., 2000; Leviten and Posakony, 1996; Villa-Cuesta et al., 2003). Additionally, recessive phenotypes other than lethality associated with gain-of-function alleles is not without precedence: dominant *Drop* mutations are associated with recessive phenotypes such as patterning and bristle defects in the eye (Mozer, 2001), and the phenotypes associated with gain-of-function *Brd* mutations are dosage-sensitive—*Brd* homozygotes have a more severe phenotype than *Brd* heterozygotes (Leviten and Posakony, 1996). Yet, the inability of *bru-3* to phenocopy all elements of the *gfr* phenotype is either (1) a consequence of insufficient tools to effectively overexpress *bru-3* to levels seen in *gfr* mutant cells or (2) supports a model in which *bru-3* is not the sole effector of *gfr* alleles. However, since *gfr* maps very close to *bru-3*, another possibility that must be considered is that *gfr* alleles affect the expression of multiple genes in the *bru-3* region (for example, by disrupting a chromatin

insulator element) and that the *gfr* phenotypes are the product of altered expression of multiple genes (Figure II.20).

Figure II.20. Models of *gfr* action.

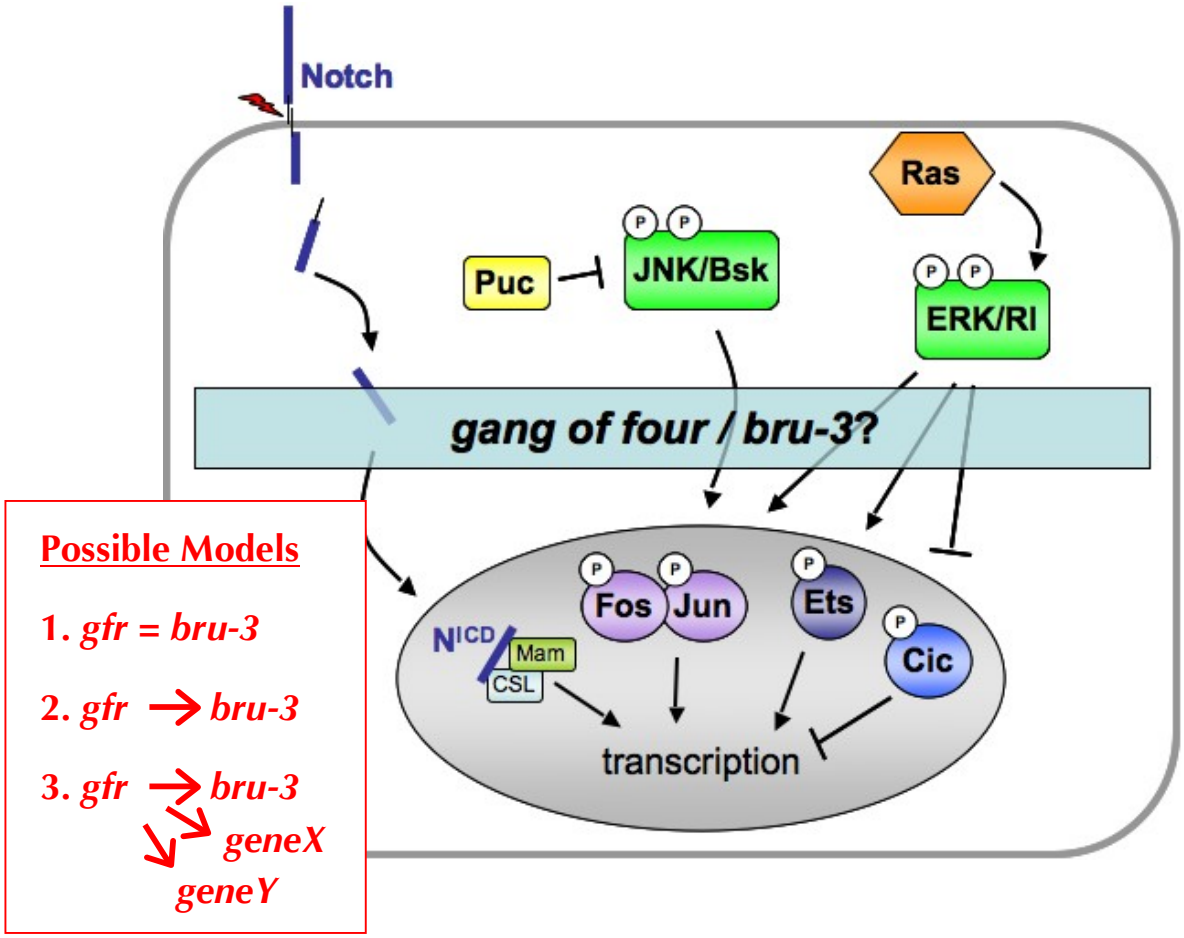

Schematic summarizing possible models of *gfr* mechanisms of action. As shown, *gfr* affects signaling through the Notch, JNK, and Ras/ERK pathways. *gfr* alleles also increase the transcription of *bru-3*. Therefore, *gfr* mutant phenotypes could be the result of several scenarios (shown in red, see also Discussion): (1) the *gfr* complementation group represents alleles of *bru-3*; (2) overexpression of *bru-3* is the primary downstream consequence of mutations in the *gfr* gene; or (3) *gfr* alleles affect the expression of multiple genes in the *bru-3* region.

II.E. MATERIALS AND METHODS

Genetics: Crosses were performed at 25°C, unless otherwise indicated. The following genotypes were used for *gfr* analysis: *y,w,eyFLP;P[m-w$^+$;ubi>GFP],FRT80B*, *y,w,ubxFLP;P[m-w$^+$;ubi>GFP],FRT80B*, *y,w,eyFLP;FRT82B,P[m-w$^+$;ubi>GFP]* (gift of I.K. Hariharan), *y,w,eyFLP;P[m-w$^+$]RpL14^1,FRT80B*, *y,w,ubxFLP;P[m-w$^+$]RpL14^1,FRT80B*, *FRT80B*, *Df(3L)H99,FRT80B*, *gfr^{1}FRT80B/TM6B*, *gfr^{2}FRT80B/TM6B*, *gfr^{x}FRT80B/TM6B*, *gfr^x,Df(3L)H99,FRT80B/TM6B* (gift of M.M. Gilbert), *gfr^{4}FRT80B/TM6B* (stock no longer extant), *y,w,eyFLP,E(spl)mß-CD2,P[m-w$^+$;ubi>GFP],FRT80B*, *cdc2^{B47}/CyO;gfr^1,FRT80B/Tm6B*, *N^{54l9}/Fm7c;gfr^1,FRT80B/Tm6B*, *bsk^1/CyO;gfr^1,FRT80B/Tm6B*, *gfr^1,FRT80B,Ras85D^{e2F}/Tm6B*, *rl^{10a}/CyO;gfr^1,FRT80B/Tm6B* (*rl^{10a}* gift of A. Vrailas Mortimer), *FRT42D,yki^{B5}/CyO;gfr^1,FRT80B/Tm6B* (*yki^{B5}* gift of K. Irvine), *y,w^a,N^{54l9}/Fm6*, *FRT82B*, *puc^{E69}/Tm6B* (gift of A. Vrailas Mortimer), *puc$^{A251.1F3}$/Tm3, FRT82B,cic^{Q474X}/Tm6B* (gift of I.K. Hariharan), *gfr^1,FRT80B,cic^{Q474X}/Tm6B*. The following genotypes were used for *bru-3* analysis: *Df(3L)Exel6119/Tm6B*, *P{PZ}l(3)05871^{05871}/Tm3*, *w^{1118}*, *P{EPgy2}EY08487*, *y,w,eyFLP;act>y$^+$>Gal4*, *l(3)05871*, *puc^{E69}/Tm6B*, *Df(3L)Exel6119,puc^{E69}/Tm6B*, *w^{1118}*, *GMR-gal4,UAS-hep^{act}* (gift of R. Jones), *EGFR^{Elp}* (gift of D. Marenda). General mapping stocks: *Df(3L)ED4502/Tm6c*, *Df(3L)Exel6119/Tm6B*, *P{SUPor-P}tRNA:CR32123:Ψ^{KG01069}*, *P{GT1}BG00690*. Bellen mapping *P*-element stocks (Zhai et al., 2003) obtained from Bloomington *Drosophila* Stock Center: *KG02776*, *KG09489*, *KG00023*, *KG02042*, *EY07351*, *EY04154*, *KG00330*, *EY01866*, *KG07481*, *KG01069*, *BG00690*, *BG01582*, *BG02493*, *BG01780*. Other stocks obtained from Bloomington *Drosophila* Stock Center.

Eye/wing pictures and measurements: Adult eyes and wings were photographed with a Leica DFC500 CCD digital camera. For measurements, areas were quantitated with Adobe Photoshop.

Immunohistochemistry & Microscopy: Immunostaining and confocal microscopy was performed using a 4% paraformaldehyde fixative as described previously (Moberg et al., 2004); α-CycE staining was performed according to the same protocol but used a PLP fixative. Primary antibodies and dilutions used in immunostaining: mouse α-CycA 1:50 (A12,DSHB); mouse α-CycB 1:50 (F2F4, DSHB); mouse α-CycE 1:5 (8B10, gift of H. Richardson); guinea pig α-Sens 1:1000 ((Nolo et al., 2000); gift of H. Bellen); mouse α-Dlg 1:50 (4F3, DSHB); rabbit α-BarH1 1:50 (S12, (Higashijima et al., 1992); gift of K. Saigo); mouse α-Notch 1:200 (9C6, DSHB); rat α-CD2 1:100 (Research Diagnostics, Inc); guinea pig α-Cic1501 and guinea pig α-Cic1503 1:300 ((Tseng et al., 2007); gift of I. Hariharan); rabbit α-phospho-Histone H3 1:200 (Ser10, Upstate); mouse α-BrdU 1:50 (Becton Dickinson); rabbit α-Jra/dJun 1:1000 (gift of D. Bohmann). For immunoblotting, imaginal disc extracts were prepared in sample buffer containing DTT and resolved on SDS-PAGE prior to Western blotting with guinea pig α-Cic1503 (1:1000), rabbit α-pJNK 1:1000 (Cell Signaling, gift of R. Jones), or α-ß-tubulin (1:1000; Santa Cruz Biotechnology). Secondary antibodies conjugated to Cy3, Cy5, and HRP were used as recommended (Jackson ImmunoResearch). A 1.5-hour pulse was used for imaginal disc BrdU incorporation.

Real Time RT-PCR (qPCR): Total RNA isolated from 30 eye discs (TRIzol/Invitrogen) was reverse transcribed (SuperScript II RT/Invitrogen) and analyzed by qPCR (SYBR Green 1 Master/Roche) Primers: *puc* 5'-GCCACATCAGAACATCAAGC-3', 5'-

CCGTTTTCCGTGCATCTT-3’; *dpp* 5’-GTGCGAAGTTTTACACACAAAGA-3’, 5’CGCCTTCAGCTTCTCGTC-3’; *bru-3-RA* 5’-TTGCCATCATCCATTAATACCA-3’, 5’TTCAGCTGTAAAGCACGGTTC-3’; *bru-3-RB* 5’-CTACCCTGCAACATGCCTTC-3’, 5’GGTGGTAAAGCTTGTGGAAACT-3’ *ß-tub* 5’-CGCACAGAGTCC ATGGTG-3’, 5’-AAATCGTTCACATCCAAGCTG-3’.

II.F. REFERENCES

Baker, N. E. (2007). Patterning signals and proliferation in Drosophila imaginal discs. *Curr Opin Genet Dev* **17**, 287-93.

Baker, N. E. and Rubin, G. M. (1989). Effect on eye development of dominant mutations in Drosophila homologue of the EGF receptor. *Nature* **340**, 150-3.

Bellen, H. J., Levis, R. W., Liao, G., He, Y., Carlson, J. W., Tsang, G., Evans-Holm, M., Hiesinger, P. R., Schulze, K. L., Rubin, G. M. et al. (2004). The BDGP gene disruption project: single transposon insertions associated with 40% of Drosophila genes. *Genetics* **167**, 761-81.

Biggs, W. H., 3rd and Zipursky, S. L. (1992). Primary structure, expression, and signal-dependent tyrosine phosphorylation of a Drosophila homolog of extracellular signal-regulated kinase. *Proc Natl Acad Sci U S A* **89**, 6295-9.

Brennecke, J., Hipfner, D. R., Stark, A., Russell, R. B. and Cohen, S. M. (2003). bantam Encodes a Developmentally Regulated microRNA that Controls Cell Proliferation and Regulates the Proapoptotic Gene hid in Drosophila. *Cell* **113**, 25-36.

Brock, H. W. (1987). Sequence and genomic structure of ras homologues Dmras85D and Dmras64B of Drosophila melanogaster. *Gene* **51**, 129-37.

Brogiolo, W., Stocker, H., Ikeya, T., Rintelen, F., Fernandez, R. and Hafen, E. (2001). An evolutionarily conserved function of the Drosophila insulin receptor and insulin-like peptides in growth control. *Curr Biol* **11**, 213-21.

Chen, B., Chu, T., Harms, E., Gergen, J. P. and Strickland, S. (1998). Mapping of Drosophila mutations using site-specific male recombination. *Genetics* **149**, 157-63.

Craig, E. A., Stevens, M. V., Vaillancourt, R. R. and Camenisch, T. D. (2008). MAP3Ks as central regulators of cell fate during development. *Dev Dyn* **237**, 3102-14.

de Celis, J. F. and Garcia-Bellido, A. (1994). Modifications of the notch function by Abruptex mutations in Drosophila melanogaster. *Genetics* **136**, 183-94.

de Celis, J. F., Tyler, D. M., de Celis, J. and Bray, S. J. (1998). Notch signalling mediates segmentation of the Drosophila leg. *Development* **125**, 4617-26.

Delaunay, J., Le Mee, G., Ezzeddine, N., Labesse, G., Terzian, C., Capri, M. and Ait-Ahmed, O. (2004). The Drosophila Bruno paralogue Bru-3 specifically binds the EDEN translational repression element. *Nucleic Acids Res* **32**, 3070-82.

Dexter, J. S. (1914). The analysis of a case of continuous variation in Drosophila by a study of its linkage relations. *Am. Nat.* **48**, 712.

Dominguez, M. and de Celis, J. F. (1998). A dorsal/ventral boundary established by Notch controls growth and polarity in the Drosophila eye. *Nature* **396**, 276-8.

Doroquez, D. B. and Rebay, I. (2006). Signal integration during development: mechanisms of EGFR and Notch pathway function and cross-talk. *Crit Rev Biochem Mol Biol* **41**, 339-85.

Edwards, P. A. (1999). The impact of developmental biology on cancer research: an overview. *Cancer Metastasis Rev* **18**, 175-80.

Fan, X. C. and Steitz, J. A. (1998). Overexpression of HuR, a nuclear-cytoplasmic shuttling protein, increases the in vivo stability of ARE-containing mRNAs. *EMBO J* **17**, 3448-60.

Fortini, M. E., Simon, M. A. and Rubin, G. M. (1992). Signalling by the sevenless protein tyrosine kinase is mimicked by Ras1 activation. *Nature* **355**, 559-61.

Frankfort, B. J., Nolo, R., Zhang, Z., Bellen, H. and Mardon, G. (2001). senseless repression of rough is required for R8 photoreceptor differentiation in the developing Drosophila eye. *Neuron* **32**, 403-14.

Hariharan, I. K. and Bilder, D. (2006). Regulation of imaginal disc growth by tumor-suppressor genes in Drosophila. *Annu Rev Genet* **40**, 335-61.

Harvey, K. F., Pfleger, C. M. and Hariharan, I. K. (2003). The Drosophila Mst ortholog, hippo, restricts growth and cell proliferation and promotes apoptosis. *Cell* **114**, 457-67.

Higashijima, S., Kojima, T., Michiue, T., Ishimaru, S., Emori, Y. and Saigo, K. (1992). Dual Bar homeo box genes of Drosophila required in two photoreceptor cells, R1 and R6, and primary pigment cells for normal eye development. *Genes Dev* **6**, 50-60.

Huang, J., Wu, S., Barrera, J., Matthews, K. and Pan, D. (2005). The Hippo signaling pathway coordinately regulates cell proliferation and apoptosis by inactivating Yorkie, the Drosophila Homolog of YAP. *Cell* **122**, 421-34.

Igaki, T., Pagliarini, R. A. and Xu, T. (2006). Loss of cell polarity drives tumor growth and invasion through JNK activation in Drosophila. *Curr Biol* **16**, 1139-46.

Jimenez, G., Guichet, A., Ephrussi, A. and Casanova, J. (2000). Relief of gene repression by torso RTK signaling: role of capicua in Drosophila terminal and dorsoventral patterning. *Genes Dev* **14**, 224-31.

Kauffmann, R. C., Li, S., Gallagher, P. A., Zhang, J. and Carthew, R. W. (1996). Ras1 signaling and transcriptional competence in the R7 cell of Drosophila. *Genes Dev* **10**, 2167-78.

Kockel, L., Homsy, J. G. and Bohmann, D. (2001). Drosophila AP-1: lessons from an invertebrate. *Oncogene* **20**, 2347-64.

Kockel, L., Zeitlinger, J., Staszewski, L. M., Mlodzik, M. and Bohmann, D. (1997). Jun in Drosophila development: redundant and nonredundant functions and regulation by two MAPK signal transduction pathways. *Genes Dev* **11**, 1748-58.

Lai, E. C., Bodner, R., Kavaler, J., Freschi, G. and Posakony, J. W. (2000). Antagonism of notch signaling activity by members of a novel protein family encoded by the bearded and enhancer of split gene complexes. *Development* **127**, 291-306.

Leviten, M. W. and Posakony, J. W. (1996). Gain-of-function alleles of Bearded interfere with alternative cell fate decisions in Drosophila adult sensory organ development. *Dev Biol* **176**, 264-83.

Levy, N. S., Chung, S., Furneaux, H. and Levy, A. P. (1998). Hypoxic stabilization of vascular endothelial growth factor mRNA by the RNA-binding protein HuR. *J Biol Chem* **273**, 6417-23.

Maillard, I. and Pear, W. S. (2003). Notch and cancer: Best to avoid the ups and downs. *Cancer Cell* **3**, 203-5.

Martin-Blanco, E., Gampel, A., Ring, J., Virdee, K., Kirov, N., Tolkovsky, A. M. and Martinez-Arias, A. (1998). puckered encodes a phosphatase that mediates a feedback loop regulating JNK activity during dorsal closure in Drosophila. *Genes Dev* **12**, 557-70.

McEwen, D. G. and Peifer, M. (2005). Puckered, a Drosophila MAPK phosphatase, ensures cell viability by antagonizing JNK-induced apoptosis. *Development* **132**, 3935-46.

Moberg, K. H., Bell, D. W., Wahrer, D. C., Haber, D. A. and Hariharan, I. K. (2001). Archipelago regulates Cyclin E levels in Drosophila and is mutated in human cancer cell lines. *Nature* **413**, 311-6.

Moberg, K. H., Mukherjee, A., Veraksa, A., Artavanis-Tsakonas, S. and Hariharan, I. K. (2004). The Drosophila F box protein archipelago regulates dMyc protein levels in vivo. *Curr Biol* **14**, 965-74.

Moore, L. A., Broihier, H. T., Van Doren, M., Lunsford, L. B. and Lehmann, R. (1998). Identification of genes controlling germ cell migration and embryonic gonad formation in Drosophila. *Development* **125**, 667-78.

Mozer, B. A. (2001). Dominant Drop mutants are gain-of-function alleles of the muscle segment homeobox gene (msh) whose overexpression leads to the arrest of eye development. *Dev Biol* **233**, 380-93.

Muller, D., Kugler, S. J., Preiss, A., Maier, D. and Nagel, A. C. (2005). Genetic modifier screens on Hairless gain-of-function phenotypes reveal genes involved in cell differentiation, cell growth and apoptosis in Drosophila melanogaster. *Genetics* **171**, 1137-52.

Nicholson, S. C., Gilbert, M. M., Nicolay, B. N., Frolov, M. V. and Moberg, K. H. (2009). The archipelago Tumor Suppressor Gene Limits Rb/E2F-Regulated Apoptosis in Developing Drosophila Tissues. *Curr Biol*.

Nolo, R., Abbott, L. A. and Bellen, H. J. (2000). Senseless, a Zn finger transcription factor, is necessary and sufficient for sensory organ development in Drosophila. *Cell* **102**, 349-62.

Paillard, L., Legagneux, V., Maniey, D. and Osborne, H. B. (2002). c-Jun ARE targets mRNA deadenylation by an EDEN-BP (embryo deadenylation element-binding protein)-dependent pathway. *J Biol Chem* **277**, 3232-5.

Pan, D. (2007). Hippo signaling in organ size control. *Genes Dev* **21**, 886-97.

Peng, S. S., Chen, C. Y., Xu, N. and Shyu, A. B. (1998). RNA stabilization by the AU-rich element binding protein, HuR, an ELAV protein. *EMBO J* **17**, 3461-70.

Pignoni, F. and Zipursky, S. L. (1997). Induction of Drosophila eye development by decapentaplegic. *Development* **124**, 271-8.

Riesgo-Escovar, J. R., Jenni, M., Fritz, A. and Hafen, E. (1996). The Drosophila Jun-N-terminal kinase is required for cell morphogenesis but not for DJun-dependent cell fate specification in the eye. *Genes Dev* **10**, 2759-68.

Saeboe-Larssen, S., Urbanczyk Mohebi, B. and Lambertsson, A. (1997). The Drosophila ribosomal protein L14-encoding gene, identified by a novel Minute mutation in a dense cluster of previously undescribed genes in cytogenetic region 66D. *Mol Gen Genet* **255**, 141-51.

Stofanko, M., Kwon, S. Y. and Badenhorst, P. (2008). A misexpression screen to identify regulators of Drosophila larval hemocyte development. *Genetics* **180**, 253-67.

Su, Y. C., Treisman, J. E. and Skolnik, E. Y. (1998). The Drosophila Ste20-related kinase misshapen is required for embryonic dorsal closure and acts through a JNK MAPK module on an evolutionarily conserved signaling pathway. *Genes Dev* **12**, 2371-80.

Sundaram, M. V. (2005). The love-hate relationship between Ras and Notch. *Genes Dev* **19**, 1825-39.

Tapon, N., Harvey, K. F., Bell, D. W., Wahrer, D. C. R., Schiripo, T. A., Haber, D. A. and Hariharan, I. K. (2002). salvador Promotes Both Cell Cycle Exit and Apoptosis in Drosophila and Is Mutated in Human Cancer Cell Lines. *Cell* **110**, 467-478.

Tapon, N., Ito, N., Dickson, B. J., Treisman, J. E. and Hariharan, I. K. (2001). The Drosophila tuberous sclerosis complex gene homologs restrict cell growth and cell proliferation. *Cell* **105**, 345-55.

Theisen, H., Purcell, J., Bennett, M., Kansagara, D., Syed, A. and Marsh, J. L. (1994). dishevelled is required during wingless signaling to establish both cell polarity and cell identity. *Development* **120**, 347-60.

Tseng, A. S., Tapon, N., Kanda, H., Cigizoglu, S., Edelmann, L., Pellock, B., White, K. and Hariharan, I. K. (2007). Capicua regulates cell proliferation downstream of the receptor tyrosine kinase/ras signaling pathway. *Curr Biol* **17**, 728-33.

Villa-Cuesta, E., de Navascues, J., Ruiz-Gomez, M., Diez del Corral, R., Dominguez, M., de Celis, J. F. and Modolell, J. (2003). Tufted is a gain-of-function allele that promotes ectopic expression of the proneural gene amos in Drosophila. *Genetics* **163**, 1403-12.

Wagner, E. F. and Nebreda, A. R. (2009). Signal integration by JNK and p38 MAPK pathways in cancer development. *Nat Rev Cancer* **9**, 537-49.

Weber, U., Paricio, N. and Mlodzik, M. (2000). Jun mediates Frizzled-induced R3/R4 cell fate distinction and planar polarity determination in the Drosophila eye. *Development* **127**, 3619-29.

White, K., Grether, M. E., Abrams, J. M., Young, L., Farrell, K. and Steller, H. (1994). Genetic control of programmed cell death in Drosophila. *Science* **264**, 677-83.

Zhai, R. G., Hiesinger, P. R., Koh, T. W., Verstreken, P., Schulze, K. L., Cao, Y., Jafar-Nejad, H., Norga, K. K., Pan, H., Bayat, V. et al. (2003). Mapping Drosophila mutations with molecularly defined P element insertions. *Proc Natl Acad Sci U S A* **100**, 10860-5.

Chapter III: The role of Notch activity in *ago* tumorigenesis

III.A. ABSTRACT

The *Drosophila* gene *archipelago* (*ago*) encodes the F-box specificity subunit of an SCF-type E3 ubiquitin ligase required for proteolysis of the Cyclin E, dMyc, and Trachealess proteins. It has been proposed that human *ago* degrades several additional targets, including the intracellular domain of the Notch receptor. Mutations in human *ago* (*hAgo*/*Fbw7*/*hCDC4*/*SEL-10*) are common in human cancers, yet the specific contribution of each Ago target to the overall biological consequences of *hAgo* loss is not clear. Here we assess the role of Notch signaling in growth and differentiation phenotypes resulting from loss of *ago* in the developing *Drosophila* eye. We show that *ago* antagonizes Notch activity but that Notch protein does not hyper-accumulate in *ago* mutant clones; therefore, Notch does not behave as a conventional *in vivo* target of Ago-mediated proteolysis in *Drosophila*. Additionally, transgenic overexpression of the Notch intracellular domain reduces overall Notch levels downstream of *ago* loss. As a result, we present evidence of a novel feedback loop in which a second, unidentified mechanism compensates for the lack of *ago* and downregulates Notch protein levels in cells. We characterize the role of Notch hyperactivity in *ago* mutant cells, showing that it affects both differentiation and growth pathways and present evidence of a link among *ago*, *Notch* and the pro-growth G1 cyclin *Cyclin D* (*CycD*). Unexpectedly, decreasing the dosage of either *Notch* or the CycD binding partner *cdk4* in an eye entirely mutant for *ago* results in a larger adult eye. This observation led to us to identify a role for *ago* in limiting p53-mediated apoptosis in the differentiating fly eye. Such a role in p53-dependent cell death mimics loss of *Fbw7* in the murine hematopoietic stem cell lineage. We are therefore currently testing the relationship among these genes and rates of

apoptosis in *ago* mutant eye discs as a means of further elucidating *ago*'s mechanisms in mammalian tumorigenesis.

In sum, these data indicate that a second pathway regulates Notch in parallel to *ago* and that elevated *Notch* activity in *ago* mutant tissues disrupts normal patterns of differentiation. This Notch hyperactivity is hypothesized to also promote apoptosis of *ago* cells in part via effects on levels of the G1 regulator CycD. The work presented here is a work in progress; therefore, additional experiments necessary to address gaps in the data will also be discussed.

III.B. INTRODUCTION

The *archipelago* (*ago*; variously known as *hAgo*/*Fbw7*/*CDC4*/*SEL-10*) gene encodes a conserved protein that inhibits cell proliferation in *Drosophila* and suppresses tumorigenesis in mammals. Alleles of *ago* were originally identified in a forward genetic screen in the *Drosophila* eye for genes that restrict cell proliferation in the larval eye disc (Moberg et al., 2001). The *ago* gene encodes an F-box/WD-repeat protein that acts as the substrate adaptor for an SCF E3 ubiquitin ligase complex. SCF-Ago targets the G1/S cell cycle regulator Cyclin E (CycE), the fly ortholog of the c-Myc proto-oncogene, dMyc, and the Trachealess transcription factor for degradation *in vivo* (Moberg et al., 2001; Moberg et al., 2004; Mortimer and Moberg, 2007). In *ago* mutant cells of the fly eye, CycE and dMyc proteins hyper-accumulate and drive a balanced increase in rates of division and growth, producing enlarged clones composed of normally sized cells (Moberg et al., 2004).

The human ortholog of *ago* is frequently mutated in a wide array of human tumor types, including those of endometrial, colorectal, and hematopoietic origin (reviewed in Welcker and Clurman, 2008). Moreover, loss of a single allele of murine *Fbw7* increases cancer incidence and collaborates with *p53* mutations to promote epithelial carcinogenesis (Mao et al., 2004). As with *ago*, growth suppression by *Fbw7* is linked to the defective degradation of various SCF substrates including CycE, c-Myc, the Notch intracellular domain, Presenilin, c-Jun, SREBP, and mTor kinase (reviewed in Mao et al., 2008; Welcker and Clurman, 2008). However, the roles of specific Ago/Fbw7 substrates in driving *in vivo* overgrowth phenotypes are not clear.

Fbw7 knock-out mice are embryonic lethal due to a combination of defects in

heart, vascular, and hematopoietic development (Tetzlaff et al., 2004; Tsunematsu et al., 2004). These phenotypes were primarily attributed to the stabilization of Notch protein and subsequent increase in Notch signaling. Likewise, conditional inactivation of *Fbw7* specifically in the T-cell lineage of mice demonstrated that Fbw7 regulates not only proliferation but also p53-dependent apoptosis and in a cell differentiation-dependent manner (Onoyama et al., 2007). Among known Fbw7 targets, only c-Myc and Notch accumulated in *Fbw7*-deficient thymocytes, and most of these conditional knock-out animals developed lymphomas. Accordingly, the highest *Fbw7* mutation rates (30%) in human cancer have been found in T-cell acute lymphoblastic leukemias (T-ALL) (O'Neil et al., 2007), and deregulation of the Notch pathway is central to T-ALL development (reviewed in Demarest et al., 2008). Therefore, understanding the role of Notch downstream of *ago/Fbw7* inactivation is an essential question in cancer biology.

Mammals have four *Notch* genes, but *Drosophila* has only one; moreover, misexpression of the N^{ICD} not only promotes tumor formation in mice and humans (Ellisen et al., 1991; Robbins et al., 1992; Uyttendaele et al., 1996; Zagouras et al., 1995) but also induces organ overgrowth in the fly (Hariharan and Bilder, 2006; Pan, 2007). Therefore, *Drosophila*'s simplicity provides and ideal system in which to study the evolutionarily conserved Notch pathway. Signaling through the Notch transmembrane receptor is primarily mediated by its intracellular domain (N^{ICD}), which controls a transcriptional program that is terminated upon its polyubiquitin and proteolytic degradation (reviewed in Bray, 2006). Although mammalian Fbw7 and its *Caenorhabditis elegans* ortholog Sel-10 have been shown to bind to and promote the polyubiquitination of Notch/Lin-12 both *in vitro* and *in vivo* (Gupta-Rossi et al., 2001;

Hubbard et al., 1997; Oberg et al., 2001; Wu et al., 2001), the interactions between fly Notch and Ago have not previously been studied. Therefore, the goal of this work is to determine the role of Notch in *ago* mutant tissue in order to establish a foundation for comparative analysis between invertebrate and vertebrate systems.

Here we report a work in progress to characterize Notch-dependent phenotypes downstream of *ago* inactivation. We show that Notch activity is increased in *ago* mutant tissue but that *ago* loss does not promote the stabilization of Notch protein, suggesting that Notch does not behave as a conventional *in vivo* target of Ago-mediated proteolysis in *Drosophila*. However, *in vivo* pulse-chase studies point toward the existence of a novel feedback mechanism that reduces levels of N^{ICD} in the absence of *ago*. We go on to characterize the role of Notch hyperactivity in *ago* mutant cells and show that it influences both differentiation and growth pathways, presenting evidence of a conserved link between Notch and the pro-growth G1 cyclin, *Cyclin D* (*CycD*). Unexpectedly, decreasing the dosage of either *Notch* or the CycD binding partner *cdk4* in an eye entirely mutant for *ago* results in a larger adult eye, meaning that *Notch* and *cdk4* can act as anti-growth factors in *ago* mutant tissues. This finding led to the identification of a role for *ago* in limiting p53-mediated apoptosis in the differentiating cells of the pupal eye, potentially via the misexpression of Notch and subsequent transcriptional up-regulation of *CycD*. However, the precise apoptotic signals remain to be determined. Thus, our findings describe the initial characterization of Notch-dependent phenotypes in *ago* mutant tissue with the aim of shedding light on the roles of the specific Ago/Fbw7 substrates in cellular transformation. Additional experiments are necessary to fill gaps in

the data. Such experiments will be suggested here, and long-term project goals will be addressed in the future directions (see Chapter V.B).

III.C. RESULTS

III.C1. *ago* antagonizes *Notch in vivo*

To address the question of whether the Notch intracellular domain (N^{ICD}) is an *in vivo* target of Ago polyubiquitination and subsequent proteolytic degradation in *Drosophila*, we tested two main predictions of this model: (1) *ago* behaves as a genetic and molecular antagonist of Notch activity; and (2) N^{ICD} is stabilized in *ago* mutant tissue. A third prediction is that Ago physically binds to the N^{ICD} via its WD repeats; this remains to be tested. The first of these predictions will be addressed in this section.

The *C. elegans ago* ortholog, *sel-10*, was first identified in a genetic screen as a suppressor of *Notch/Lin-12* loss-of-function phenotypes (Sundaram and Greenwald, 1993) and was later shown to physically interact with the intracellular domains of *C. elegans* Lin12 and mammalian Notch1 and Notch4 (Gupta-Rossi et al., 2001; Hubbard et al., 1997). Consistent with the model that Notch is an Ago substrate in flies, we confirmed that, like *sel-10*, *ago* is a suppressor of Notch loss-of-function phenotypes *in vivo*: females heterozygous for the null allele N^{54l9} have a stereotypical notching phenotype in the adult wing margin (Figure III.1B, as in Dexter, 1914); creating a *trans*-heterozygous combination by introducing a null or strong loss-of-function *ago* allele into this background suppresses the wing notching phenotype (Figure III.1C,D). Consistent with this observed genetic interaction, *ago* mutant eye tissue exhibits previously described *Notch* gain-of-function phenotypes (Fortini et al., 1993): adult eyes mutant for *ago* have moderate bristle defects and reduced numbers of photoreceptors (see Figure III.6). We discuss below that *Notch* is indeed responsible for these phenotypes. Thus, *ago*

has characteristic phenotypes of *Notch* overexpression and behaves as a genetic antagonist of *Notch* in our system.

To test whether *ago* restricts Notch activity *in vivo*, clones of *ago* mutant cells were generated in the presence of the Notch-inducible transcriptional reporter, *E(spl)mß-CD2* (de Celis et al., 1998). Posterior to the morphogenetic furrow (MF), *CD2* expression is detected in the interommatidial cells, outlining a single cell from each photoreceptor cluster in a mirror-image pattern along the equator (Figure III.2A, Dominguez and de Celis, 1998). In *ago* mutant clones, reporter activity is strongly elevated; the degree of activation exceeds that observed in wild-type twinspots (marked by Bgal, blue; Figure III.2B-B'). While the reporter is active in both the dividing cells anterior to the MF and in the differentiating cells posterior to the MF, *ago*-dependent reporter up-reguation is most strongly pronounced posterior to the MF. Notch hyperactivity is not limited to the larval eye; the same reporter also detects increased Notch activity in ago^{1} clones in the pupal eye (Figure III.2D-D'). Though Notch transcriptional activity is increased in *ago* mutant eye tissue, the same Notch hyperactivity is not evident in the wing: we observe no significant elevation of *E(spl)mß-CD2* reporter expression or of other standard read-outs of Notch activity in the wing, such as the Wingless or Cut proteins (data not shown). The genetic antagonism between *ago* and *Notch* in the wing may therefore be more complex than we previously assumed. Thus, mutations in *ago* promote increased Notch activity most strongly in differentiating eye tissue—posterior to the MF and in the pupal eye.

Together, these data show that *ago* behaves as a genetic antagonist of *Notch* in the wing and as a molecular antagonist of Notch in the eye, thereby fulfilling the first prediction of our model.

Figure III.1. *ago* dominantly suppresses *Notch* wing phenotypes.

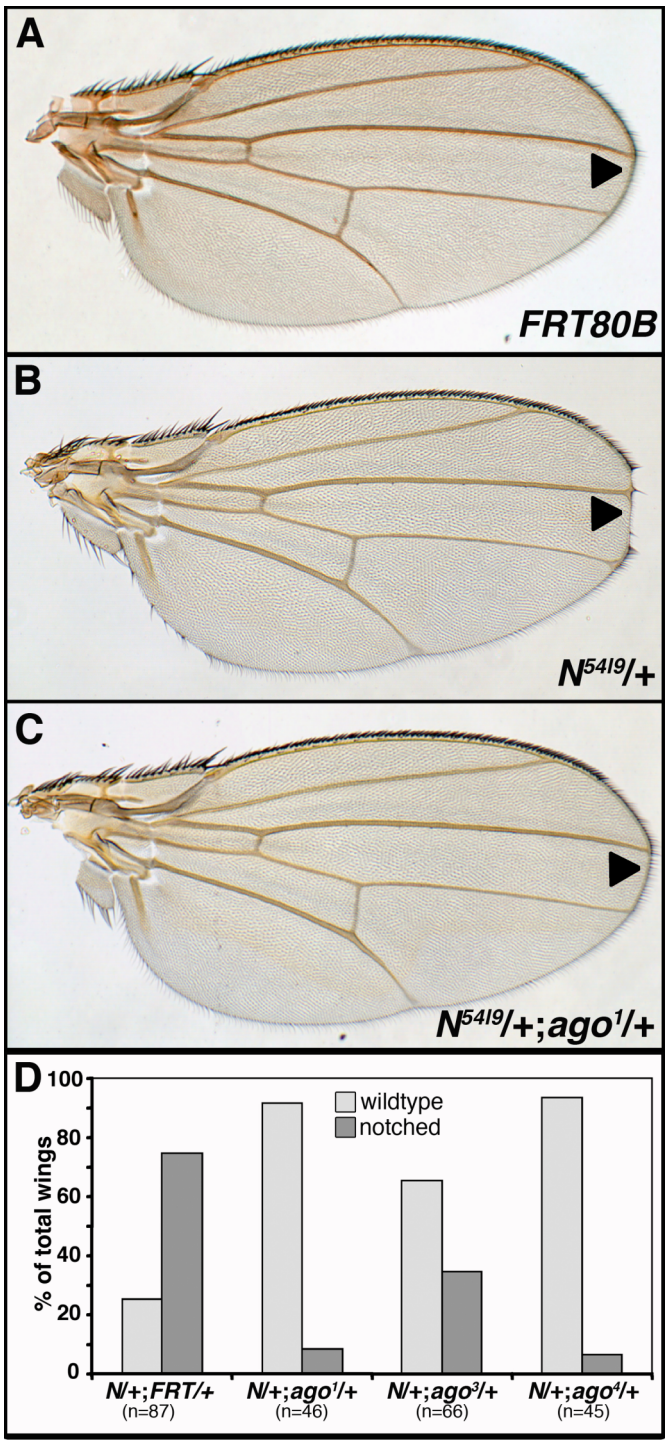

(A-C) Light microscopic images of (A) *FRT80B*, (B) $N^{54/9}$/+;;*FRT80B*/+, and (C) $N^{54/9}$/+;;*FRT,ago*^{1}/+ female adult wings tracking wing notching (*arrowhead*). (D) Quantification of this interaction shows that *ago* behaves as a *Notch* antagonist in this assay. Bars indicate percentage of wings with indicated phenotype: light gray, wildtype; dark gray, notched.

Figure III.2. *ago* restricts Notch activity in eye cells.

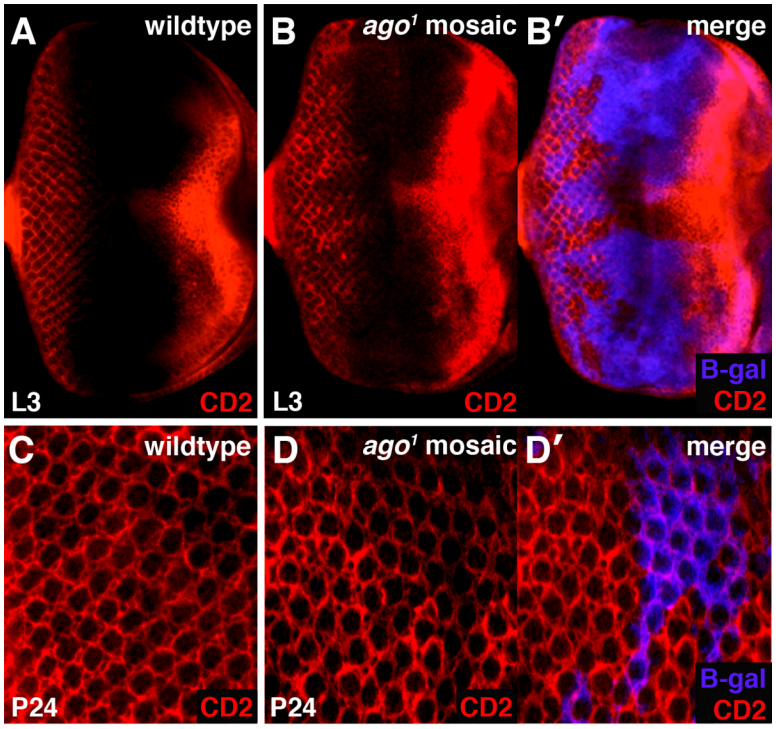

Activity of the *E(spl)mß-CD2* Notch reporter assessed via levels of CD2 (red) is increased in *ago*^{1} clones in both the third instar larval (B, B') and the 24 hour pupal (C, C') eye imaginal disc. (B', C') Clones are marked by the absence of blue B-gal staining. Panels A and C show wild-type Notch reporter expression in the larval and pupal eye, respectively. In this an all subsequent figures, posterior is to the left.

III.C2. *ago* loss does not stabilize Notch protein *in vivo*

We showed that *ago* antagonizes N^{ICD} transcriptional activity in differentiating eye tissue (see above), but mutations in the *ago* ortholog *Fbw7* lead to a stabilization of N^{ICD} protein in mouse tissues (Tetzlaff et al., 2004; Tsunematsu et al., 2004). Therefore, if Notch is an *in vivo* target of Ago-mediated proteolysis, then a second prediction is that Notch protein should be selectively stabilized and, as a result, accumulate in *ago* mutant clones. The ago^1 allele is a functional null containing a premature stop codon in the fourth WD repeat that interferes with the ability of the Ago protein to bind substrates like Cyclin E and dMyc. These bona fide Ago targets are indeed stabilized in ago^1 eye clones (Moberg et al., 2001; Moberg et al., 2004). But unlike Cyclin E and dMyc, an antibody recognizing the cytoplasmic domain of Notch (anti-N9C6) reveals no accumulation of N^{ICD} in *ago* mutant eye or wing clones by immunofluorescence or Western blot analysis (Figure III.3).

This lack of N^{ICD} stabilization upon *ago* loss could be the result of several scenarios: (1) Ago does not play a role in degrading N^{ICD}, so the levels of N^{ICD} are not significantly increased above background in *ago* mutant tissue; (2) Ago does regulate N^{ICD} levels, but the epitope recognized by anti-N9C6 is 'hidden' in *ago* mutant cells by association with other proteins; or (3) a parallel mechanism exists that retards the build-up of excess N^{ICD} in *ago* mutant cells. The second scenario has already been addressed by performing a Western blot for N^{ICD} in *ago* mutant eye discs (see Figure III.3C). If the epitope were endogenously hidden, then the denaturing conditions of Western blot analysis would have allowed us to observe any increase in Notch protein. Moreover, nuclear accumulation of N^{ICD} has been observed with the same anti-N9C6 antibody in

cells lacking other factors involved in the turnover of Notch (eg., *phyl*, Nagaraj and Banerjee, 2009), suggesting that the lack of N^{ICD} accumulation in *ago* cells is not due to the limits of the 9C6 antibody. However, to further address this possibility, we also performed immunofluorescence on *ago*^{1} mosaic eye discs with a second antibody that recognizes the cleaved, active form of human Notch1 (anti-Notch1,Val1744). We also observed no effect of *ago* loss on this epitope, suggesting either that the antibody does not cross-react with fly Notch or that there is no selective stabilization of N^{ICD} in *ago* cells (data not shown).

Although the Notch-induced transcription of genes has been extensively reported, the endogenous, nuclear N^{ICD} is virtually undetectable in normal cells. Therefore, we tested whether exogenously expressed N^{ICD} could be stabilized upon *ago* loss. To do so, we performed an *in vivo* pulse-chase experiment. Briefly, we subjected the fly to a heat-shock pulse of N^{ICD} expression and then fixed discs at several time points post-heat shock to detect N^{ICD} levels. If the *Drosophila* N^{ICD} is indeed an *in vivo* target of Ago, then we would expect to see selective N^{ICD} stabilization in *ago* mutant tissue coincident with effective N^{ICD} turnover in adjacent wild-type tissue. Such protein stabilization following a N^{ICD} heat-shock pulse has been shown in wing disc cells expressing a dominant negative subunit of the proteosome (Figure 4A, Schweisguth, 1999), and we were able to recapitulate this experiment as a positive control for our assay (Figure III.4B). Unexpectedly, the N^{ICD} is not stabilized in *ago* mutant clones as early as 30 min following heat shock, and overall levels of membrane-associated, endogenous Notch are lower specifically in *ago* mutant cells in both the larval wing and eye imaginal discs (Figure III.4C-E"). Thus, loss of *ago* appears to synergize with exogenous N^{ICD} to

downregulate levels of endogenous Notch protein. This downregulation of Notch is not simply due to an increase in cell death: we detect no increase in cleaved Caspase-3 in these same cells, and Notch levels are also decreased upon N^{ICD} transgenic overexpression in apoptosis-deficient *ago*^{X2}*,H99* clones (data not shown). A similar phenomenon has also been observed in the early pupal eye (KHM, unpublished): when full-length Notch is transgenically expressed under the control of an eye-specific driver, an overall reduction in Notch protein is obeserved in *ago*^{1} clones relative to wild-type tissue (Figure III.4F-F").

Collectively, these data suggest that Notch does not behave as a conventional Ago target in flies (eg., CycE, dMyc) but argue strongly for proposed scenario three—the existence of a parallel feedback mechanism that blocks the accumulation of excess Notch protein upon loss of *ago*. Based on our data, we can speculate as to some of the features of this mechanism. In this hypothetical feedback model (see Figures V.2-V.3), transgenic overexpression of N^{ICD} increases the already high levels of Notch activity in *ago* mutant tissue. This extremely elevated Notch activity triggers a signal that feeds back to hyperactivate a parallel mechanism. This second, unidentified mechanism then downregulates Notch to levels below baseline, resulting in an *ago*-specific decrease in Notch protein. Such a feedback model provides a possible explanation for our inability to observe N^{ICD} stabilization in *ago* mutant tissue under normal conditions: increased Notch activity promotes the upregulation of a parallel mechanism that compensates for lack of *ago* and downregulates Notch protein to baseline levels in cells, thereby limiting the amount of N^{ICD} and appearing as no change in Notch protein levels in *ago*^{1} mosaic imaginal discs (see Figure III.3).

While these data are indicative of a feedback mechanism, the results are insufficient to directly address the aim of this part of the project—whether Notch an *in vivo* Ago substrate. Indeed, *ago* behaves as a Notch antagonist, and the fly N^{ICD} contains two putative Ago binding sites as defined for Fbw7 binding to CycE, c-Myc, c-Jun, and Notch1 (Figure III.5, Hao et al., 2007). However, Presenilin (Psn), a component of the gamma-secretase complex responsible for releasing N^{ICD} from the membrane (Struhl and Greenwald, 2001), is also a proposed Fbw7 substrate (Li et al., 2002; Wu et al., 1998). Therefore, if Psn, rather than N^{ICD}, is the actual Ago target in flies, then the machinery responsible for N^{ICD} turnover would remain intact in *ago* mutant tissue and accumulation of Psn could result in the phenotypes we observe—a genetic interaction between *ago* and *Notch* and an increase in Notch activity without subsequent N^{ICD} accumulation. Notably, Psn and other proteins involved in Notch signaling, including Delta, Serrate, Su(H) and Mastermind, do not contain consensus Ago binding sites and do not accumulate in ago^{1} eye clones (data not shown). It is therefore likely that Notch is a bona fide target of Ago. However, to confirm this interaction, future experiments should be conducted to show that Notch physically binds Ago WD repeats *in vitro*. If binding occurs, then the proposed feedback mechanism could be legitamitely suspected.

Figure III.3. Levels of the N^{ICD} are unchanged in *ago* mutant tissues.

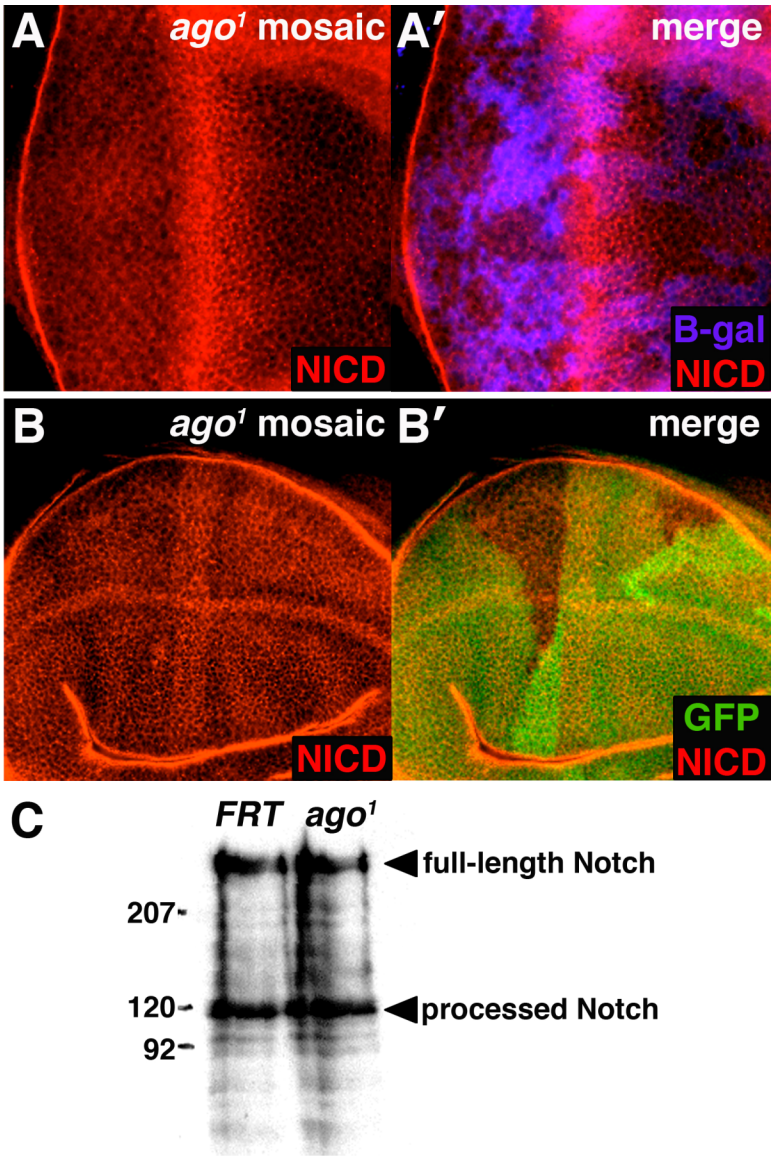

Confocal images of larval eye (A, A') and wing (B, B') imaginal discs show no change in the levels of the Notch intracellular domain in *ago* mutant clones (A-B'; N^{ICD} in red, mutant tissue lacks fluorescence). Immunoblot for the N^{ICD} in *FRT* control and *ago* mutant larval eye tissue lysates also shows no change in protein levels (C; 20 pairs of eye discs loaded in each lane).

Figure III.4. Transgenic Notch is not stabilized in *ago* mutant tissues.

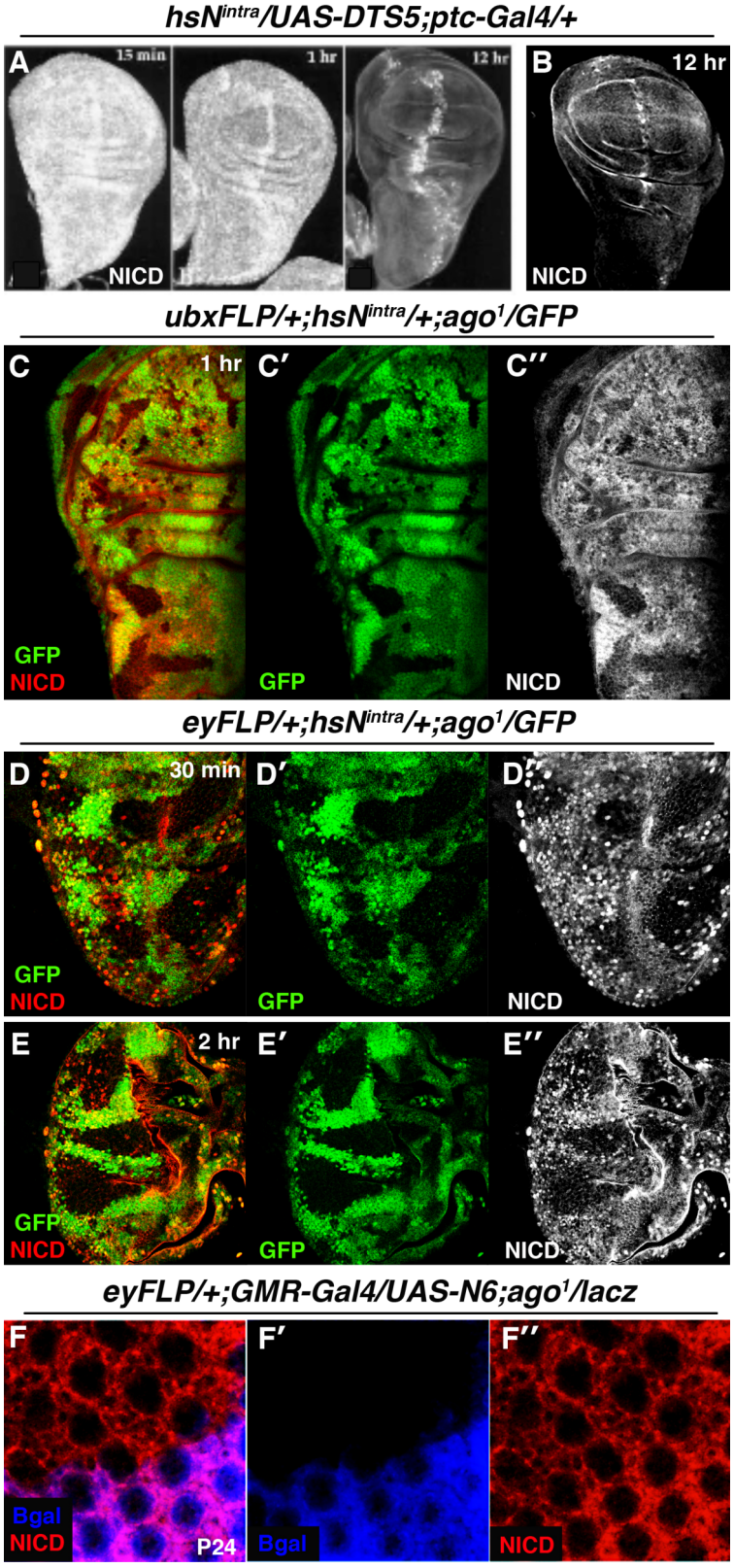

Confocal images of the indicated genotypes. (A-E") Time indicated is time of fixation post heat-shock pulse of $Notch^{intra}$. (A) Schweisguth *et al*. showed that N^{ICD} is stabilized in the *ptc-Gal4* wing disc domain expressing a dominant negative proteosomal subunit (DTS5, Belote and Fortier, 2002) at 15 min, 1 hour, and 12 hours post heat shock (Schweisguth, 1999). (B) Recapitulation of the experiment in panel A; N^{ICD} is stabilized in cells expressing a dominant negative proteosomal subunit at 12 hours following heat shock. (C-F") Merged confocal sections of ago^{1} clones marked by the absence of fluorescence. N^{ICD} is downregulated in ago^{1} larval wing clones 1 hour post heat shock (C-C") and in larval eye clones 30 min (D-D") or 2 hours (E-E") post heat shock. (F-F") N^{ICD} is downregulated in ago^{1} P24 eye clones upon transgenic expression of full-length Notch (N6).

Figure III.5. Fly Notch has consensus Ago binding sites.

MQSQRSRRRSRAPNTWICFWINKMHAVASLPASLPLLLLTLAFANLPNTVRGTDTALVAASCTSVGCQNGGTCVTQLN
GKTYCACDSHYVGDYCEHRNPCNSMRCQNGGTCQVTFRNGRPGISCKCPLGFDESLCEIAVPNACDHVTCLNGGTC
QLKTLEEYTCACANGYTGERCETKNLCASSPCRNGATCTALAGSSSFTCSCPPGFTGDTCSYDIEECQSNPCKYGGTC
VNTHGSYQCMCPTGYTGKDCDTKYKPCSPSPCQNGGICRSNGLSYECKCPKGFEGKNCEQNYDDCLGHLCQNGGTC
IDGISDYTCRCPPNFTGRFCQDDVDECAQRDHPVCQNGATCTNTHGSYSCICVNGWAGLDCSNNTDDCKQAACFYGA
TCIDGVGSFYCQCTKGKTGLLCHLDDACTSNPCHADAICDTSPINGSYACSCATGYKGVDCSEDIDECDQGSPCEHNGI
CVNTPGSYRCNCSQGFTGPRCETNINECESHPCQNEGSCLDDPGTFRCVCMPGFTGTQCEIDIDECQSNPCLNDGTC
HDKINGFKCSCALGFTGARCQINIDDCQSQPCRNRGICHDSIAGYSCECPPGYTGTSCEININDCDSNPCHRGKCIDDV
NSFKCLCDPGYTGYICQKQINECESNPCQFDGHCQDRVGSYYCQCQAGTSGKNCEVNVNECHSNPCNNGATCIDGIN
SYKCQCVPGFTGQHCEKNVDECISSPCANNGVCIDQVNGYKCECPRGFYDAHCLSDVDECASNPCVNEGRCEDGINE
FICHCPPGYTGKRCELDIDECSSNPCQHGGTCYDKLNAFSCQCMPGYTGQKCETNIDDCVTNPCGNGGTCIDKVNGY
KCVCKVPFTGRDCESKMDPCASNRCKNEAKCTPSSNFLDFSCTCKLGYTGRYCDEDIDECSLSSPCRNGASCLNVPG
SYRCLCTKGYEGRDCAINTDDCASFPCQNGGTCLDGIGDYSCLCVDGFDGKHCETDINECLSQPCQNGATCSQYVNS
YTCTCPLGFSGINCQTNDEDCTESSCLNGGSCIDGINGYNCSCLAGYSGANCQYKLNKCDSNPCLNGATCHEQNNEYT
CHCPSGFTGKQCSEYVDWCGQSPCENGATCSQMKHQFSCKCSAGWTGKLCDVQTISCQDAADRKGLSLRQLCNNG
TCKDYGNSHVCYCSQGYAGSYCQKEIDECQSQPCQNGGTCRDLIGAYECQCRQGFQGQNCELNIDDCAPNPCQNGG
TCHDRVMNFSCSCPPGTMGIICEINKDDCKPGACHNNGSCIDRVGGFECVCQPGFVGARCEGDINECLSNPCSNAGTL
DCVQLVNNYHCNCRPGHMGRHCEHKVDFCAQSPCQNGGNCNIRQSGHHCICNNGFYGKNCELSGQDCDSNPCRVG
NCVVADEGFGYRCECPRGTLGEHCEIDTLDECSPNPCAQGAACEDLLGDYECLCPSKWKGKRCDIYDANYPGWNGG
SGSGNDRYAADLEQQRAMCDKRGCTEKQGNGICDSDCNTYACNFDGNDCSLGINPWANCTANECWNKFKNGKCNE
ECNNAACHYDGHDCERKLKSCDSLFDAYCQKHYGDGFCDYGCNNAECSWDGLDCENKTQSPVLAEGAMSVVMLMN
VEAFREIQAQFLRNMSHMLRTTVRLKKDALGHDIIINWKDNVRVPEIEDTDFARKNKILYTQQVHQTGIQIYLEIDNRKCTE
CFTHAVEAAEFLAATAAKHQLRNDFQIHSVRGIKNPGDEDNGEPPANVKYVITGIILVIIALAFFGMVLSTQRKRAHGVTW
FPEGFRAPAAVMSRRRRDPHGQEMRNLNKQVAMQSQGVGQPGAHWSDDESDMPLPKRQRSDPVSGVGLGNNGGY
ASDHTMVSEYEEADQRVWSQAHLDVVDVRAIMTPPAHQDGGKHDVDARGPCGLTPLMIAAVRGGGLDTGEDIENNED
STAQVISDLLAQGAELNATMDKTGETSLHLAARFARADAAKRLLDAGADANCQDNTGRTPLHAAVAADAMGVFQILLRN
RATNLNARMHDGTTPLILAARLAIEGMVEDLITADADINAADNSGKTALHWAAAVNNTEAVNILLMHHANRDAQDDKDET
PLFLAAREGSYEACKALLDNFANREITDHMDRLPRDVASERLHHDIVRLLDEHVPRSPQMLSMTPQAMIGSPPPGQQQ
PQLITQPTVISAGNGGNNGNGNASGKQSNQTAKQKAAKKAKLIEGSPDNGLDATGSLRRKASSKKTSAASKKAANLNG
LNPGQLTGGVSGVPGVPPTNSAAQAAAAAAAAVAAMSHELEGSPVGVGMGGNLPSPYDTSSMYSNAMAAPLANGNP
NTGAKQPPSYEDCIKNAQSMQSLQGNGLDMIKLDNYAYSMGSPFQQELLNGQGLGMNGNGQRNGVGPGVLPGGLC
GMGGLSGAGNGNSHEQGLSPPYSNQSPPHSVQSSLALSPHAYLGSPSPAKSRPSLPTSPTHIQAMRHATQQKQFGGS
NLNSLLGGANGGGVVGGGGGGGGGVGQGPQNSPVSLGIISPTGSDMGIMLAPPQSSKNSAIMQTISPQQQQQQQQQ
QQQQHQQQQQQQQQQQQQQQQQLGGLEFGSAGLDLNGFCGSPDSFHSGQMNPPSIQSSMSGSSPSTNM**LSPSS**
QHNQQAFYQY**LTPSSQH**SGGHTPQHLVQTLDSYPTPSPESPGHWSSSSPRSNSDWSEGVQSPAANNLYISGGHQA
NKGSEAIYI

The amino acid sequence of *Drosophila* Notch contains two putative Ago binding sites (red) in its C-terminal domain. The Fbw7 consensus substrate binding sequence is defined as H-X-H-H-H-pT/S-P-P-X-pS/T, with H representing a hydrophobic residue and X any amino acid.

III.C3. *Notch* influences differentiation and growth downstream of *ago*

Notch has been shown to be an Ago substrate in other systems, and we have shown that *ago* behaves as a Notch antagonist in flies. Therefore, in an attempt to further elucidate mechanisms of mammalian tumorigenesis due to mutations in *hAgo/Fbw7*, we focused on determining which of the *ago* mutant phenotypes can be attributed to deregulation of Notch activity. We found that the Notch hyperactivity in *ago* mutant cells affects both differentiation and growth pathways.

The *ago* complementation group was initially identified in a screen for growth suppressors because clones of *ago* mutant tissue have a growth advantage in the fly eye—the white homozygous mutant clones overgrow relative to the red wild-type tissue (Figure III.6A). Upon closer examination, *ago* mutant clones in the eye also have a slight roughness due to defects in the number and location of interommatidial bristles. Additionally, each ommatidium should contain eight photoreceptors arranged in a trapezoidal pattern (Ready et al., 1976). However, thin tissue sections of the adult eye reveal underlying differentiation defects—*ago* mutant cells have fewer than the wild-type number of photoreceptors (Figure III.6D), a phenotype also observed following expression of Notch transgenes in the eye (Fortini et al., 1993). Therefore, *ago* mutations result in defects in two main cellular processes in the eye—differentiation and growth. To test if any of these cellular phenotypes are due to increased Notch activity, we again examined each *ago* mutant phenotype but in a background heterozygous for *Notch*. While genetic reduction of *Notch* does not strongly affect the ratio of red:white tissue in the ago mosaic eye, *Notch* heterozygosity rescues the bristle roughness on the surface of the adult eye and the photoreceptor number defect. The N^{54l9}/+,ago^{1} mosaic eye appears smoother

than the ago mosaic control (Figure III.6B; CKB, pers. obs.), and the eye sections show an increase in the number of ommatidium with a wild-type complement of photoreceptors (Figure III.6E,F). Therefore, Notch plays an obvious role in *ago* mutant differentiation defects but does not play a dosage-sensitive role in the clonal overgrowth associated with *ago* alleles.

Because Notch has known roles not only in differentiation but also in growth of the eye (e.g., Dominguez and de Celis, 1998), we searched further for a connection between Notch activity and *ago*'s growth-suppressive properties. In the initial phenotypic characterization of *ago* mutations, we noticed that levels of the pro-growth G1 cyclin, Cyclin D (CycD), are increased in *ago* mutant larval eye clones posterior to the MF and in pupal eye clones (Figure III.7A-B'). As measured by quantitative realtime PCR (qPCR), levels of the *CycD* transcript are also increased in the *ago* mutant eye (Figure III.7E). Because CycD is increased at the same space and time in development as we observe for the Notch reporter (in the differentiating cells posterior to the MF and in the pupal eye), we tested the hypothesis that this *CycD* up-regulation is a consequence of increased Notch activity. Indeed, not only is overexpression of Notch posterior to the MF sufficient to phenocopy the up-regulation of *CycD* (compare Figure III.7C&D, III.7E), but reducing *Notch* activity also dominantly restores CycD protein to normal levels in *ago* mutant cells (Figure III.7F-F'). Likewise, an allele of the CycD partner *cdk4* is a strong enhancer of *Notch* mutant wing phenotypes (Figure III.8). Thus, genetic interactions confirm our basic model that *CycD* is downstream of Notch activity and indicate that *Notch* may affect the CycD pathway in other tissues as well. This Notch

transcriptional regulation of *CycD* is a conserved function—*cyclin D1* is a known Notch target in mammalian systems (Ronchini and Capobianco, 2001).

We showed that Notch is responsible for CycD elevation in *ago* clones and that overexpression of Notch is sufficient to increase *CycD* transcript (see Figure III.7). We next tested whether Notch is required for baseline *CycD* expression by detecting CycD protein levels in eye clones mutant for Notch pathway members. Endogenous CycD expression remains unchanged in tissue mutant for *Psn* or doubly mutant for the Notch ligands *Delta* (*Dl*) and *Serrate* (*Ser*) (Figure III.9), indicating that while Notch is sufficient for the ectopic overexpression of *CycD*, Notch pathway activity is not required for the normal patterns of CycD expression.

With this established link between *Notch* and *CycD* downstream of *ago*, we sought to determine roles for these genes in *ago* mutant growth phenotypes. We therefore looked for effects on eye size. *Drosophila* eyes/heads composed almost entirely of *ago* mutant tissue were generated using the ago^{1} allele and the 3L *Minute* (*M(3)*) allele $RpL14^{1}$ (Saeboe-Larssen et al., 1997). $RpL14^{1}$ is a recessive, cell-lethal mutation that kills *M(3)/M(3)* cells, allowing ago^{1}/ago^{1} cells to populate the eye-antennal disc and adult structures derived from it. While alleles of *ago* are sufficient to induce hyperplasia of some organs, they paradoxically shrink the size of the adult eye—$ago^{1}/M(3)$ adult eyes are smaller than control eyes (Figure 9, Nicholson et al., 2009). This small eye phenotype reflects a requirement for *ago* to restrict apoptotic activity of the *rbf1/e2f1* pathway adjacent to the eye-specific MF: *ago* mutant cells display elevated *de2f1* activity, express the pro-death dE2f targets *hid* and *rpr*, and undergo high rates of apoptosis, resulting in a 'stripe of death' just anterior to the MF in *ago* mutant eye tissue (Nicholson et al., 2009).

Blocking death by making the eye doubly mutant for both *ago* and either the *H99* deletion, which removes *rpr*, *grm*, and *hid* (White et al., 1994), or an allele of *hid* completely rescues the $ago^{1}/M(3)$ small eye size (see quantification in Figure 9, Nicholson et al., 2009). Notch and CycD can both promote tissue growth in *Drosophila* (Datar et al., 2000; Hariharan and Bilder, 2006; Meyer et al., 2000; Pan, 2007). We therefore hypothesized that reducing the pro-growth activities of Notch and/or CycD would further enhance this *ago/M(3)* phenotype, resulting in a smaller eye. Because available *CycD* alleles have dominant eye phenotypes (CKB, pers. obs.), we used an allele of Cdk4 to reduce CycD activity in these assays. However, we saw the opposite result: decreasing the dosage of either *Notch* or *cdk4* in an $ago^{1}/M(3)$ eye results in a larger adult eye (Figure III.10). In fact, the *Notch* and *cdk4* alleles dominantly rescue the *ago/M(3)* small eye size to the same extent as alleles of members of the *rbf1/e2f1* pathway, including $cycE^{AR95}$ and $e2f1^{rM729}$ (see quantification in Figure III.10B). Therefore, we tested the ability of N^{54l9} and $cdk4^{3}$ to dominantly rescue the *e2f1*-dependent stripe of death in the ago^{1} mutant larval eye, but neither allele affected the observed rates of apoptosis at this stage (SCN, pers. comm.). To more firmly establish roles for Notch and CycD in apoptosis resulting from *ago* loss, we performed a genetic test and showed that a block in cell death using the *H99* deficiency is epistatic to the effects of reducing *Notch* activity: N^{54l9}/+ cannot further increase the size of the ago^{x2},*H99/M(3)* eye (Figure III.10B). This interaction further supports a model whereby *Notch* and, by extension, *cdk4* rescue $ago^{1}/M(3)$ eye size by reducing cell death rather than by increasing cell proliferation, perhaps suggesting roles for Notch and CycD in cell death of *ago* cells at a later stage in eye development.

In sum, these data identify a role for Notch-dependent *CycD* transcription downstream of *ago*, indicate that elevated *Notch* activity disrupts normal patterns of differentiation in *ago* mutant tissues, and suggest roles for Notch and CycD in promoting apoptosis downstream of mutations in the *ago* gene. Additionally, although *Notch* and *cdk4* act in the same direction with respect to ago eye size, the activities of Notch and CycD appear to behave differently with respect to differentiation phenotypes: as previously mentioned, *Notch* heterozygosity not only rescues *ago* photoreceptor defects but also results in a smoother adult eye; however, reducing *cdk4* does not markedly affect the bristle roughness of the *ago* mutant eye (see Figure III.6). We, therefore, may have uncovered a pathway bifurcation of effects on differentiation and growth/death downstream of Notch acitvity in *ago* mutant tissue (Figure III.11). Since *Notch* and *cdk4* both dominantly rescue $ago^{1}/M(3)$ eye size, this model would be further confirmed if future experiments found that *cdk4* heterozygosity is unable to rescue defects in photoreceptor number in the *ago* mutant eye. These additional data would support the idea that Notch regulates differentiation downstream of *ago* independently of its effects on *CycD*.

Figure III.6. Effects of *Notch* and *cdk4* gene dosage on *ago* differentiation defects.

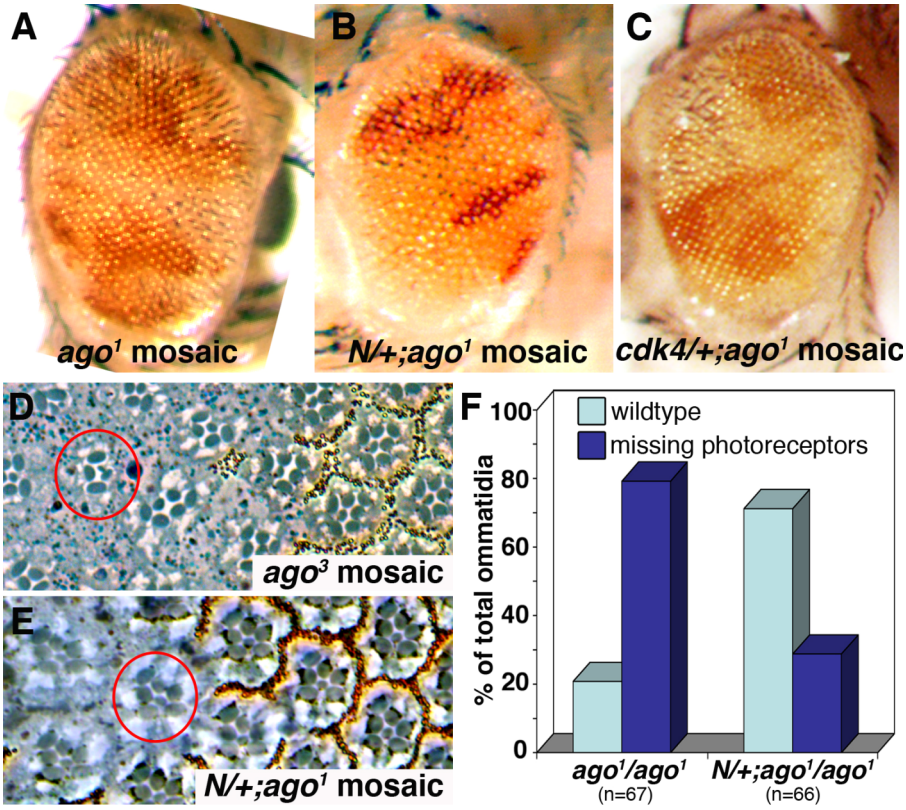

(A-C) Light microscopic images of *ago*^{1} mosaic adult female eyes of the indicated genotypes. Note that reducing *Notch* (B) but not *cdk4* (C) rescues bristle roughness of *ago*^{1} mosaic eye (A). (D, E) Thin tissue sections of the adult eye; *ago* clones on left marked by lack of pigment granules. (D) *ago*^{3} mutant ommatidia have reduced numbers of photoreceptors (red circle). (E) Reducing *Notch* restores wild-type numbers of photoreceptors in *ago* mutant ommatidia (red circle). (F) Quantification of effect in D, E shows percentage of ommatidia with wild-type numbers (light blue bars) or missing (dark blue bars) photoreceptors in the indicated genotypes.

Figure III.7. Notch up-regulates *Cyclin D* transcription in *ago* mutant tissue.

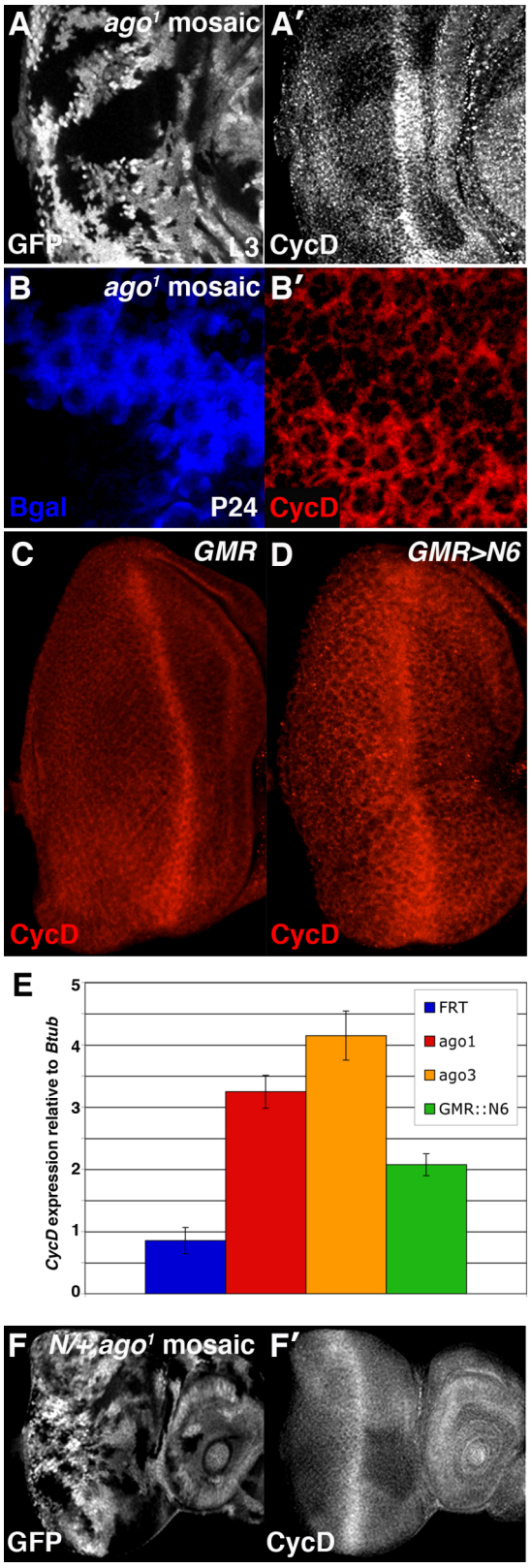

(A-B') Merged confocal sections show elevated Cyclin D protein in *ago*^{1} clones in larval (A, A') and 24h pupal (B, B') eye discs. (C, D) CycD protein expression in control (C) and Notch-overexpressing (GMR-Gal4/UAS-N6) larval eye discs. (E) *CycD* transcription is increased greater than 2.5 fold in both *ago* mutant and Notch-overexpressing eye tissue by qPCR analysis. (F, F') Reducing *Notch* dosage is sufficient to restore wild-type Cyclin D levels in *ago*^{1} clones. *ago* mutant clones marked by the absence of fluorescence.

Figure III.8. *cdk4* is a strong enhancer of *Notch* mutant wing phenotypes.

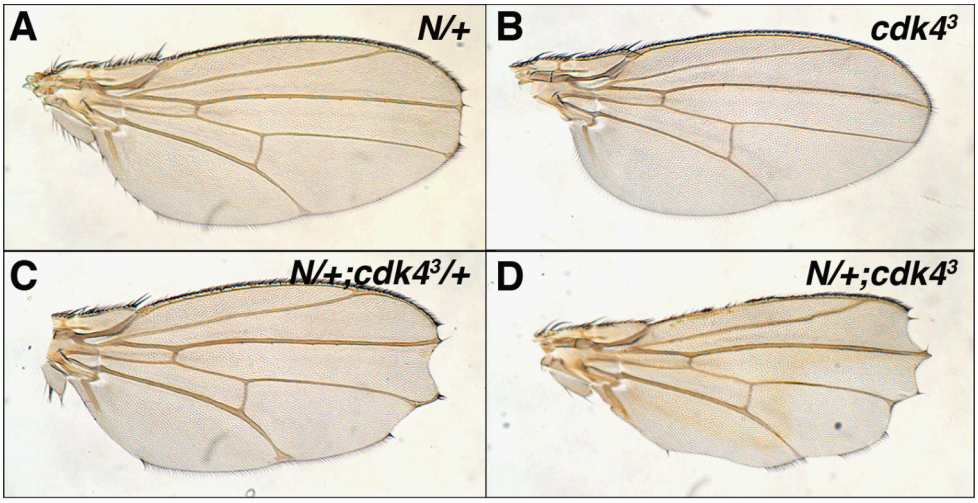

(A-D) Light microscopic images of (A) $N^{54/9}$/+, (B) $cdk4^{3}/cdk4^{3}$, (C) $N^{54/9}$/+;$cdk4^{3}$/+, and (D) $N^{54/9}$/+;$cdk4^{3}/cdk4^{3}$ female adult wings tracking wing notching.

Figure III.9. Notch pathway activity is not required for baseline CycD expression.

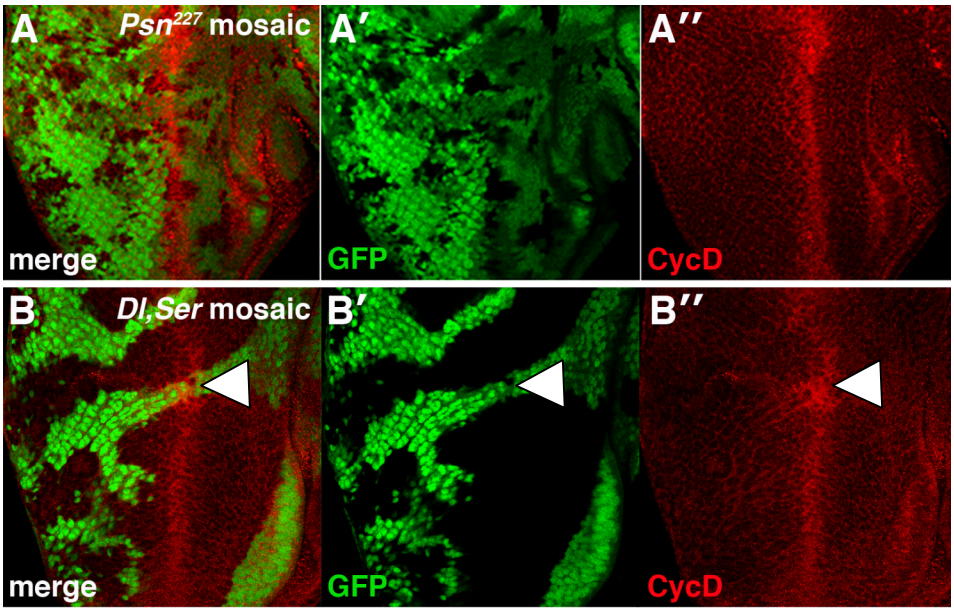

Merged confocal sections detecting CycD expression in larval eye discs. (A-A") *Psn*^{227} clones marked by the absence of GFP. (B-B") *Dl*^{RevF10},*Ser*^{RX82} double mutant clones marked by the absence of GFP; the bright spot of CycD expression (arrowhead) is due to a tear in the disc. Note that normal patterns of CycD are not altered in mutant tissue.

Figure III.10. Modification of *ago* mutant eye size by growth regulators and signaling components.

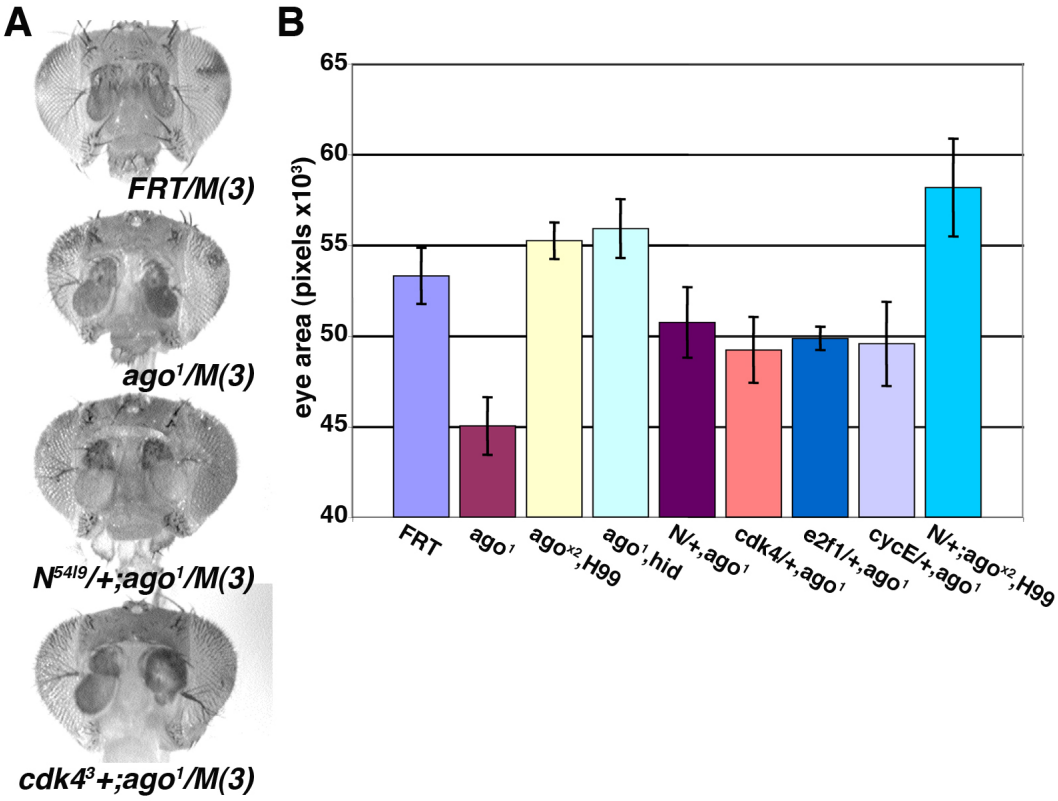

(A) Composite image of *FRT80B/M(3)*, *ago*^{1}*/M(3)*, *N*^{54l9}*/+;;ago*^{1}*/M(3)*, and *cdk4*^{3}*/+;ago*^{1}*/M(3)* adult female heads. Note the *N*^{54l9}*/+;;ago*^{1}*/M(3)* and *cdk4*^{3}*/+;ago*^{1}*/M(3)* eyes are larger than *ago*^{1}*/M(3)*. (B) Graphic summary of the effect of the indicated genotypes on adult eye area. n ≥ 10 for each genotype. Error bars represent 95% confidence intervals.

Figure III.11. Working model for effects of Notch on growth and differentiation downstream of Ago.

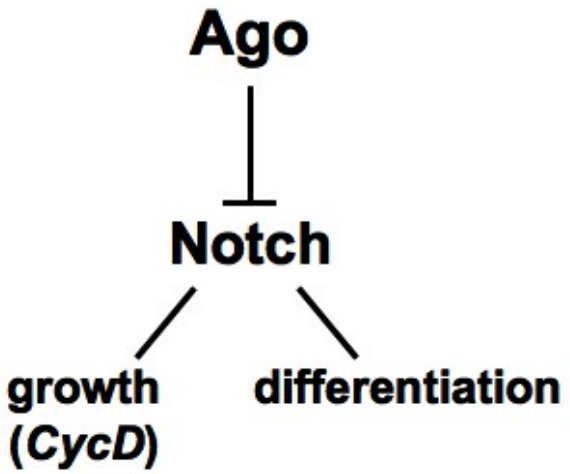

Model for effects of Notch downstream of Ago. Current data indicate a birfurcation of *ago*'s growth/death and differentiation phenotypes downstream of Notch activity. *CycD* transcriptional upregulation has potential roles in regulating *ago* mutant eye size but does not appear to affect its differentiation defects.

III.C4. *ago* limits p53-mediated apoptosis in the pupal eye

While *ago* behaves as a growth suppressor in some tissues, it is required for the developing eye to reach its normal size, and we have found that *Notch* and *cdk4* are involved in this process (see above). One explanation may be that *Notch* and *cdk4* are required to promote the *de2f1*-dependent apoptosis that we observe in *ago* mutant larval eyes (Nicholson et al., 2009). However, we have been unsuccessful in finding a role for these genes in cell death at the larval stage. Because the larval death observed in *ago* mutant tissue occurs in the dividing cells anterior to the MF, but Notch and CycD are most strongly affected by *ago* mutations in the differentiating cells posterior to the MF, we searched for *ago*-regulated apoptosis later in development. Waves of developmental programmed cell death normally occur during the pupal stage to cull excess, unspecified cells from the epithelium (Cagan and Ready, 1989). An early wave of programmed cell death begins around 18 hours after pupariation formation (APF) and is complete by 24 hours APF; signals from Wingless and Notch promote this early-stage death (Cordero et al., 2004). A later wave of programmed cell death occurs from 26-36 hours APF and is dependent on both Notch and EGFR pathway signaling (Cagan and Ready, 1989; Miller and Cagan, 1998; Sawamoto et al., 1994; Yu et al., 2002). Compared with the parental *FRT* control, *ago* mutant tissue exhibits high rates of cell death around 22-25 hours APF as detected with an antibody to cleaved Caspase-3 (C3) (Figure III.12A-B"). Preliminary data suggest that this *ago*-dependent increase in cell death is dominantly suppressed by $cdk4^{3}$ (n = 1, Figure III.12C-C"). Notch signaling is required for developmental cell death in the pupal retina. Likewise, we have shown that (1) Notch hyperactivity is epistatic to elevated levels of *CycD* in *ago* mutant larval eye tissue, (2) heterozygosity for *Notch* or

cdk4 rescue the *ago*^{1}*/M(3)* eye size to the same extent, and (3) a block in cell death is epistatic to a genetic reduction in *Notch* with respect to *ago*^{x2}*/M(3)* eye size (see above). We therefore hypothesize that elevated Notch activity promotes the ectopic apoptosis of *ago* mutant cells in part via effects on *CycD*. However, it remains to be determined whether Notch drives apoptosis here. Notch1 has been shown to promote apoptosis downstream of *Fbw7* mutations in mouse embryonic fibroblasts; this death was rescued by deletion of *Rbpj* (Ishikawa et al., 2008). Therefore, future experiments should determine whether reducing *Notch* or the *Rbpj* homolog, *Su(H)*, in the background of *ago*^{1} mutations at 24 hours APF rescues the death at this stage. If this turns out to be the case, we may have discovered the time in fly eye development in which roles for *ago* most closely mimic its roles in a mammalian system.

Although we predict that apoptosis downstream of *ago* mutations in the differentiating eye results from elevated Notch activity, the death may simply be the result of a simultaneous increase in multiple Ago substrates. However, heterozygosity for the known Ago substrate *cycE* does not rescue the ectopic pupal death in *ago*^{1} clones (Figure III.12D-D"). Likewise, the same cells that stabilize CycE in *ago* mutant tissue at this stage do not express C3: CycE is elevated in a pattern consistent with the Sensless-positive bristle cell complexes (Moberg et al., 2001), and Caspase-3 does not co-localize with Sensless (Sens) here (Figure III.13A-A"). Therefore, the pupal eye death in *ago* mutant tissue is not due a general increase in Ago targets; however, the role of dMyc remains unknown. In vertebrates, oncogenic levels of c-Myc activate p53-mediated apoptosis (Hermeking and Eick, 1994). Since *ago* loss elevates both Notch activity and dMyc protein (this work, Moberg et al., 2004), and Notch has the potential to further

upregulate *c-myc* transcriptionally (Sharma et al., 2006; Weng et al., 2006), it is quite possible that 'oncogenic' levels of dMyc are reached in the pupal eye tissue harboring *ago* mutations and that this dMyc contributes to the high rates of apoptosis observed here.

Like in mammals, dE2F and dp53 induce apoptosis when overexpressed in the fly (Brodsky et al., 2000; Moon et al., 2005; Ollmann et al., 2000). However, unlike mammalian systems, the pro-apoptotic activities of E2F and p53 are independent of one another in the context of fly development because *Drosophila* lacks clear p19/ARF and Mdm2 homologs (Figure III.14, Moon et al., 2008). Therefore, to first test whether *ago* limits pupal eye death by the same *e2f1*-dependent mechanism as it limits death in the larval eye, the dE2F-reporter transgene *PCNA-GFP* (Thacker et al., 2003) was placed into the background of ago^{1} mosaic eye discs. The bristle cell complexes are the last cells to divide in the pupal stage, and because these cell divisions are largely complete by 24 hours APF (Perry, 1968), dE2F is not normally active at this stage in development, as observed in the wild-type twinspots (Bgal+, red; Figure III.13B-B"). Although dE2F activity is high in ago^{1} clones (Figure III.13B-B"), *PCNA-GFP* expression is specifically elevated in the Sens-positive cells of the bristle complexes (see overlap in Figure III.13C"). Therefore, high dE2F1 activity does not correlate spatially with the location of C3 expression in *ago* mutant cells (see Figure III.12B-B"). Likewise, although *de2f1* is a dominant modifier of the $ago^{1}/M(3)$ small eye size (see Figure III.10B), heterozygosity for *de2f1* does not rescue the death in *ago* mutant cells at the pupal stage (compare Figure III.12B-B" and III.12E-E"). On the other hand, expressing a dominant negative p53 (DNp53) transgene in the background of ago^{1} clones almost completely rescues the death at this stage (Figure III.12F-F"), indicating a p53-mediated apoptotic mechanism.

Therefore, ectopic cell death in the *ago* mutant pupal retina is distinct from the *ago*-regulated E2F1-mediated apoptosis in the larval eye (Nicholson et al., 2009).

To summarize, *ago* limits p53-mediated apoptosis in the pupal eye in a differentiation-dependent manner: apoptosis occurs in the post-mitotic interommatidial cells and not in the dividing bristle cells. Although CycE levels and dE2F1 activity are elevated in bristle cell complex nuclei, this expression does not overlap with C3-positive cells in ago^{1} clones, and neither $cycE^{AR95}$ nor $de2f1^{rM729}$ dominantly rescues the levels of apoptosis at this stage. Alternatively, C3 expression in *ago* mutant tissue occurs in the differentiating interommatidial cells and correlates spatially with the previously observed increases in Notch reporter activity and CycD protein levels. Additional immunofluorescence data are necessary to definitely show that C3 indeed colocalizes with elevated CycD levels and Notch reporter activity (see Figures III.2 and III.7). However, the spacial correlation between pathway activity and cell death together with genetic data showing that reducing *Notch* rescues the *ago* small eye size (see Figure III.10) leads us to hypothesize that elevated Notch activity may promote apoptosis of ago^{1} cells in part via effects on the G1 regulator CycD. Future studies should test this hypothesis and additionally determine whether Notch and p53 work in the same or parallel pathways to promote developmental apoptosis downstream of *ago* inactivation. If Notch hyperactivity is indeed confirmed to promote apoptosis in *ago* mutant cells, then these questions could be addressed by testing whether Notch overexpression in the wild-type eye is sufficient to induce apoptosis at 24 hours APF and, subsequently, whether this Notch-regulated death can be rescued by DN-p53. Moreover, the role of dMyc remains to be determined. c-Myc is stabilized upon *Fbw7* loss (Welcker et al., 2004a; Welcker et al.,

2004b; Yada et al., 2004), is further transcriptionally up-regulated by Notch (Sharma et al., 2006; Weng et al., 2006), and has been implicated in p53-dependent apoptosis in *Fbw7*$^{-/-}$ T cells (Onoyama et al., 2007); thus, potential roles for dMyc in proliferation and apoptosis upon *ago* loss merits investigation. Another prediction is that p53 levels and activity are increased in *ago* mutant cells at this stage; this is also a subject of future study to more fully characterize *ago*-regulated apoptosis in the pupal retina.

Figure III.12. *ago* limits p53-mediated apoptosis in the early pupal eye.

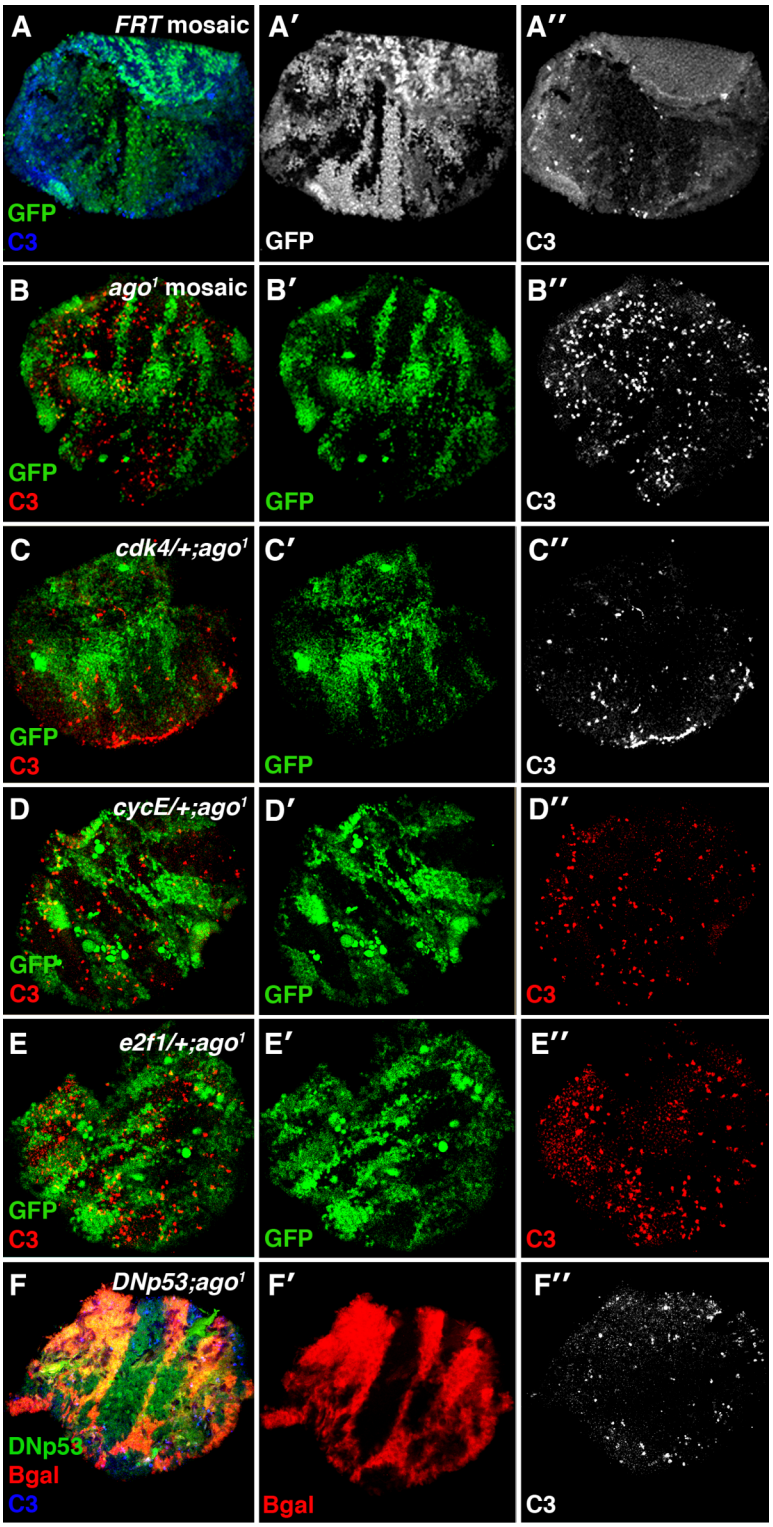

(A-F") Merged confocal sections of pupal eye discs ~24h APF detecting expression of cleaved Caspase-3 (C3) in the indicated genotypes; *FRT80B* control (A-A") or *ago*^{1} clones marked by the absence of GFP (B-E"). (F-F") *ago*^{1} clones marked by the absence of B-gal (red); expression of the dominant-negative p53 (DNp53) transgene detected by GFP fluorescence. Compared with the parental *FRT* (A-A"), *ago* mutant tissue exhibits high rates of cell death (B-B") that is rescued by reducing p53 expression (F-F").

Figure III.13. *ago* mutant bristle cells exhibit high E2F1 activity and do not express cleaved Caspase-3.

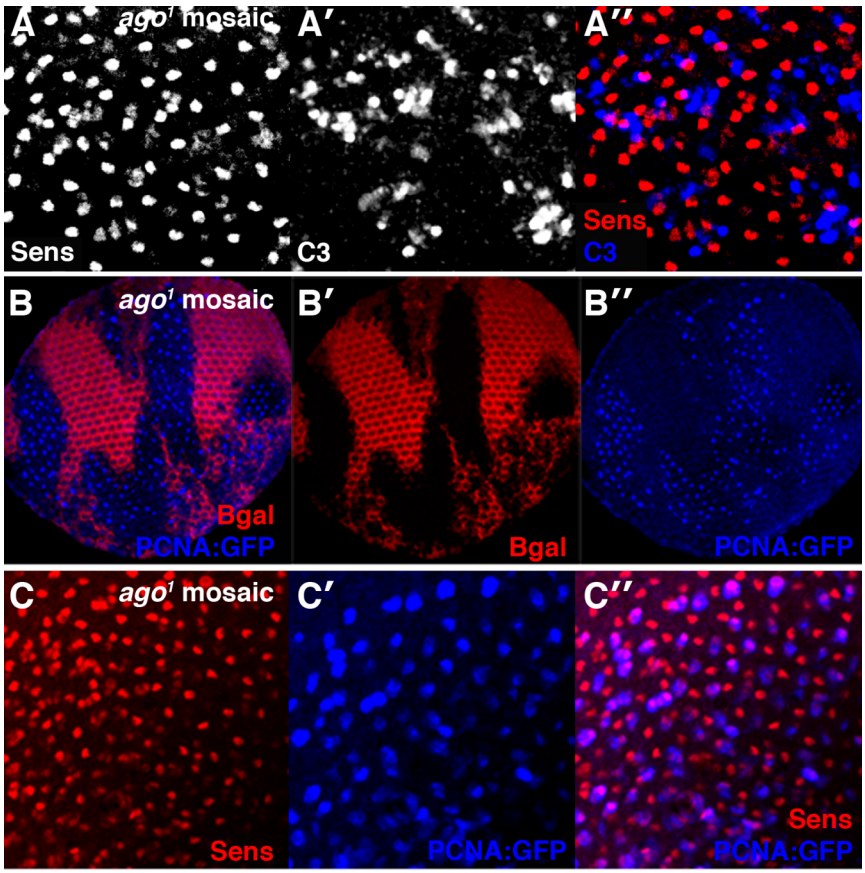

Merged confocal sections of pupal eye discs ~24h APF. (A-A") High magnification image of *ago*^{1} clone indicates disruption of Sens-positive bristle cell organization (A) and ectopic C3 expression (A'). Bristle cell complexes (red) do not colocalize with C3 (blue) expression (A"); clonal boundaries not shown. (B-B") PCNA:GFP (blue) reporter expression reveals high E2F1 activity in *ago*^{1} clones marked by the absence of Bgal (red). (C-C") High magnification image of *ago*^{1} clone detecting Sens (red) and E2F1 activity (PCNA:GFP, blue) shows high degree of colocalization between Sens-positive bristle cell complexes and PCNA:GFP reporter expression (purple, C"); clonal boundaries not shown.

Figure III.14. E2F and p53 pathways in mammals and flies.

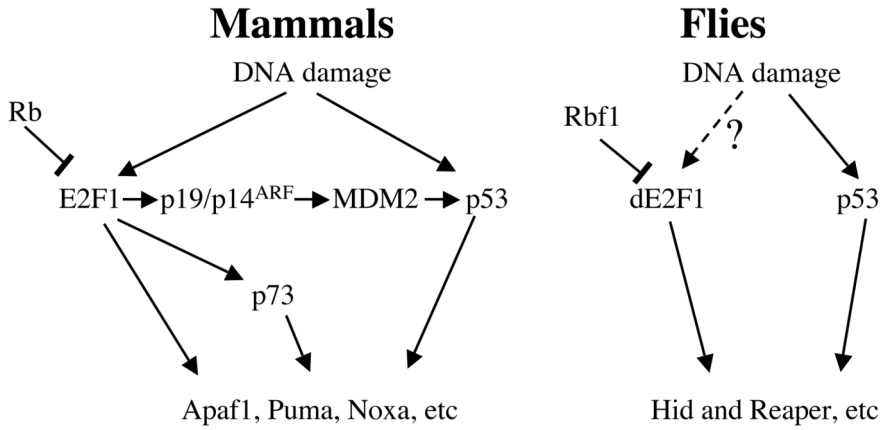

Comparison of E2F and p53 apoptotic networks in mammals and flies. In mammals, crosstalk between E2F1 and p53 occurs via p19/p14^{ARF} and Mdm2. However, *Drosophila* lacks any clear orthologs of these genes, so crosstalk between dE2F1 and dp53 may be limited during development. In the context of DNA damage, however, dE2F1 and dp53 may cooperate to induce a common set of pro-apoptotic targets. (Courtesy of Moon et al., 2008)

III.D. DISCUSSION

The tumor suppressor gene *ago/Fbw7* is responsible driving the proteolytic degradation of pro-growth factors involved in a wide range of human cancers. While known Ago targets in *Drosophila* include CycE, dMyc, and Trachealess, Fbw7 is implicated in the turnover of several additional substrates, including the Notch intracellular domain (N^{ICD}). However, the full consequences of Notch deregulation in *Fbw7* mutants are unclear. We therefore took advantage of *Drosophila*'s conserved simplicity to investigate Notch-dependent mechanisms downstream of *ago*.

This current work is a work in progress, and while conceptual gaps remain to be addressed experimentally, it is apparent that Notch misexpression in *ago* mutant tissue has many consequences. We show that while Notch protein does not hyper-accumulate in *ago* mutant cells, Notch activity is increased. This elevated Notch signaling contributes to differentiation phenotypes, such as reduced photoreceptor number, in the *ago* mutant eye. Although Notch does not behave as a classical Ago target, overall levels of Notch protein are specifically downregulated in *ago* mutant cells that transgenically overexpress the either the N^{ICD} or full-length Notch protein, suggesting the upregulation of a parallel mechanism that acts to maintain baseline levels of Notch in the absence of *ago*. We have also uncovered a role for Notch-dependent transcription of *CycD* downstream of *ago*. Genetic evidence suggests that this interaction may, in part, promote ectopic p53-mediated apoptosis in *ago* mutant tissue, specifically in the differentiating cells of the early pupal retina. In mice and in humans, inactivation of *Fbw7* can collaborate with loss of *p53* to promote leukemogenesis; the combined elevation in Notch activity and inactivation of the p53 tumor surveillance mechanism are central to T-ALL development

(reviewed in Demarest et al., 2008). In *Drosphila*, we have also shown a concurrent increase in Notch activity and p53-mediated apoptosis upon *ago* loss, thereby identifying the early pupal retina as a stage in fly development that recapitulates the expected consequences of *Fbw7* mutations in vertebrate T-ALL models.

In fact, the molecular mechanisms observed in the *ago* mutant pupal retina are reminiscent of conditional *Fbw7* inactivation in the murine T-cell lineage. In *Drosophila*, primordial eye cells proliferate during the larval stages, begin maturation at the end of the third instar, and these post-mitotic cells complete differentiation during the pupal stage into specialized cells that form the adult eye. Therefore, fly eye development is not unlike most vertebrate cell lineages where precursor cells divide a limited number of times before becoming quiescent and undergoing terminal differentiation into specialized post-mitotic cells (Conlon and Raff, 1999). This is especially true in the mouse T-cell lineage: T-cell progenitors are produced in the bone marrow, undergo maturation in the thymus, and finally populate the peripheral lymphoid organs, such as the spleen and lymph nodes. Upon *Fbw7* inactivation in the T-cell lineage, immature T cells hyper-proliferate and mature T cells undergo p53-mediated cell-cycle arrest and apoptosis (Onoyama et al., 2007). These events parallel our observations in the *Drosophila* pupal eye: *ago* loss promotes hyper-proliferation of the mitotic, 'immature' bristle precursor cells and p53-mediated apoptosis of the post-mitotic, 'mature' interommatidial cells. Such phenotypes in both the *Fbw7*-deficient thymocytes and the *ago*-deficient pupal eye cells can potentially be attributed to ectopic activities of c-Myc/dMyc and Notch proteins (this work; Moberg et al., 2004; Onoyama et al., 2007). Thus, roles for *Fbw7* in the mammalian T-cell lineage appear conserved in the early pupal eye, providing the

opportunity more fully understand the basic signaling networks active in an analogous system—valuable information in the development of novel therapeutic strategies for *Fbw7*-dependent lymphomas and leukemias.

Initial evidence points to the N^{ICD} as a bona fide Ago substrate in flies: *ago* alleles suppress *Notch* loss-of-function phenotypes, and Notch activity is elevated in *ago* mutant cells. However, we observe a downregulation of N^{ICD} specifically in *ago* mutant cells when the N^{ICD} is overexpressed (see Figure III.4). As a result, we favor a model in which another factor capable of degrading Notch is up-regulated in the absence of *ago*; this could also explain why we do not observe N^{ICD} stabilization in ago^{1} clones. One candidate to be involved in such a compensatory mechanism is *phyllopod* (*phyl*), a transcriptional target of the EGFR pathway that is thought to encode an E3 ligase adaptor protein (Nagaraj and Banerjee, 2009). Phyl acts to modulate the amount of transcriptional activity from the Notch and Wingless pathways by degrading endocytic pools of these activated receptors (Nagaraj and Banerjee, 2009). Therefore, if elevated Phyl levels or activity is observed in *ago* mutant cells, this could explain why we observe increased Notch reporter activity without N^{ICD} accumulation. Because Notch misregulation upon loss of *Fbw7* is key to cellular transformation, identification of this proposed feedback mechanism could lead to yet another target for therapeutic development.

Therefore, although these data represent a work in progress, roles for Notch downstream of *ago* and its involvement in *ago*-regulated, p53-mediated apoptosis clearly warrant futher investigation.

III.E. MATERIALS AND METHODS

Genetics: Crosses were performed at 25°C. The following genotypes were used for Notch genetic interactions: N^{59l9}/+;*FRT80B*/+, N^{59l9}/+;ago^{1},*FRT80B*/+, N^{59l9}/+;ago^{3},*FRT80B*/+, N^{59l9}/+;ago^{4},*FRT80B*/+, N^{59l9}/+;$cdk4^{3}$/+, N^{59l9}/+;$cdk4^{3}$/$cdk4^{3}$. The following genotypes were used for mosaic experiments: ago^{1},*FRT80B/TM6B*, ago^{3},*FRT80B/TM6B*, ago^{x2},*Df(3L)H99,FRT80B/TM6B*, *eyFLP;P[m-*w^{+}*;ubi>GFP],FRT80B*, *eyFLP;P[m-*w^{+}*;arm-LacZ],FRT80B/TM6B*, *eyFLP;FRT82B,P[m-*w^{+}*;ubi>GFP]*, *ubxFLP;P[m-*w^{+}*;ubi>GFP],FRT80B*, *w;P[m-w+;PCNA-EmGFP];*ago^{1}*,FRT80B/TM6B* (*PCNA-EmGFP* gift of R. Duronio), *eyFLP,E(spl)mß-CD2,P[m-*w^{+}*;arm-LacZ],FRT80B*, Psn^{227},*FRT80B/Tm6B*, *FRT82B,*Dl^{RevF10},Ser^{RX82}/*Tm6B*, N^{59l9}/+;ago^{1},*FRT80B*/+, $cdk4^{3}$/*CyO;*ago^{1}*FRT80B/TM6B*, $cycE^{AR95}$/*CyO;*ago^{1}*FRT80B/TM6B*, and ago^{1},*FRT80B,*$de2f1^{rM729}$/*TM6B*. The following genotypes were used for cell lethal experiments: *eyFLP;P[m-*w^{+}*]*$RpL14^{1}$,*FRT80B,* ago^{1}*FRT80B/TM6B*, ago^{x2},*Df(3L)H99,FRT80B/TM6B*, N^{59l9}/+;ago^{1},*FRT80B*/+, $cdk4^{3}$/*CyO;*ago^{1}*FRT80B/TM6B*, ago^{1},hid^{05014},*FRT80B/TM6B*, $cycE^{AR95}$/*CyO;*ago^{1}*FRT80B/TM6B*, ago^{1},*FRT80B,*$de2f1^{rM729}$/*TM6B*, and N^{59l9}/+; ago^{x2},*Df(3L)H99,FRT80B/TM6B*. The following genotypes were used for transgenic experiments: *GMR-Gal4/UAS-N6*; *w;UAS-dp53*^{R155H}/+;ago^{1},*FRT80B/TM6B, eyFLP;act>*y^{+}*>Gal4;P[m-*w^{+}*,arm-LacZ],FRT80B/TM6B*, hsN^{intra}/*UAS-DTS5;ptc-Gal4*/+, hsN^{intra}/*CyO*;ago^{1}*FRT80B* (*UAS-DTS5* gift of J. Belote).

Eye/wing pictures and measurements: Adult eyes and wings were photographed with a Leica DFC500 CCD digital camera. For measurements, areas were quantitated with Adobe Photoshop; a minimum of 10 eyes and wings were counted per genotype.

Immunohistochemistry & Microscopy: Thin-section analysis of adult eyes was performed according to standard protocols. Immunostaining and confocal microscopy was performed using a 4% paraformaldehyde fixative as previously described (Moberg et al., 2004). In pulse-chase experiments, flies were heat-shocked for 1 hour at 37^{o} prior to dissection and fixation. Primary antibodies used: mouse α-Notch 1:200 (9C6, DSHB); rat α-CD2 1:100 (Research Diagnostics, Inc); mouse α-βgal 1:1000 (Promega); mouse α-DCD3/6 1:15 each (CycD; gift of N. Dyson); rabbit α-cleaved Caspase-3 (Cell Signaling) 1:100; rabbit α-GFP (Molecular Probes) 1:1000; guinea pig α-Sens 1:1000 (gift of H. Bellen, Nolo et al., 2000). For immunoblotting, imaginal disc extracts were prepared in sample buffer containing DTT and resolved on SDS-PAGE prior to Western blotting with mouse α-N9C6 (1:400). Secondary antibodies conjugated to Cy3, Cy5, and HRP were used as recommended (Jackson ImmunoResearch).

Real Time RT-PCR (qPCR): Total RNA isolated from 30 eye discs (TRIzol/Invitrogen) was reverse transcribed (SuperScript II RT/Invitrogen) and analyzed by qPCR (SYBR Green 1 Master/Roche) Primers: *CycD* 5'-GCCGAATGGATGATGGAA-3', 5'-CCATGTAATTTAATGCCAGTAATACG-3'; *β-tub* (5'-CGCACAGAGTCCATGGTG-3', 5'-AAATCGTTCACATCCAAGCTG-3'.

III.F. REFERENCES

Belote, J. M. and Fortier, E. (2002). Targeted expression of dominant negative proteasome mutants in Drosophila melanogaster. *Genesis* **34**, 80-2.

Bray, S. J. (2006). Notch signalling: a simple pathway becomes complex. *Nat Rev Mol Cell Biol* **7**, 678-89.

Brodsky, M. H., Nordstrom, W., Tsang, G., Kwan, E., Rubin, G. M. and Abrams, J. M. (2000). Drosophila p53 binds a damage response element at the reaper locus. *Cell* **101**, 103-13.

Cagan, R. L. and Ready, D. F. (1989). The emergence of order in the Drosophila pupal retina. *Dev Biol* **136**, 346-62.

Conlon, I. and Raff, M. (1999). Size control in animal development. *Cell* **96**, 235-44.

Cordero, J., Jassim, O., Bao, S. and Cagan, R. (2004). A role for wingless in an early pupal cell death event that contributes to patterning the Drosophila eye. *Mech Dev* **121**, 1523-30.

Datar, S. A., Jacobs, H. W., de la Cruz, A. F., Lehner, C. F. and Edgar, B. A. (2000). The Drosophila cyclin D-Cdk4 complex promotes cellular growth. *EMBO J* **19**, 4543-54.

de Celis, J. F., Tyler, D. M., de Celis, J. and Bray, S. J. (1998). Notch signalling mediates segmentation of the Drosophila leg. *Development* **125**, 4617-26.

Demarest, R. M., Ratti, F. and Capobianco, A. J. (2008). It's T-ALL about Notch. *Oncogene* **27**, 5082-91.

Dexter, J. S. (1914). The analysis of a case of continuous variation in Drosophila by a study of its linkage relations. *Am. Nat.* **48**, 712.

Dominguez, M. and de Celis, J. F. (1998). A dorsal/ventral boundary established by Notch controls growth and polarity in the Drosophila eye. *Nature* **396**, 276-8.

Ellisen, L. W., Bird, J., West, D. C., Soreng, A. L., Reynolds, T. C., Smith, S. D. and Sklar, J. (1991). TAN-1, the human homolog of the Drosophila notch gene, is broken by chromosomal translocations in T lymphoblastic neoplasms. *Cell* **66**, 649-61.

Fortini, M. E., Rebay, I., Caron, L. A. and Artavanis-Tsakonas, S. (1993). An activated Notch receptor blocks cell-fate commitment in the developing Drosophila eye. *Nature* **365**, 555-7.

Gupta-Rossi, N., Le Bail, O., Gonen, H., Brou, C., Logeat, F., Six, E., Ciechanover, A. and Israel, A. (2001). Functional interaction between SEL-10, an F-box protein, and the nuclear form of activated Notch1 receptor. *J Biol Chem* **276**, 34371-8.

Hao, B., Oehlmann, S., Sowa, M. E., Harper, J. W. and Pavletich, N. P. (2007). Structure of a Fbw7-Skp1-cyclin E complex: multisite-phosphorylated substrate recognition by SCF ubiquitin ligases. *Mol Cell* **26**, 131-43.

Hariharan, I. K. and Bilder, D. (2006). Regulation of imaginal disc growth by tumor-suppressor genes in Drosophila. *Annu Rev Genet* **40**, 335-61.

Hermeking, H. and Eick, D. (1994). Mediation of c-Myc-induced apoptosis by p53. *Science* **265**, 2091-3.

Hubbard, E. J., Wu, G., Kitajewski, J. and Greenwald, I. (1997). sel-10, a negative regulator of lin-12 activity in Caenorhabditis elegans, encodes a member of the CDC4 family of proteins. *Genes Dev* **11**, 3182-93.

Ishikawa, Y., Onoyama, I., Nakayama, K. I. and Nakayama, K. (2008). Notch-dependent cell cycle arrest and apoptosis in mouse embryonic fibroblasts lacking Fbxw7. *Oncogene* **27**, 6164-74.

Li, J., Pauley, A. M., Myers, R. L., Shuang, R., Brashler, J. R., Yan, R., Buhl, A. E., Ruble, C. and Gurney, M. E. (2002). SEL-10 interacts with presenilin 1, facilitates its ubiquitination, and alters A-beta peptide production. *J Neurochem* **82**, 1540-8.

Mao, J. H., Kim, I. J., Wu, D., Climent, J., Kang, H. C., DelRosario, R. and Balmain, A. (2008). FBXW7 targets mTOR for degradation and cooperates with PTEN in tumor suppression. *Science* **321**, 1499-502.

Mao, J. H., Perez-Losada, J., Wu, D., Delrosario, R., Tsunematsu, R., Nakayama, K. I., Brown, K., Bryson, S. and Balmain, A. (2004). Fbxw7/Cdc4 is a p53-dependent, haploinsufficient tumour suppressor gene. *Nature* **432**, 775-9.

Meyer, C. A., Jacobs, H. W., Datar, S. A., Du, W., Edgar, B. A. and Lehner, C. F. (2000). Drosophila Cdk4 is required for normal growth and is dispensable for cell cycle progression. *EMBO J* **19**, 4533-42.

Miller, D. T. and Cagan, R. L. (1998). Local induction of patterning and programmed cell death in the developing Drosophila retina. *Development* **125**, 2327-35.

Moberg, K. H., Bell, D. W., Wahrer, D. C., Haber, D. A. and Hariharan, I. K. (2001). Archipelago regulates Cyclin E levels in Drosophila and is mutated in human cancer cell lines. *Nature* **413**, 311-6.

Moberg, K. H., Mukherjee, A., Veraksa, A., Artavanis-Tsakonas, S. and Hariharan, I. K. (2004). The Drosophila F box protein archipelago regulates dMyc protein levels in vivo. *Curr Biol* **14**, 965-74.

Moon, N. S., Di Stefano, L., Morris, E. J., Patel, R., White, K. and Dyson, N. J. (2008). E2F and p53 induce apoptosis independently during Drosophila development but intersect in the context of DNA damage. *PLoS Genet* **4**, e1000153.

Moon, N. S., Frolov, M. V., Kwon, E. J., Di Stefano, L., Dimova, D. K., Morris, E. J., Taylor-Harding, B., White, K. and Dyson, N. J. (2005). Drosophila E2F1 has context-specific pro- and antiapoptotic properties during development. *Dev Cell* **9**, 463-75.

Mortimer, N. T. and Moberg, K. H. (2007). The Drosophila F-box protein Archipelago controls levels of the Trachealess transcription factor in the embryonic tracheal system. *Dev Biol* **312**, 560-71.

Nagaraj, R. and Banerjee, U. (2009). Regulation of Notch and Wingless signalling by phyllopod, a transcriptional target of the EGFR pathway. *EMBO J* **28**, 337-46.

Nicholson, S. C., Gilbert, M. M., Nicolay, B. N., Frolov, M. V. and Moberg, K. H. (2009). The archipelago Tumor Suppressor Gene Limits Rb/E2F-Regulated Apoptosis in Developing Drosophila Tissues. *Curr Biol*.

Nolo, R., Abbott, L. A. and Bellen, H. J. (2000). Senseless, a Zn finger transcription factor, is necessary and sufficient for sensory organ development in Drosophila. *Cell* **102**, 349-62.

O'Neil, J., Grim, J., Strack, P., Rao, S., Tibbitts, D., Winter, C., Hardwick, J., Welcker, M., Meijerink, J. P., Pieters, R. et al. (2007). FBW7 mutations in leukemic cells mediate NOTCH pathway activation and resistance to {gamma}-secretase inhibitors. *J Exp Med*.

Oberg, C., Li, J., Pauley, A., Wolf, E., Gurney, M. and Lendahl, U. (2001). The Notch intracellular domain is ubiquitinated and negatively regulated by the mammalian Sel-10 homolog. *J Biol Chem* **276**, 35847-53.

Ollmann, M., Young, L. M., Di Como, C. J., Karim, F., Belvin, M., Robertson, S., Whittaker, K., Demsky, M., Fisher, W. W., Buchman, A. et al. (2000). Drosophila p53 is a structural and functional homolog of the tumor suppressor p53. *Cell* **101**, 91-101.

Onoyama, I., Tsunematsu, R., Matsumoto, A., Kimura, T., de Alboran, I. M., Nakayama, K. and Nakayama, K. I. (2007). Conditional inactivation of Fbxw7 impairs cell-cycle exit during T cell differentiation and results in lymphomatogenesis. *J Exp Med* **204**, 2875-88.

Pan, D. (2007). Hippo signaling in organ size control. *Genes Dev* **21**, 886-97.

Perry, M. M. (1968). Further studies on the development of the eye of Drosophila melanogaster. II: The inter-ommatidial bristles. *J. Morphol.* **124**, 249-262.

Ready, D. F., Hanson, T. E. and Benzer, S. (1976). Development of the Drosophila retina, a neurocrystalline lattice. *Dev Biol* **53**, 217-40.

Robbins, J., Blondel, B. J., Gallahan, D. and Callahan, R. (1992). Mouse mammary tumor gene int-3: a member of the notch gene family transforms mammary epithelial cells. *J Virol* **66**, 2594-9.

Ronchini, C. and Capobianco, A. J. (2001). Induction of cyclin D1 transcription and CDK2 activity by Notch(ic): implication for cell cycle disruption in transformation by Notch(ic). *Mol Cell Biol* **21**, 5925-34.

Saeboe-Larssen, S., Urbanczyk Mohebi, B. and Lambertsson, A. (1997). The Drosophila ribosomal protein L14-encoding gene, identified by a novel Minute mutation in a dense cluster of previously undescribed genes in cytogenetic region 66D. *Mol Gen Genet* **255**, 141-51.

Sawamoto, K., Okano, H., Kobayakawa, Y., Hayashi, S., Mikoshiba, K. and Tanimura, T. (1994). The function of argos in regulating cell fate decisions during Drosophila eye and wing vein development. *Dev Biol* **164**, 267-76.

Schweisguth, F. (1999). Dominant-negative mutation in the beta2 and beta6 proteasome subunit genes affect alternative cell fate decisions in the Drosophila sense organ lineage. *Proc Natl Acad Sci U S A* **96**, 11382-6.

Sharma, V. M., Calvo, J. A., Draheim, K. M., Cunningham, L. A., Hermance, N., Beverly, L., Krishnamoorthy, V., Bhasin, M., Capobianco, A. J. and Kelliher, M. A. (2006). Notch1 contributes to mouse T-cell leukemia by directly inducing the expression of c-myc. *Mol Cell Biol* **26**, 8022-31.

Struhl, G. and Greenwald, I. (2001). Presenilin-mediated transmembrane cleavage is required for Notch signal transduction in Drosophila. *Proc Natl Acad Sci U S A* **98**, 229-34.

Sundaram, M. and Greenwald, I. (1993). Suppressors of a lin-12 hypomorph define genes that interact with both lin-12 and glp-1 in Caenorhabditis elegans. *Genetics* **135**, 765-83.

Tetzlaff, M. T., Yu, W., Li, M., Zhang, P., Finegold, M., Mahon, K., Harper, J. W., Schwartz, R. J. and Elledge, S. J. (2004). Defective cardiovascular development and elevated cyclin E and Notch proteins in mice lacking the Fbw7 F-box protein. *Proc Natl Acad Sci U S A* **101**, 3338-45.

Thacker, S. A., Bonnette, P. C. and Duronio, R. J. (2003). The contribution of E2F-regulated transcription to Drosophila PCNA gene function. *Curr Biol* **13**, 53-8.

Tsunematsu, R., Nakayama, K., Oike, Y., Nishiyama, M., Ishida, N., Hatakeyama, S., Bessho, Y., Kageyama, R., Suda, T. and Nakayama, K. I. (2004). Mouse Fbw7/Sel-10/Cdc4 is required for notch degradation during vascular development. *J Biol Chem* **279**, 9417-23.

Uyttendaele, H., Marazzi, G., Wu, G., Yan, Q., Sassoon, D. and Kitajewski, J. (1996). Notch4/int-3, a mammary proto-oncogene, is an endothelial cell-specific mammalian Notch gene. *Development* **122**, 2251-9.

Welcker, M. and Clurman, B. E. (2008). FBW7 ubiquitin ligase: a tumour suppressor at the crossroads of cell division, growth and differentiation. *Nat Rev Cancer* **8**, 83-93.

Welcker, M., Orian, A., Grim, J. A., Eisenman, R. N. and Clurman, B. E. (2004a). A nucleolar isoform of the Fbw7 ubiquitin ligase regulates c-Myc and cell size. *Curr Biol* **14**, 1852-7.

Welcker, M., Orian, A., Jin, J., Grim, J. A., Harper, J. W., Eisenman, R. N. and Clurman, B. E. (2004b). The Fbw7 tumor suppressor regulates glycogen synthase kinase 3 phosphorylation-dependent c-Myc protein degradation. *Proc Natl Acad Sci U S A* **101**, 9085-90.

Weng, A. P., Millholland, J. M., Yashiro-Ohtani, Y., Arcangeli, M. L., Lau, A., Wai, C., Del Bianco, C., Rodriguez, C. G., Sai, H., Tobias, J. et al. (2006). c-Myc is an important direct target of Notch1 in T-cell acute lymphoblastic leukemia/lymphoma. *Genes Dev* **20**, 2096-109.

White, K., Grether, M. E., Abrams, J. M., Young, L., Farrell, K. and Steller, H. (1994). Genetic control of programmed cell death in Drosophila. *Science* **264**, 677-83.

Wu, G., Hubbard, E. J., Kitajewski, J. K. and Greenwald, I. (1998). Evidence for functional and physical association between Caenorhabditis elegans SEL-10, a Cdc4p-related protein, and SEL-12 presenilin. *Proc Natl Acad Sci U S A* **95**, 15787-91.

Wu, G., Lyapina, S., Das, I., Li, J., Gurney, M., Pauley, A., Chui, I., Deshaies, R. J. and Kitajewski, J. (2001). SEL-10 is an inhibitor of notch signaling that targets notch for ubiquitin-mediated protein degradation. *Mol Cell Biol* **21**, 7403-15.

Yada, M., Hatakeyama, S., Kamura, T., Nishiyama, M., Tsunematsu, R., Imaki, H., Ishida, N., Okumura, F., Nakayama, K. and Nakayama, K. I. (2004). Phosphorylation-dependent degradation of c-Myc is mediated by the F-box protein Fbw7. *EMBO J* **23**, 2116-25.

Yu, S. Y., Yoo, S. J., Yang, L., Zapata, C., Srinivasan, A., Hay, B. A. and Baker, N. E. (2002). A pathway of signals regulating effector and initiator caspases in the developing Drosophila eye. *Development* **129**, 3269-78.

Zagouras, P., Stifani, S., Blaumueller, C. M., Carcangiu, M. L. and Artavanis-Tsakonas, S. (1995). Alterations in Notch signaling in neoplastic lesions of the human cervix. *Proc Natl Acad Sci U S A* **92**, 6414-8.

Chapter IV: The *Drosophila* tumor suppressor gene *ept/tsg101* hyperactivates the JAK-STAT pathway[3]

[3] Adapted from **Gilbert, M. M., Beam, C. K., Robinson, B. S. and Moberg, K. H.** (2009). Genetic interactions between the Drosophila tumor suppressor gene ept and the stat92E transcription factor. *PLoS One* **4**, e7083.

IV.A. ABSTRACT

Tumor Susceptibility Gene-101 (TSG101) promotes the endocytic degradation of transmembrane proteins and is implicated as a mutational target in cancer, yet the effect of *TSG101* loss on cell proliferation in vertebrates is uncertain. By contrast, *Drosophila* epithelial tissues lacking the TSG101 ortholog *erupted* (*ept*) develop as enlarged undifferentiated tumors, indicating that the gene can have anti-growth properties in a simple metazoan. A full understanding of pathways deregulated by loss of *Drosophila ept* will aid in understanding potential links between mammalian TSG101 and growth control. We find that *ept* loss alters Domeless receptor localization and levels in eye imaginal disc cells, and this correlates with accumulation of phosphorylated, activated Stat92E and subsequent JAK-STAT pathway hyperactivity. These findings identify *ept* as a cell-autonomous inhibitor of the JAK-STAT pathway and, together with data published in Gilbert, *et al*., suggest that excess JAK-STAT signaling makes a significant contribution to proliferative and tissue architectural phenotypes that occur in *ept* mutant tissues.

IV.B. INTRODUCTION

The *Drosophila* gene *erupted* (*ept*) encodes an ortholog of human Tumor Susceptibility Gene-101 (TSG101) and yeast Vps23p, which function as part of the ESCRT-I complex to sort proteins to the multi-vesicular body for ultimate lysosomal degradation (Bishop and Woodman, 2001; Katzmann et al., 2001; Stuffers et al., 2008). Mutations in the *ept/tsg101* gene (referred to hereafter as *ept*) or the ESCRT-II subunit gene *vps25* block endocytic degradation of certain transmembrane proteins, including the Notch receptor and the apical polarity determinant Crumbs (Crb), and lead to dramatic overgrowth of *Drosophila* imaginal discs (Herz et al., 2006; Moberg et al., 2005; Thompson et al., 2005; Vaccari and Bilder, 2005). This imaginal disc overgrowth occurs in part by a non-cell autonomous process: *ept* and *vps25* mutant cells themselves undergo very high rates of apoptosis but can potently induce hyperplastic growth of surrounding genetically normal tissue due to overproduction of secreted factors like Unpaired (Upd) (Moberg et al., 2005; Thompson et al., 2005; Vaccari and Bilder, 2005), a secreted cytokine-like mitogen that activates JAK-STAT signaling via the receptor Domeless (Dome) (Harrison et al., 1998). Because the death of *ept* and *vps25* mutant cells eventually limits Upd production, the phenotypic outcome of clonal loss of either gene is limited to enlargement of the affected organ. However, both *ept* and *vps25* also display a conditional, cell-autonomous tumor suppressor activity: if the death of mutant cells is prevented, either by the expression of anti-apoptotic genes or by the removal of competing normal cells from the disc, they overgrow into large, disorganized tumors that kill the host animal (Moberg et al., 2005; Thompson et al., 2005; Vaccari and Bilder, 2005). Thus, *ept* and *vps25* behave both as non-cell autonomous growth suppressors and as conditional, cell-autonomous

neoplastic tumor suppressors. While mechanisms underlying the non-autonomous effects of mutations in *ept* have been previously reported (Moberg et al., 2005), its cell-autonomous roles are not known. Both mutational inactivation and overexpression of the vertebrate *ept* ortholog, TSG101, have been implicated in human cancers (Li et al., 1997; Oh et al., 2007; Young et al., 2007a; Young et al., 2007b). Therefore, a more complete understanding of how *ept* mutations affect growth pathways will establish the basis for comparative analysis of vertebrate and invertebrate TSG101 developmental phenotypes and may lead to the identification of similar oncogneic mechanisms in mammals.

Here we show that the autonomous growth of *ept* mutant cells is dependent upon high levels of JAK-STAT pathway signaling. The data presented are a portion of a larger published work wherein my colleagues in the Moberg lab demonstrated that *ept* mutant eye-antennal tumors require the *stat92E* gene (Gilbert et al., 2009), which encodes the sole fly member of the Signal Transducer and Activator of Transcription (STAT) family of mammalian transcription factors that are well known for their ability to promote tissue growth in *Drosophila* (Bach et al., 2003; Chao et al., 2004; Tsai and Sun, 2004) and mammals (reviewed in Calo et al., 2003). Gilbert, *et al*. showed that removing a single copy of *stat92E* gene significantly reduced the overgrowth of eye imaginal discs composed entirely of *ept* cells (Figure IV.1A-C). This correlated with a more normal G1/S cell cycle phasing in *ept* mutant discs and a partial reversion of an *ept* enlarged-cell phenotype (Figure IV.1D). These effects of *stat92E* heterozygosity on the proliferative properties of *ept* cells were accompanied by an ameliorating effect on the epithelial architecture of *ept* mutant tissues (Figure IV.2), coincident with the observation that lowering *stat92E* gene dosage reduced expression of the epithelial polarity factor *crumbs*

(*crb*) in *ept* mutant eye discs (Figure IV.3). Together, these data indicated that *stat92E* contributes not only to deregulated cell cycling, excessive cell size, but also to defects in tissue organization observed in *ept* mutant tumors.

To some degree the genetic evidence of a role for *stat92E* in *ept* phenotypes was not surprising: the excess Upd produced by *ept* mutant cells is known to drive Stat92E-dependent proliferation in immediately surrounding wild-type cells (Moberg et al., 2005). However, it had not previously been determined whether excess Stat activation contributes to the growth and polarity phenotypes of *ept* mutant cells themselves. We find that multiple sensors of JAK-STAT activity indeed detect strong activation of the JAK-STAT pathway within mutant cells. This phenomenon is coincident with accumulation of the Upd receptor Dome in intracellular puncta in *ept* mutant cells that co-stains with the endosomal protein Hrs (Lloyd et al., 2002). Stat92E hyperactivity therefore correlates with an autonomous effect of *ept* alleles on Dome localization and levels.

Figure IV.1. *stat92E* promotes growth of *ept* tumors.

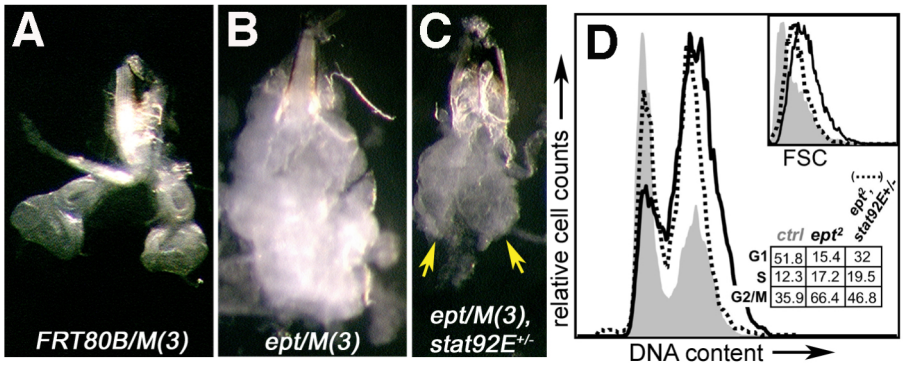

Bright-field images of (A) control discs [*FRT80B/M(3)*], (B) *ept* mutant discs [$ept^2/M(3)$], or *ept* mutant, *stat92E* heterozygous discs [$ept^2/M(3),stat92E^{06346}/+$] from wandering-stage larvae. Yellow arrows in (C) denote the two lobes of tissue resembling eye discs. (D) Flow cytometric analysis of control (grey fill), $ept^2/M(3)$ mutant (black line), and $ept^2/M(3),stat92E^{06346}/+$ (dotted line) eye-antennal discs shows that reducing *stat92E* gene dosage partially rescues of cell cycle and cell size (inset) defects in ept^2 mutant tissues. Percentages of cells in each stage of the cell cycle are indicated. The FACS data are representative of multiple experiments.

Figure IV.2. ***stat92E*** **affects tissue architecture in** ***ept*** **tumors.**

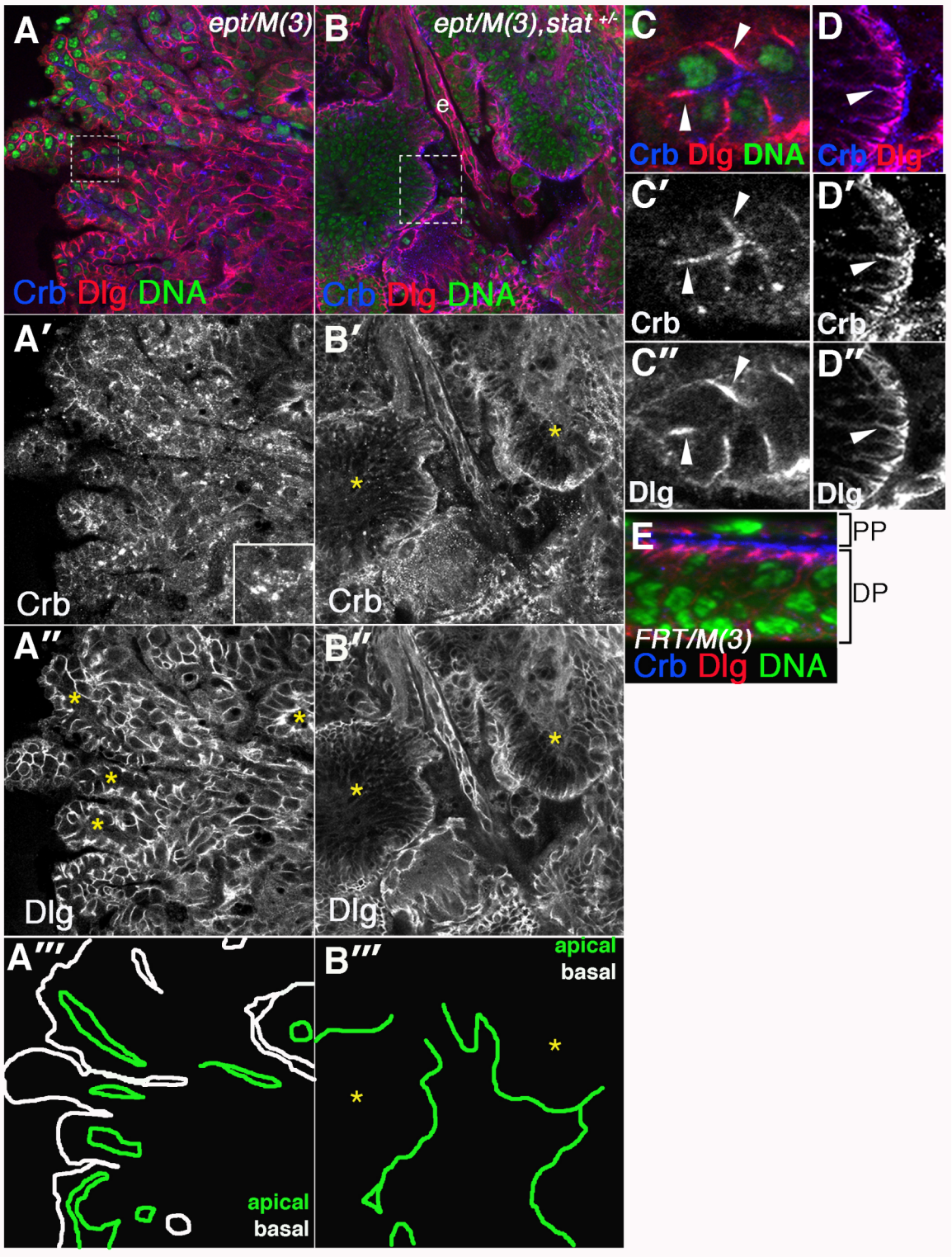

Confocal images of *ept*^{2}*/M(3)* (A-A″) and *ept*^{2}*/M(3),stat92E*^{06346}/+ (B-B″) eye discs stained for Dlg (red), Crb (blue) and DNA (green). The two main tissue lobes in panel B are separated by the esophagus (e), which remained embedded in the tissue mass during dissection. Areas outlined by dashed boxes in (A) and (B) are magnified in (C-C″) and (D-D″) respectively. Asterisks in (A″) denote internal lumens bounded by Dlg-negative apical membrane of *ept*^{2}*/M(3)* mutant cells. Asterisks in B-B‴ denote tissue lobes of *ept*^{2}*/M(3),stat92E*^{06346}/+ discs. Note the dominant effect of *stat92E*^{06346} on the appearance of Crb aggregates (A′ vs B′) and the lack of the 'inverted' tissue phenotype in *ept*^{2}*/M(3),stat92E*^{06346}/+ tumors (A″ vs B″). The *stat92E*^{06346} allele does not have a dominant effect on the mislocalization of Crb onto the Dlg-positive basolateral membrane domain of *ept*^{2} mutant cells (arrowhead in D-D″). (E) A control *FRT80B/M(3)* disc stained for Crb (blue), Dlg (red), and DNA (green). The peripodial cell layer (PP) and disc proper (DP) are indicated. Panels A‴ and B‴ are tracings of the apical (green) and basal (white) membranes of the tissues in A" and B" respectively.

Figure IV.3. *stat92E* promotes *crb* expression in *ept* mutant cells.

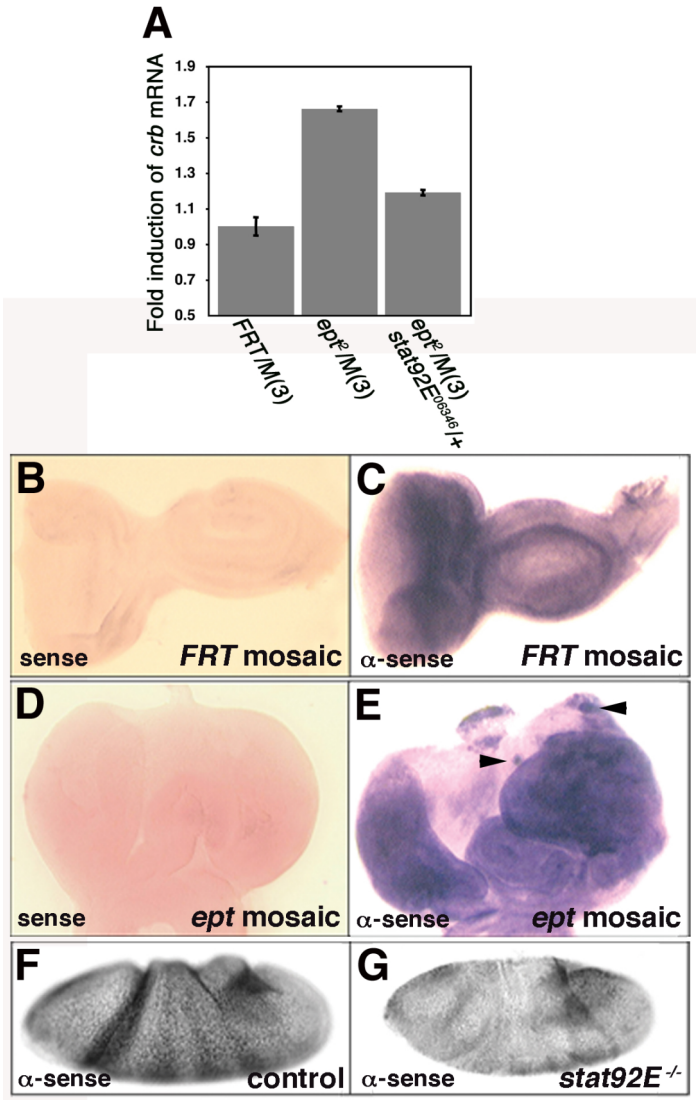

(A) *crb* transcript levels in the indicated genotypes as determined by quantitative realtime PCR. Levels of *crb* mRNA were normalized to control reactions to *rp49* mRNA. Data represents an average of two separate experiments. (B-G) RNA in situ hybridization analysis with *crb* sense (B,D) or anti-sense (C,E,F,G) probes in eye discs (B-E) or stage 3 embryos (F,G) of the indicated genotypes. Arrowheads in (E) indicate patches of cells that appear to contain higher levels of *crb* mRNA than surrounding cells.

IV.C. RESULTS

IV.C1. Activation of JAK-STAT signaling in *ept* mutant cells

Stat92E has been shown to be required for the non-autonomous pro-growth effect of *ept* mutant cells on surrounding normal cells (Moberg et al., 2005). The genetic requirement for *stat92E* in the overgrowth of *ept* mutant tumors indicates that the gene is also required for the autonomous growth effects of *ept* alleles (see Figure IV.1). The mechanism of this effect is not known. *ept* mutant cells are known to overexpress the *upd* gene (Moberg et al., 2005), which encodes a secreted cytokine-like ligand protein that binds the Dome receptor and signals through the Jak kinase to the Stat92E transcription factor (reviewed in Zeidler et al., 2000). As *upd* overexpression is alone sufficient to drive eye-antennal disc enlargement (Bach et al., 2003), high levels of extracellular Upd produced by *ept* cells might be predicted to feed back onto nearby cells (irrespective of their genotype) to elicit the growth and proliferation phenotypes observed in FACS analysis (see Figure IV.1).

To test the effect of *ept* alleles on Stat92E signaling, we first used an antibody reported to detect ligand-stimulated tyrosine phosphorylation of Stat92E by Jak kinase (anti-pY-Stat92E), which is necessary for Stat92E activity *in vivo* (reviewed in Hombria and Brown, 2002). This antibody has been used in other studies of *Drosophila* Stat92E activity (Herz et al., 2006; Li et al., 2003), including one in which it was used to assess JAK-STAT activity in eyes discs mosaic for an allele of the ESCRT-II component *vps25* (Herz et al., 2006). In eye-antennal discs composed of patches of normal and *ept* mutant cells, the anti-pY-Stat92E antibody detects strong accumulation of the pY-Stat92E epitope within clones of *ept* mutant cells (Figure IV.4A-A″). A high magnification view

of a clonal boundary confirms this effect (Figure IV.4B-B″). This epitope is also elevated in mutant areas of *ept* disc tumors relative to wild type areas of *FRT80B/M(3)* control discs (Figures IV.4C vs. D).

To test the relationship between *ept* and JAK-STAT activity further, two Stat92E reporter transgenes were placed in the background of *ept* mutations. The first, *3xGAS-lacZ* (Gilbert et al., 2005), is located on the same chromosome arm as *ept*, such that mitotic recombination of a *3xGAS-lacZ,ept*^{2}*,FRT80B* chromosome produces clones of *ept* cells carrying two copies of the *3xGAS-lacZ* transgene that can be compared to discs carrying control *FRT80B* clones with two copies of *3xGAS-lacZ*. When these cells are imaged under identical optical settings (Figure IV.5A-B), the *3xGAS-lacZ* reporter is up-regulated in patches of *ept* eye disc cells (Figure IV.5A-A″) relative to control *FRT80B* clones (Figure IV.5B-B″). The inset in Figure IV.5A shows a small *ept*^{2} clone in the posterior region of the eye disc that stains brightly for β-galactosidase expressed from the *3xGAS-lacZ* transgene. This small-clone phenotype is due to increased rates of apoptosis (see Moberg et al., 2005), which make it difficult to recover large *ept* mutant clones in the eye-antennal disc. To bypass this problem, expression of the second Stat92E reporter, *10xStat92E>GFP* (Bach et al., 2007), was analyzed in two backgrounds in which the death of *ept* mutant cells was blocked. The first of these was *ept/M(3)* tumors, in which removal of competing normal cells allows mutant cells to overgrow into large tumors (Moberg et al., 2005). *10xStat92E>GFP* is very strongly expressed in this background relative to its expression in control *FRT80B/M(3)* discs composed of normal cells (Figure IV.5F-G). The magnitude of the difference is so substantial that the fluorescent signal from the disc in Figure IV.5F was only detectable following a doubling of the gain setting

used to visualize the disc in Figure IV.5G. *10xStat>GFP* was also analyzed in a second background in which the death of *ept* mutant cells was blocked by simultaneous loss of the *H99* chromosomal region, which contains genes required for apoptotic cell death (White et al., 1994). We first confirmed that loss of the *H99* region alone had no effect on expression of *10xStat>GFP* (Figure IV.5C). By contrast, expression of *10xStat>GFP* is very strongly up-regulated in eye-antennal discs carrying clones of *ept,H99* cells (Figure IV.5D). An interesting pattern of GFP expression was observed in this experiment: some clones of *ept,H99* mutant cells located in the eye disc express *10xStat>GFP* highly both within clonal boundaries and in surrounding cells (see arrow in 5D′ and D″), whereas other nearby eye clones do not (see arrowhead in 5D′ and D″). This difference appears to be due to anterior/posterior positioning: clones that activate *10xStat>GFP* tend to be located anterior to the presumptive morphogenetic furrow, whereas those that do not tend to be located in posterior regions of the disc. Autonomous and non-autonomous activation of *10xStat>GFP* by *ept,H99* clones is also observed in the antennal disc (Figure IV.5D-E). *10xStat>GFP* can be strongly activated both within clones and in cells located 5-10 cell diameters away from the mutant clones (Figure IV.5E-E″, arrows and white outlines). This evidence of non-autonomous *10xStat>GFP* expression fits very well with previous models in which excess Upd produced by *ept* or *vps25* mutant cells is able to activate Stat in surrounding cells (Moberg et al., 2005; Vaccari and Bilder, 2005). The more novel observation of autonomous *10xStat>GFP* activation within *ept,H99* mutant clones agrees with the data gathered with the pY-Stat92E and *3xGAS-lacZ* reporters. The differences in the readouts provided by these three pathway reporters also

suggest that *10xStat>GFP* may be a more faithful reporter of Stat92E activity in larval discs than either pY-Stat92E or *3xGAS-lacZ*.

In aggregate, these observations indicate that the effect of *stat92E* heterozygosity on *ept* tumor growth is a reflection of a role for JAK-STAT hyperactivity in the growth, cell cycle, and polarity characteristics of *ept* mutant cells.

Figure IV.4. pY-Stat92E levels in *ept* mutant eye disc cells.

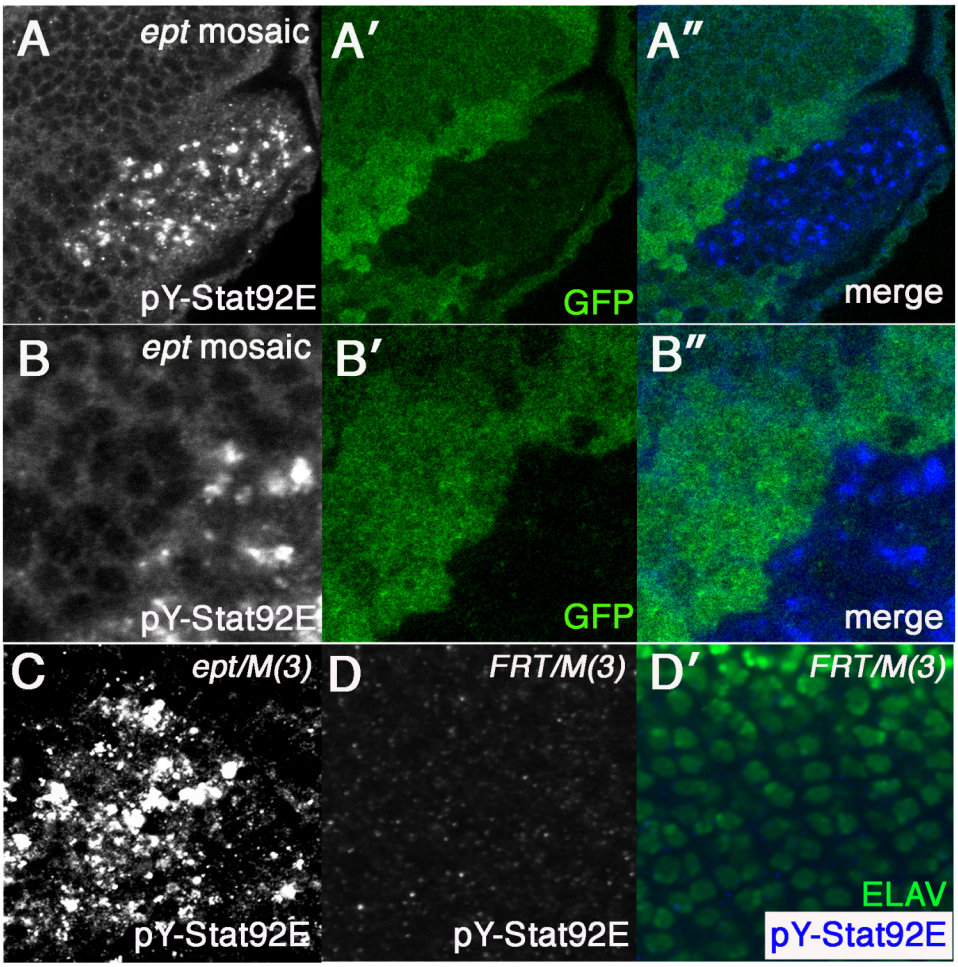

A clone of *ept*^{2} mutant eye disc cells (A-B) marked by the absence of GFP (green) and stains brightly for the pTyr-Stat92E epitope (blue). Note the pY-Stat92E epitope is specifically enriched within *ept*^{2} mutant clones. Anti-pY-Stat92E signal in an *ept*^{2}*/M(3)* eye-antennal tumor (C) and in a control *FRT80B/M(3)* eye antennal disc posterior to the morphogenetic furrow (D). Areas imaged in panels A, B, and D are posterior to the MF; the tumor in panel C has no MF.

Figure IV.5. Stat92E sensor activity in *ept* mutant eye-antennal cells.

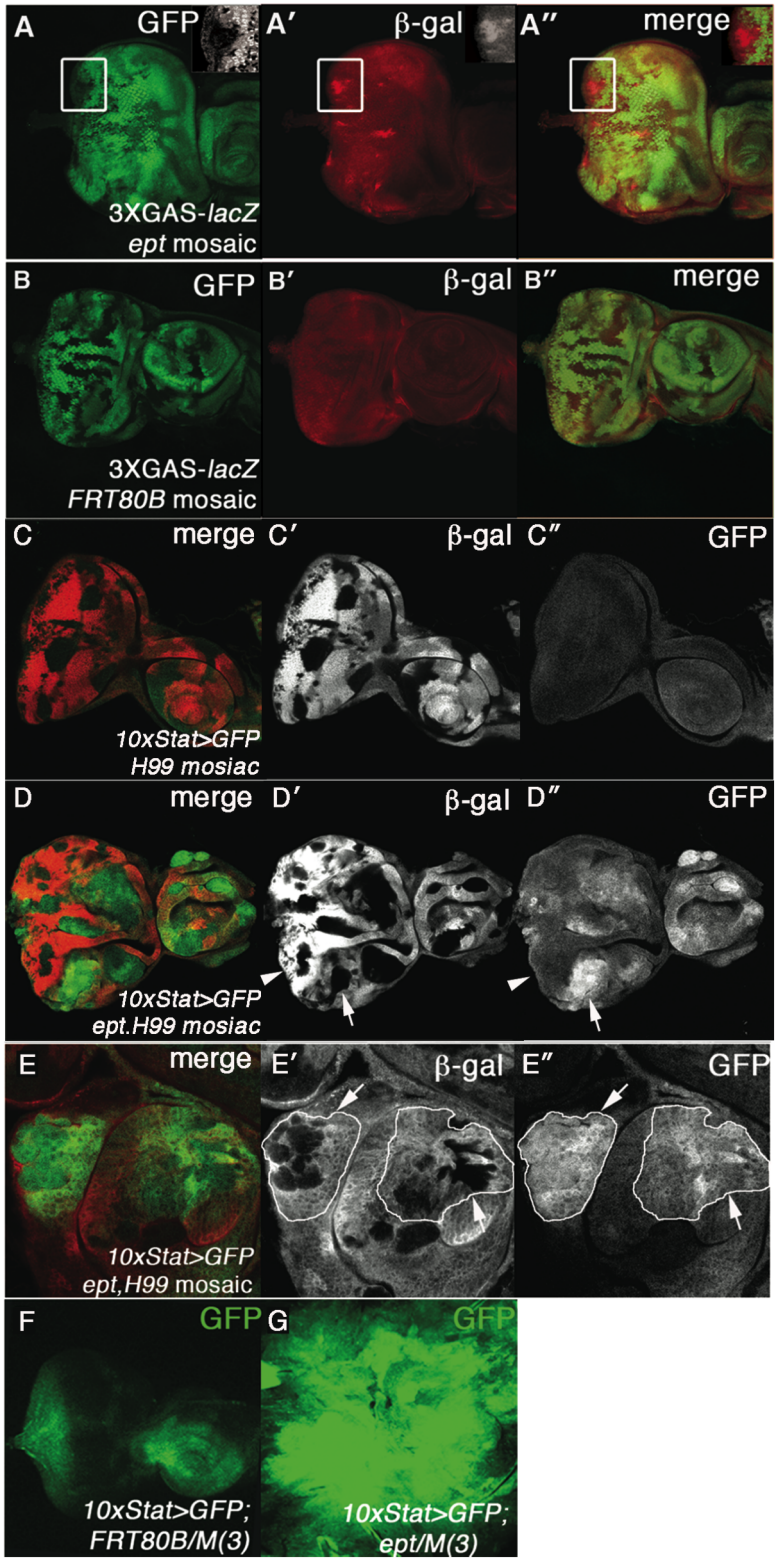

Eye discs carrying clones of *ept*^{2} mutant cells (A-A") or *FRT80B* control cells (B-B") marked by the absence of GFP (green) and stained for expression of β-galactosidase (β-gal; red in A' and B') to detect expression of the *3xGAS-lacZ* Stat-reporter. Inset in (A-A") shows an *ept*^{2} mutant clone that shows cell autonomous activation of *3xGAS-lacZ*. Because the *3xGAS-lacZ* transgene and the *ept* gene are both located on chromosome arm 3L, the reporter is present in two copies in both *FRT80B* and *ept* mutant clones; images in A' and B' were captured using exactly the same optical settings. (C-E) Expression of the *10xStat>GFP* transgene (green) in *ept*^{X1}*,H99* mosaic discs in which mutant cells are marked by the absence of β-gal (red). Arrowhead marks clone of *ept*^{X1}*,H99* mutant cells in the eye disc that do not activate *10xStat>GFP*; arrow marks an example of an antennal clone that activates *10xStat>GFP* within the clone and in surrounding wild type cells. Images in (E-E") are of the antennal region of an *ept*^{X1}*,H99* mosaic disc. White outlines in panel (E″) denotes boundaries of GFP-expressing cells. Expression of the Stat reporter *10xStat>GFP* (green) in a control *FRT80B/M(3)* eye disc (F) and an *ept*^{2} eye-antennal tumor (G). The disc in (F) was imaged at half the fluorescence intensity relative to the control disc in (G).

IV.C2. Cell-autonomous effect of *ept* loss on Dome

The autonomous effect of *ept* loss of pY-Stat92E suggests that this phenotype is not only an indication of JAK-STAT activation, but may also reveal a requirement for *ept* in controlling an intracellular step in the JAK-STAT cascade. Consequently, we sought to test whether *ept* loss affects trafficking of the transmembrane receptor Dome. Dome traffics through the late endosome (Ghiglione et al., 2002), and loss of the *hrs* gene, which acts at the step immediately preceding *ept* (reviewed in Raiborg et al., 2003), blocks Dome trafficking and activation even in the presence of Upd (Devergne et al., 2007). These observations have led to the proposal that movement of Dome into and through the endosomal system is a significant regulatory step in JAK-STAT signaling (Devergne et al., 2007). Since loss of *ept* leads to accumulation of certain apical trans-membrane proteins in the late endosome (Moberg et al., 2005), we tested whether *ept* loss might also affect levels or localization of Dome. An antibody specific to the Dome protein (Ghiglione et al., 2002) detects much higher levels of Dome in *ept* cells than in surrounding normal cells (Figure IV.6A-A"). This Dome appears as puncta that partially colocalize with the endosomal protein Hrs (see arrowheads in Figure IV.6). Loss of *ept* may also have more mild non-autonomous effects on Dome (see cells to the right of the clone in Figure IV.5A″). Since Hrs-dependent movement of Dome into the late-endosome has been proposed to be required for activation of Stat92E (Devergne et al., 2007), we next tested whether the accumulation of the pY-Stat92E epitope in *ept* mutant cells was dependent on Dome activity. The *Actin>CD2>Gal4* 'flip-out' chromosome (Pignoni and Zipursky, 1997) was used in combination with a *UAS-GFP* transgene and a transgene carrying a dominant-negative form of *dome* that lacks the C-terminal tail (*UAS-*

dome$^{\Delta CYT}$) (Brown et al., 2001) to produce GFP-positive/ *dome*$^{\Delta CYT}$ -expressing clones in the background of an *ept* tumor. *ept* mutant cells that express the *dome*$^{\Delta CYT}$ allele (GFP-positive area in Figure IV.6B-B″) do not display excess anti-pY-Stat92E staining, whereas those that do not express *dome*$^{\Delta CYT}$ (GFP-negative area in Figure IV.6B-B″) retain high levels of the pY-Stat92E epitope. From these data, we conclude that *ept* loss alters Dome localization and levels in eye imaginal disc cells, and this correlates with Dome-dependent accumulation of the pY-Stat92E epitope. These data agree with a proposed model in which Dome must access the Hrs-positive late endosome in order to activate signaling (Devergne et al., 2007). The trapping of Dome in this activation compartment in *ept* mutants may therefore contribute to high-level activation of the JAK-STAT pathway observed in these cells.

Figure IV.6. Dome localization in *ept* mutant tissue.

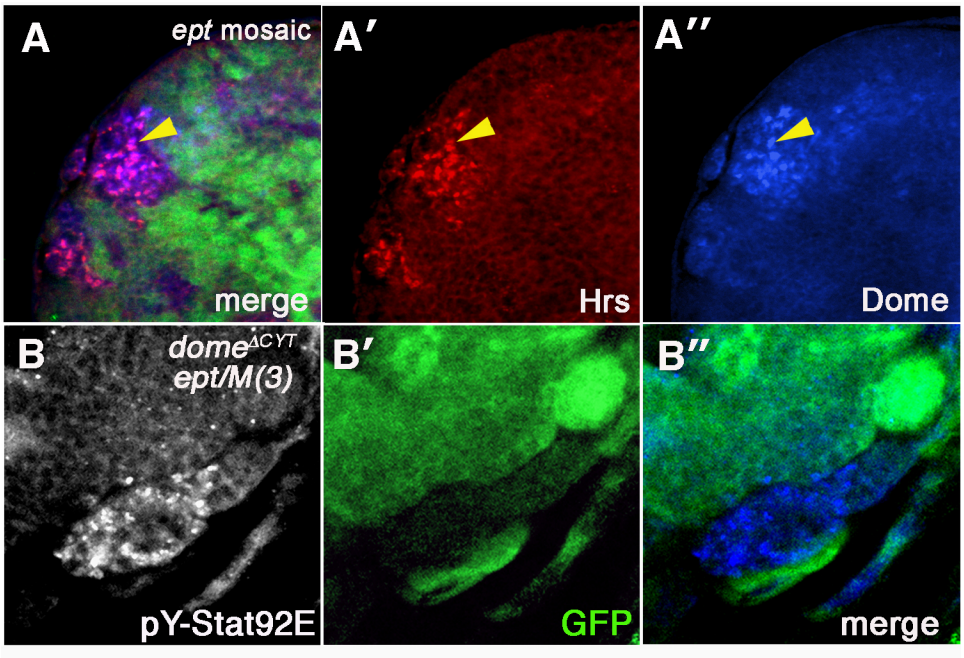

(A-A") A clone of *ept*^{2} mutant eye disc cells marked by the absence of GFP (green) stained for Dome (blue) and the endocytic marker Hrs (red) shows extensive accumulation of Dome in Hrs-positive structures (yellow arrowhead denotes example of magenta overlap). (B-B") A confocal image of a section of an *ept*^{2} eye-antennal tumor expressing *dome*$^{\Delta CYT}$ (using the *eyFLP;Actin>CD2>Gal4, UAS-GFP* system) and stained for anti-pYStat92E (blue); GFP (green) marks cells that express the *dome*$^{\Delta CYT}$ transgene. The anti-pY-Stat92E epitope is strongly reduced in cells that express *dome*$^{\Delta CYT}$ but not in the patch of GFP-negative, *ept*^{2} mutant cells that do not express *dome*$^{\Delta CYT}$.

IV.D. DISCUSSION

We have sought to identify pathways that mediate the cell-autonomous growth suppressor activity of the *Drosophila* endocytic gene *ept*, which encodes a homolog of mammalian Tumor Susceptibility Gene-101. We find that *ept* is required *in vivo* to restrict cell-autonomous activation of the JAK-STAT pathway. As described in Gilbert, *et al*., pathway activation correlates with effects of the *Drosophila stat92E* gene on G1/S cell cycle control, cell size, and epithelial organization of *ept* mutant tumors (Gilbert et al., 2009). A previous study in the cultured *Drosophila* hemocyte S2 cell line also identified *ept* as a negative regulator of JAK-STAT signaling (Muller et al., 2005), but the extent to which this relationship is conserved in developing tissues in the whole organism and its contribution to *ept* loss-of-function phenotypes were not addressed.

We also find that trafficking of Dome, which acts upstream of Stat92E, is altered in *ept* mutant cells. Since Upd can stimulate the endocytic uptake of Dome (Ghiglione et al., 2002), the effect of *ept* loss on Dome protein could theoretically be a secondary consequence of the fact that these cells express highly elevated levels of Upd (Moberg et al., 2005). In addition, it has been shown that *dome* itself is a transcriptional target of Stat92E as part of a positive feedback loop (Bach et al., 2003). Alternatively, the relationship between *ept* and Dome localization could indicate a direct requirement for *ept* in Dome endolysosomal trafficking in much the same way that ESCRT mutants block the vesicular movement and lysosomal turnover of the Notch receptor (Moberg et al., 2005; Thompson et al., 2005; Vaccari and Bilder, 2005; Vaccari et al., 2008). The simple observation that Dome can be trapped in an Hrs-positive compartment agrees with other studies that have shown that the Dome receptor also fluxes through the ESCRT

endosomal system in imaginal disc and ovarian follicle cells and that endocytic trafficking of Dome can modulate the output of the downstream JAK-STAT pathway (Devergne et al., 2007; Ghiglione et al., 2002). The oncogenic properties of this pathway are well-established in flies (Bach et al., 2003; Hanratty and Dearolf, 1993; Harrison et al., 1995; Luo et al., 2002; Tsai and Sun, 2004) and mammals (reviewed in Calo et al., 2003), but its pro-growth targets are not fully understood.

The *Drosophila* and mammalian forms of TSG101 are quite similar at a primary sequence level (46% identical/61% similar), share the same domain structure (Moberg et al., 2005), and are predicted to have very similar molecular properties. Each has also been shown to function as part of the same conserved complex, ESCRT-I, and to be involved in the same biological process: endocytic trafficking of internalized receptors and membrane proteins. However, both gain and loss of mammalian TSG101 have been shown to contribute to tumorigenesis, rendering its relationship to the roles of *ept* in *Drosophila* epithelia unclear. Mammalian TSG101 was first identified based on its ability to inhibit cell transformation (Li and Cohen, 1996) and by its apparent mutational inactivation in some cancers (Li et al., 1997). Subsequent analysis of mice carrying a targeted deletion of the *TSG101* gene revealed a requirement for *TSG101* in embryonic viability but found no effect on cancer incidence or progression (Krempler et al., 2002; Ruland et al., 2001). More recent work showing that the *TSG101* gene is overexpressed in some human cancers (Oh et al., 2007; Young et al., 2007a; Young et al., 2007b) and that transgenic overexpression of TSG101 in the mouse mammary gland mildly increases the frequency of breast carcinoma (Oh et al., 2007) tends to support the idea that excess TSG101 promotes, rather than inhibits, cell survival and proliferation. Since signaling via

the EGF receptor, which is sorted to the lysosome via an ESCRT-dependent pathway in mammalian cells (Bache et al., 2006; Lu et al., 2003; Malerod et al., 2007; Raiborg et al., 2007), is elevated in cells that overexpress TSG101 (Oh et al., 2007), excessively high levels of TSG101 may be capable of acting in a dominant-negative manner to reduce endocytic degradation of its normal targets thereby enhancing cell proliferation.

The somewhat discordant views of the growth regulatory properties of TSG101-like proteins provided by mammalian and insect models may reflect stage- or tissue-specific differences in the spectrum of proteins routed into the ESCRT pathway in each type of organism. In addition to Crb and Notch, *Drosophila ept* has now been shown to affect localization and levels of the Dome receptor. Loss of the ESCRT-II subunit and tumor suppressor gene *vps25* additionally affects trafficking of the Thickveins TGFß receptor (Thompson et al., 2005), and loss of the *hrs* gene affects a wide spectrum of cell surface receptors (Jekely and Rorth, 2003). Therefore, *ept* may influence the trafficking of as yet unidentified transmembrane proteins. It remains to be determined whether or not the effect of *ept* on Dome is direct and whether Dome homologs in other species are also affected by alterations in ESCRT-mediated trafficking. However, if these proteins require TSG101 to traffic through the ESCRT pathway in a specific subset of mammalian epithelia, it may be that impaired TSG101 function in these tissues will result in growth phenotypes similar to those observed in *Drosophila* imaginal disc epithelia lacking *ept*.

IV.E. MATERIALS AND METHODS

Genetics: Crosses were done at 25°C unless otherwise indicated. *ept* clones were generated by crossing *w;ept^{2},FRT80B/TM6B* and *yweyFLP;P[m-w^{+};ubiGFP],FRT80B*. *ept,H99* clones were generated by crossing *w;ept^{X1},H99,FRT80B/TM6B* and *yweyFLP;P[m-w^{+};ubiGFP],FRT80B*. *ept* mutant eye-antennal tumors were generated by crossing *w;ept^{2},FRT80B* and *yweyFLP;P[m-w^{+}]RpL14^{1},FRT80B/TM6B*. The *3xGAS-lacZ* reporter was placed into control or *ept* mutant backgrounds by crossing *3xGAS-lacZ,FRT80B/TM6B* or *3xGAS-lacZ,ept^{2},FRT80B/TM6B* males to *yweyFLP;P[mw^{+};ubiGFP],FRT80B* females. *10xStat-GFP* (gift of E. Bach) activity was measured by crossing *10xStat-GFP;ept^{2}FRT80B/TM6B* or *10xStat-GFP;FRT80B* to *yweyFLP;P[m-w^{+}]L14^{1},FRT80B/TM6B*. '*ept,stat92E^{06346}/+*' animals were obtained by crossing *w;ept^{2},FRT80B,stat92E^{06346}/TM6B* to *yweyFLP;P[w^{+}]RpL14^{1},FRT80B/TM6B*. '*DN-dome; ept/M(3)*' animals were obtained by crossing *UAS- dome$^{\Delta CYT}$;ept/TM6B* and *yweyFLP;act<y^{+}<Gal4/*CyO:*twi*-GFP;*P[m-w^{+}]RpL14^{1} FRT80B/TM6B* animals.

Molecular biology: Total RNA from *FRT80B/M(3), ept/M(3)* and *ept/M(3), stat92E^{06346}/+* animals was isolated using TRIzol (Invitrogen) and reverse transcribed (SuperScript II RT/Invitrogen). *crb* transcript was analyzed by qPCR (SYBR Green 1 Master/Roche). *rp49* was used as a control to normalize *crb* transcript levels in each sample. Primers used: *crb* 5'-cgtgctcgtttgacagttgta-3' and 5'-cgattcggagtgcgtagg-3'; *rp49* 5'-cttcatccgccaccagtc-3' and 5'-cgacgcactctgttgtcg-3'. RNA in situ hybridization was performed as described previously (Mortimer and Moberg, 2007). A DIG labeled *crb* riboprobe was synthesized from the linearized *crb* cDNA (DGRC) and visualized with anti-DIG-AP (1:2000, Roche).

Flow Cytometry: Discs were dissociated in PBS Trypsin-EDTA, 20 μM DRAQ-5 (Biostatus Limited). Sample data were acquired on a Becton Dickinson LSR II flow cytometer via a 755 nM Red laser with a 780/60 nM BP collection filter and analyzed with FACSDiva Software.

Microscopy & Immunohistochemistry: Immunostaining and confocal microscopy was performed as described previously (Moberg et al., 2001). Antibodies used: rat α-Crb-extra (gift of U. Tepass and E. Knust) 1:500; guinea pig a-Hrs (gift of H. Bellen) 1:1000; rabbit anti-pYStat92E (Cell Signaling) 1:1000; mouse a-Dlg (DSHB) 1:20; rabbit a-Domeless-intra (gift of S. Noselli) 1:200; goat a-rabbit Cy5, goat a-mouse Cy3, goat a-guinea pig Cy3, and goat a-rat Cy3 (Jackson Laboratories) each at 1:50; YOYO (Molecular Probes) was used at 1:2000.

IV.F. REFERENCES

Bach, E. A., Ekas, L. A., Ayala-Camargo, A., Flaherty, M. S., Lee, H., Perrimon, N. and Baeg, G. H. (2007). GFP reporters detect the activation of the Drosophila JAK/STAT pathway in vivo. *Gene Expr Patterns* **7**, 323-31.

Bach, E. A., Vincent, S., Zeidler, M. P. and Perrimon, N. (2003). A sensitized genetic screen to identify novel regulators and components of the Drosophila janus kinase/signal transducer and activator of transcription pathway. *Genetics* **165**, 1149-66.

Bache, K. G., Stuffers, S., Malerod, L., Slagsvold, T., Raiborg, C., Lechardeur, D., Walchli, S., Lukacs, G. L., Brech, A. and Stenmark, H. (2006). The ESCRT-III subunit hVps24 is required for degradation but not silencing of the epidermal growth factor receptor. *Mol Biol Cell* **17**, 2513-23.

Bishop, N. and Woodman, P. (2001). TSG101/mammalian VPS23 and mammalian VPS28 interact directly and are recruited to VPS4-induced endosomes. *J Biol Chem* **276**, 11735-42.

Brown, S., Hu, N. and Hombria, J. C. (2001). Identification of the first invertebrate interleukin JAK/STAT receptor, the Drosophila gene domeless. *Curr Biol* **11**, 1700-5.

Calo, V., Migliavacca, M., Bazan, V., Macaluso, M., Buscemi, M., Gebbia, N. and Russo, A. (2003). STAT proteins: from normal control of cellular events to tumorigenesis. *J Cell Physiol* **197**, 157-68.

Chao, J. L., Tsai, Y. C., Chiu, S. J. and Sun, Y. H. (2004). Localized Notch signal acts through eyg and upd to promote global growth in Drosophila eye. *Development* **131**, 3839-47.

Devergne, O., Ghiglione, C. and Noselli, S. (2007). The endocytic control of JAK/STAT signalling in Drosophila. *J Cell Sci* **120**, 3457-64.

Ghiglione, C., Devergne, O., Georgenthum, E., Carballes, F., Medioni, C., Cerezo, D. and Noselli, S. (2002). The Drosophila cytokine receptor Domeless controls border cell migration and epithelial polarization during oogenesis. *Development* **129**, 5437-47.

Gilbert, M. M., Beam, C. K., Robinson, B. S. and Moberg, K. H. (2009). Genetic interactions between the Drosophila tumor suppressor gene ept and the stat92E transcription factor. *PLoS One* **4**, e7083.

Gilbert, M. M., Weaver, B. K., Gergen, J. P. and Reich, N. C. (2005). A novel functional activator of the Drosophila JAK/STAT pathway, unpaired2, is revealed by an in vivo reporter of pathway activation. *Mech Dev* **122**, 939-48.

Hanratty, W. P. and Dearolf, C. R. (1993). The Drosophila Tumorous-lethal hematopoietic oncogene is a dominant mutation in the hopscotch locus. *Mol Gen Genet* **238**, 33-7.

Harrison, D. A., Binari, R., Nahreini, T. S., Gilman, M. and Perrimon, N. (1995). Activation of a Drosophila Janus kinase (JAK) causes hematopoietic neoplasia and developmental defects. *EMBO J* **14**, 2857-65.

Harrison, D. A., McCoon, P. E., Binari, R., Gilman, M. and Perrimon, N. (1998). Drosophila unpaired encodes a secreted protein that activates the JAK signaling pathway. *Genes Dev* **12**, 3252-63.

Herz, H. M., Chen, Z., Scherr, H., Lackey, M., Bolduc, C. and Bergmann, A. (2006). vps25 mosaics display non-autonomous cell survival and overgrowth, and autonomous apoptosis. *Development* **133**, 1871-80.

Hombria, J. C. and Brown, S. (2002). The fertile field of Drosophila Jak/STAT signalling. *Curr Biol* **12**, R569-75.

Jekely, G. and Rorth, P. (2003). Hrs mediates downregulation of multiple signalling receptors in Drosophila. *EMBO Rep* **4**, 1163-8.

Katzmann, D. J., Babst, M. and Emr, S. D. (2001). Ubiquitin-dependent sorting into the multivesicular body pathway requires the function of a conserved endosomal protein sorting complex, ESCRT-I. *Cell* **106**, 145-55.

Krempler, A., Henry, M. D., Triplett, A. A. and Wagner, K. U. (2002). Targeted deletion of the Tsg101 gene results in cell cycle arrest at G1/S and p53-independent cell death. *J Biol Chem* **277**, 43216-23.

Li, J., Li, W., Calhoun, H. C., Xia, F., Gao, F. B. and Li, W. X. (2003). Patterns and functions of STAT activation during Drosophila embryogenesis. *Mech Dev* **120**, 1455-68.

Li, L. and Cohen, S. N. (1996). Tsg101: a novel tumor susceptibility gene isolated by controlled homozygous functional knockout of allelic loci in mammalian cells. *Cell* **85**, 319-29.

Li, L., Li, X., Francke, U. and Cohen, S. N. (1997). The TSG101 tumor susceptibility gene is located in chromosome 11 band p15 and is mutated in human breast cancer. *Cell* **88**, 143-54.

Lloyd, T. E., Atkinson, R., Wu, M. N., Zhou, Y., Pennetta, G. and Bellen, H. J. (2002). Hrs regulates endosome membrane invagination and tyrosine kinase receptor signaling in Drosophila. *Cell* **108**, 261-9.

Lu, Q., Hope, L. W., Brasch, M., Reinhard, C. and Cohen, S. N. (2003). TSG101 interaction with HRS mediates endosomal trafficking and receptor down-regulation. *Proc Natl Acad Sci U S A* **100**, 7626-31.

Luo, H., Rose, P. E., Roberts, T. M. and Dearolf, C. R. (2002). The Hopscotch Jak kinase requires the Raf pathway to promote blood cell activation and differentiation in Drosophila. *Mol Genet Genomics* **267**, 57-63.

Malerod, L., Stuffers, S., Brech, A. and Stenmark, H. (2007). Vps22/EAP30 in ESCRT-II mediates endosomal sorting of growth factor and chemokine receptors destined for lysosomal degradation. *Traffic* **8**, 1617-29.

Moberg, K. H., Bell, D. W., Wahrer, D. C., Haber, D. A. and Hariharan, I. K. (2001). Archipelago regulates Cyclin E levels in Drosophila and is mutated in human cancer cell lines. *Nature* **413**, 311-6.

Moberg, K. H., Schelble, S., Burdick, S. K. and Hariharan, I. K. (2005). Mutations in erupted, the Drosophila ortholog of mammalian tumor susceptibility gene 101, elicit non-cell-autonomous overgrowth. *Dev Cell* **9**, 699-710.

Mortimer, N. T. and Moberg, K. H. (2007). The Drosophila F-box protein Archipelago controls levels of the Trachealess transcription factor in the embryonic tracheal system. *Dev Biol* **312**, 560-71.

Muller, P., Kuttenkeuler, D., Gesellchen, V., Zeidler, M. P. and Boutros, M. (2005). Identification of JAK/STAT signalling components by genome-wide RNA interference. *Nature* **436**, 871-5.

Oh, K. B., Stanton, M. J., West, W. W., Todd, G. L. and Wagner, K. U. (2007). Tsg101 is upregulated in a subset of invasive human breast cancers and its targeted overexpression in transgenic mice reveals weak oncogenic properties for mammary cancer initiation. *Oncogene* **26**, 5950-9.

Pignoni, F. and Zipursky, S. L. (1997). Induction of Drosophila eye development by decapentaplegic. *Development* **124**, 271-8.

Raiborg, C., Malerod, L., Pedersen, N. M. and Stenmark, H. (2007). Differential functions of Hrs and ESCRT proteins in endocytic membrane trafficking. *Exp Cell Res*.

Raiborg, C., Rusten, T. E. and Stenmark, H. (2003). Protein sorting into multivesicular endosomes. *Curr Opin Cell Biol* **15**, 446-55.

Ruland, J., Sirard, C., Elia, A., MacPherson, D., Wakeham, A., Li, L., de la Pompa, J. L., Cohen, S. N. and Mak, T. W. (2001). p53 accumulation, defective cell proliferation, and early embryonic lethality in mice lacking tsg101. *Proc Natl Acad Sci U S A* **98**, 1859-64.

Stuffers, S., Brech, A. and Stenmark, H. (2008). ESCRT proteins in physiology and disease. *Exp Cell Res*.

Thompson, B. J., Mathieu, J., Sung, H. H., Loeser, E., Rorth, P. and Cohen, S. M. (2005). Tumor suppressor properties of the ESCRT-II complex component Vps25 in Drosophila. *Dev Cell* **9**, 711-20.

Tsai, Y. C. and Sun, Y. H. (2004). Long-range effect of upd, a ligand for Jak/STAT pathway, on cell cycle in Drosophila eye development. *Genesis* **39**, 141-53.

Vaccari, T. and Bilder, D. (2005). The Drosophila tumor suppressor vps25 prevents nonautonomous overproliferation by regulating notch trafficking. *Dev Cell* **9**, 687-98.

Vaccari, T., Lu, H., Kanwar, R., Fortini, M. E. and Bilder, D. (2008). Endosomal entry regulates Notch receptor activation in Drosophila melanogaster. *J Cell Biol* **180**, 755-62.

White, K., Grether, M. E., Abrams, J. M., Young, L., Farrell, K. and Steller, H. (1994). Genetic control of programmed cell death in Drosophila. *Science* **264**, 677-83.

Young, T. W., Mei, F. C., Rosen, D. G., Yang, G., Li, N., Liu, J. and Cheng, X. (2007a). Up-regulation of tumor susceptibility gene 101 protein in ovarian carcinomas revealed by proteomics analyses. *Mol Cell Proteomics* **6**, 294-304.

Young, T. W., Rosen, D. G., Mei, F. C., Li, N., Liu, J., Wang, X. F. and Cheng, X. (2007b). Up-regulation of tumor susceptibility gene 101 conveys poor prognosis through suppression of p21 expression in ovarian cancer. *Clin Cancer Res* **13**, 3848-54.

Zeidler, M. P., Bach, E. A. and Perrimon, N. (2000). The roles of the Drosophila JAK/STAT pathway. *Oncogene* **19**, 2598-606.

Chapter V: Future Directions and Concluding Remarks

V.A. FUTURE DIRECTIONS: *gang of four*

We have genetically characterized the *gfr* alleles and have shown that *gfr* integrates signals from several pathways to affect growth and patterning. Future directions for this project should be aimed at molecular identification of the *gfr* lesions and subsequent molecular characterization of the *gfr* gene product.

V.A1. Mapping

Extensive meiotic mapping places the lethality associated with gfr^{1} closely linked to a genomic interval at 70A-B, but the gfr^{3} allele appears to map quite proximal to this chromosomal region (see Chapter II). In addition, all alleles except gfr^{3} promote the overexpression of a gene in this region, *bru-3*. However, aside from the effects on *bru-3* transcription, gfr^{1} and gfr^{3} have same the mutant cellular phenotypes, including the downregulation of the Ras/MAPK pathway component Capicua. So, why do such discrepancies exist in the mapping data for these two alleles? I suspect that either (1) gfr^{1} and gfr^{3} exhibit non-allelic noncomplementation or (2) the nature of each allele prevents correlation by recombination mapping. If the first hypothesis is correct, then it is expected that the two alleles would indeed share many mutant phenotypes, since the genes would be predicted to act on the same process or in the same complex. Of course, only upon identification of the molecular lesions associated with each allele or with additional mapping can these two points be firmly assessed. However, in support of this latter hypothesis, there appear to be several annotated natural transposons within and surrounding *bru-3* (FlyBase). Therefore, if either *gfr* allele was created by a local transposon hop (as observed for the ept^{2} allele isolated in the same screen, Moberg et al.,

2005), then the use of transposase in the male *P*-element mapping strategy may have promoted additional transposition events that complicated the data. Moreover, in *Drosophila*, the density of transposons is negatively correlated with recombination rate: the higher the density of transposons, the lower the recombination rate (Rizzon et al., 2002). Thus, the presence of areas within this chromosomal region that have low recombination rates, together with the finding that recombination rates vary greatly over short stretches of DNA (Zhai et al., 2003), suggest that the genetic map generated for each allele with recombination data may not correlate closely with the molecular map. All of this circumstantial evidence indicates that gfr^{1} and gfr^{3} could be closer together on the chromosome than calculations with the *P*-element meiotic recombination data lead us to assume and supports the possibility that gfr^{1} and gfr^{3} are indeed allelic.

Immediate future directions to identify the *gfr* molecular lesions should test the working hypothesis that the *gfr* complementation group represents gain-of-function alleles of *bru-3*. To further address this claim, I plan to perform genomic PCR on conserved regions upstream of *bru-3* to detect chromosomal aberrations in putative regulatory regions. Blasting 10 kb of *bru-3* upstream sequence against the *Anopheles gambiae* genome reveals three short stretches of high conservation that will be the focus of my initial analysis. Additionally, if *gfr* alleles are gain-of-function for *bru-3*, then genetics argue that reduction of *bru-3* should rescue *gfr/gfr* lethality. However, because *gfr* and *bru-3* are closely linked and alleles of the genes do not readily recombine, I am currently testing whether RNAi knock-down of *bru-3* is sufficient to rescue *gfr/gfr* lethality.

At the end of the Discussion (Chapter II.D), we suggested the possibility that '*gfr* alleles affect the expression of multiple genes in the *bru-3* region (for example, by disrupting a chromatin insulator element) and that the *gfr* phenotypes are the product of altered expression of multiple genes.' To this end, I have tested the expression levels of a few genes neighboring *bru-3*, including *CG10133*, *CG17689*, and *CG10089*, and have not detected any relative changes; nonetheless, expression of additional annotated genes in this region should be assessed to more fully test this idea. In support of this 'insulator hypothesis,' however, I have found that not only does an allele of *bru-3* or *Df(3L)Exel6119* (removing eight annotated genes spanning from *stv* to *bru-3*) rescue the synthetic lethality observed between *gfr* and *puckered* alleles (see Table II.3), but a small deficiency immediately adjacent to *Df(3L)Exel6119*, *Df(3L)Exel9017*, also rescues *gfr/puc* lethality (CKB, data not shown). The entire genome region spanned by *Df(3L)Exel9017* was sequenced in the *gfr* alleles, and no mutations were identified. Therefore, this evidence that genetic reduction of several annotated genes in the region surrounding *bru-3* is sufficient to rescue *gfr/puc* lethality lends merit to the notion that *gfr* alleles represent mutations in a regulatory DNA element. *Df(3L)Exel9017* removes *CG10089* and *CG10738*, neither of which has been specifically studied. Interestingly, *CG10089* is predicted to encode a dual specificity protein phosphatase with activity similar to *puckered*. Thus, because *CG10089* is so closely related to *puc*, rather than removing a region containing the *gfr* locus with *Df(3L)Exel9017*, we may have simply discovered a functional interaction among *gfr*, *puc*, and *CG10089* that could be further explored upon molecular identification of the *gfr* gene.

I was merely unlucky that the two alleles I chose to comprehensively map, *gfr*^{1} and *gfr*^{3}, gave different recombination mapping results and different molecular results with respect to *bru-3* expression. Therefore, long-term future directions should include the unbiased recombination mapping of *gfr*^{2} and *gfr*^{x} using the same techniques previously described (*P*-element meiotic recombination mapping and male *P* mapping; see Chapter II.C2). It is the hope that large-scale recombination mapping with additional alleles will confirm the genetic region corresponding to the lethality associated with each lesion. Once a precise chromosomal region is successfully narrowed down, and if that region is uncovered by a deficiency that complements the *gfr* alleles, such as *Df(3L)ED4502*, then genomic PCR or Southern blotting for chromosomal aberrations and additional sequencing in the region should be carried out. However, in the unlikely event that *gfr*^{2} or *gfr*^{x} map to a different location, then complementation testing with deficiencies and/or known lethals in that region should first be conducted. With the *P*-element meiotic mapping strategy as described by Zhai *et al*., it is apparently possible to define a 50-kb interval containing the lesions. After defining this region, the authors then recommend using a heteroduplex DNA mutation detection system to locate the lesions (Zhai et al., 2003). Although this technology is not currently available in our lab, it remains another possible method for molecular identification of the *gfr* gene.

V.A2. *gfr* molecular mechanism

gfr alleles appear to elicit growth and patterning phenotypes via effects on multiple signaling pathways, including Notch and Ras/MAPK. We also found that the *gfr*^{1} eye overgrowth requires a diploid dose of *yorkie* (*yki*; Figure V.1), a transcriptional

coactivator that regulates pro-growth and pro-survival target genes in response to Hippo pathway signaling (Huang et al., 2005). This genetic interaction with *yki* corresponds with a change in Yki levels/localization that is most strongly observed in *gfr* mutant clones just anterior to the MF in the larval eye disc (Figure V.1.A-A"). Since Yki protein is up-regulated in *gfr* clones anterior to the MF, we looked for evidence of increased Yki activity by detecting levels of a known target gene, *dIAP*. Although we expected to see an increase in DIAP protein, surprisingly, the same cells that appear to have increased Yki levels and nuclear localization have greatly reduced levels of DIAP relative to adjacent wild-type tissue (Figure V.1.B-B"). A recent report suggests that different transcription factors bind Yki in the anterior versus the posterior portions of the larval eye disc to promote transcription of Yki target genes (Peng et al., 2009). Thus, although the significance of the effect of yki^{B5} on *gfr* eye size and the differential expression of the Yki target *dIAP* are not clear, it may indicate a role for *gfr* in regulating transcriptional cofactors or target gene specificity downstream of the Hippo tumor suppressor pathway.

gfr alleles also overexpress the RNA-binding protein *bru-3*. While we have shown overexpression of *bru-3* can phenocopy some aspects of the *gfr* mutant phenotype (eg., decreased Cic levels; see Figure II.15), we have not tested the corollary—whether *gfr* alleles can phenocopy *bru-3* overexpression. *bru-3* misexpression has been shown to increase hemocyte number in larvae (Stofanko et al., 2008). Therefore, by driving GFP in hemocytes and observing whether the introduction a *gfr* allele is sufficient to increase GFP expression in larvae, we could assess whether *gfr* has a dominant influence on hemocyte number. While this experiment may show that *gfr* indeed affects *bru-3*

expression (this we already know), it does not give us any additional evidence that *gfr* and *bru-3* represent the same locus.

Future directions indeed include molecular characterization of the *gfr* gene product, but they also include the characterization of *gfr* expression patterns and the determination of how *gfr* itself is regulated during development. The first steps after identifying the *gfr* gene are to generate antibodies and probes to detect Gfr protein and mRNA expression, respectively. This will allow for the determination of *gfr*'s expression patterns relative to its tissue specificity or developmental stage of expression. In addition, a transgenic fly should be made to characterize *gfr*'s misexpression phenotype(s). However, if the *gfr* alleles are indeed gain-of-function, then loss-of-function alleles should be created if they are not already publically available. This can be accomplished by screening for imprecise excisions of a nearby *P*-element. The observed expression patterns and range of phenotypes will form the basis for second-site modifier screens to more fully characterize the pathways upstream and downstream of *gfr*.

Figure V.1. *gfr* mutant tissue exhibits differential expression of Yki and DIAP anterior to the morphogenetic furrow.

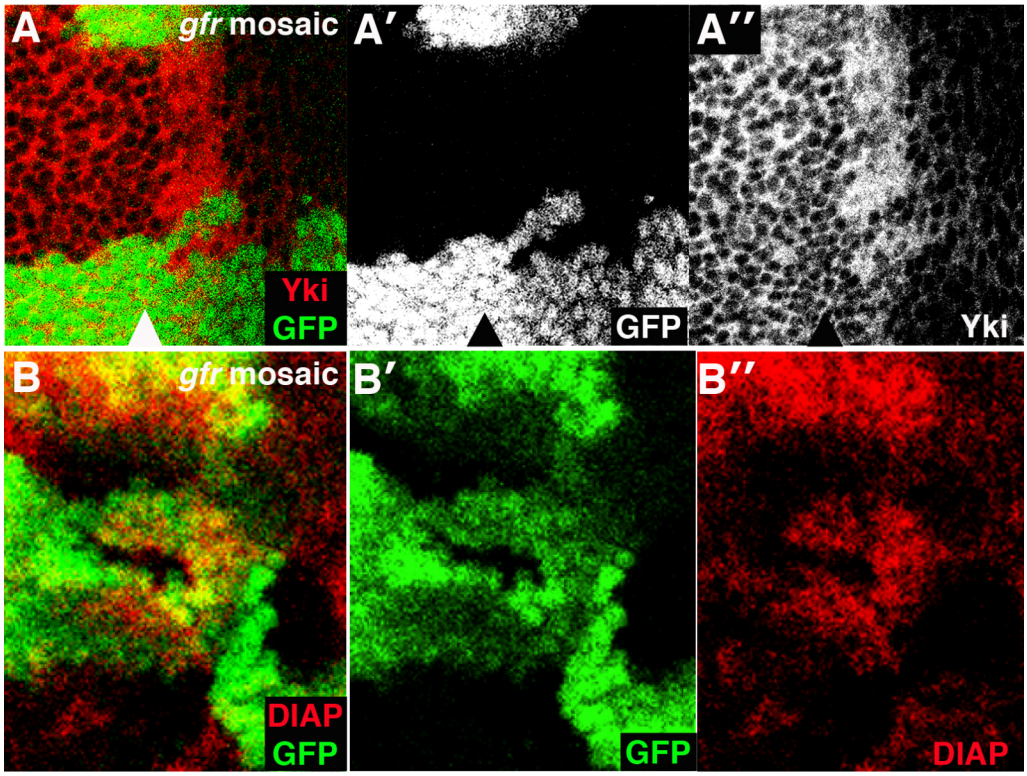

Merged confocal sections of *gfr*^{1} larval eye clones marked by the absence of GFP (green) and stained for Yorkie (Yki) (A-A") or DIAP (B-B") in red. (A-A") Yki protein levels are elevated and its localization is altered in *gfr* clones anterior to the MF. Arrowheads mark position of the MF. (B-B") DIAP protein levels are decreased in *gfr* clones anterior to the MF. Posterior is to the left in all panels.

V.B. FUTURE DIRECTIONS: *archipelago*

Our findings describe the initial characterization of Notch-dependent phenotypes in *ago* mutant tissue. For publication purposes, the presented data could be divided to address at least two main questions: (1) Is fly Notch an Ago substrate *in vivo*? and (2) What is the role of Notch in *ago* growth and differentiation defects? To fill gaps in the data, immediate future directions were discussed as results were presented (see Chapter III). Long-term future directions will be discussed here.

V.B1. Is fly Notch an Ago substrate *in vivo*?

It is currently unclear whether the Notch intracellular domain (N^{ICD}) is a target of Ago-mediated proteolysis in flies. It is necessary to address this outstanding question if we are to establish a foundation for comparative analysis between invertebrate and vertebrate systems. The conventional method of testing this hypothesis is to show that Ago physically binds and polyubiquitinates N^{ICD} *in vitro*. Because of the conserved structures of the Ago and Notch proteins and the presence of an Ago binding site in the N^{ICD} C-terminal domain (see Figure III.5), the two proteins are likely to bind *in vitro*. However, addressing whether N^{ICD} is an *in vivo* Ago substrate demands tackling the more curious question: why does exogenous N^{ICD} promote the downregulation of endogenous Notch protein in *ago* mutant cells (see Figure III.4)? These results, together with the observation that Notch activity but not N^{ICD} protein is increased upon *ago* loss, suggest the existence of a novel feedback loop in which a second, unidentified mechanism compensates for the lack of *ago* and reduces Notch protein levels in cells. Because only modest differences in Notch pathway activity suffice to determine dramatic differences in cellular behavior, this

pathway is tightly regulated by a variety of mechanisms. Therefore, the idea of a redundant mechanism to compensate for *ago* loss is not without merit. Upon characterization, such a mechanism designed to protect *ago* mutant cells against the transforming capabilities of excess Notch activity could theoretically be exploited to develop novel T-ALL treatments.

Because we observe high levels of Notch activity but no accumulation of Notch protein in *ago* mutant tissue, and Ago is the only factor implicated in the turnover of nuclear N^{ICD} in flies (Bray, 2006), it follows that a feedback mechanism activated upon *ago* loss may not act on nuclear Notch but at earlier phases of Notch signaling (Figure V.2). Endocytic sorting of Notch indeed mediates a key decision between its activation and downregulation (reviewed in Bray, 2006; Le Borgne, 2006); thus, one candidate to be involved in this feedback mechanism is *phyllopod* (*phyl*), which encodes an E3 ligase adaptor protein and is a transcriptional target of the EGFR pathway (Nagaraj and Banerjee, 2009). Phyl acts to modulate the amount of transcriptional activity from the Notch and Wingless pathways by degrading endocytic pools of these activated receptors (Nagaraj and Banerjee, 2009). Therefore, elevated Phyl levels or activity in *ago* mutant cells may explain why we observe increased Notch reporter activity without Notch accumulation. Since no antibody to Phyl currently exists, we have obtained a Phyl-YFP fusion (YD76) that can be placed in the background of ago^{1} clones to detect changes in Phyl levels. I would also hypothesize that N^{ICD} accumulation in *ago* mutant cells could be observed upon blocking this proposed feedback mechanism. In a preliminary analysis, genetic reduction of *phyl* by half in *ago* mutant tissue was insufficient to observe N^{ICD} stabilization (data not shown). However, generating a stronger knock-down of *phyl* by

using an RNAi line may prove more efficient. Since *phyl* mutant clones alone accumulate Notch (Nagaraj and Banerjee, 2009), controls must be carefully examined. Candidates other than Phyl to be tested in a similar fashion could include a Nedd4 family HECT-domain E3 ligase, Suppressor of Deltex (Su(dx))/Itch, or components of the ESCRT pathway, such as Erupted and Vps25, all of which also regulate trafficking and lysosomal degradation of the Notch receptor (reviewed in Bray, 2006; Le Borgne, 2006; Tien et al., 2009).

Another possibility remains that Ago is not the only F-box protein which binds nuclear N^{ICD}, suggesting a feedback model whereby activation of Notch target genes in the absence of *ago* triggers up-reguation of a related F-box protein (Figure V.3). Preliminary data from our lab indicate that Notch does not only act downstream of Ago, but also directly controls *ago* transcription (SCN and KHM pers. comm.). Therefore, if Notch normally directly regulates one factor implicated in its turnover, then excess N^{ICD} in *ago* mutant cells could be the signal that promotes transcription of a redundant, nuclear F-box. *Drosophila* has two additional F-box proteins structurally related to Ago: Supernumerary limbs (Slimb) and the uncharacterized CG9144. Although single F-box proteins typically recognize distinct substrates, it has recently been shown that both Ago and Slimb bind to and promote the turnover of the glial regulatory transcription factor, Glial cell missing (Gcm/Glide, Ho et al., 2009). We are currently testing this proposed feedback model by searching for Su(H) binding sites upstream of *slimb* and *CG9144* and by determining the expression of these two candidate genes in *ago* mutant eye tissue. If, in addition to Ago, Slimb or CG9144 also recognizes nuclear N^{ICD}, then only in tissue

doubly mutant for *ago* and the other F-box would nuclear accumulation of N^{ICD} be visible.

Figure V.2. Feedback Model 1.

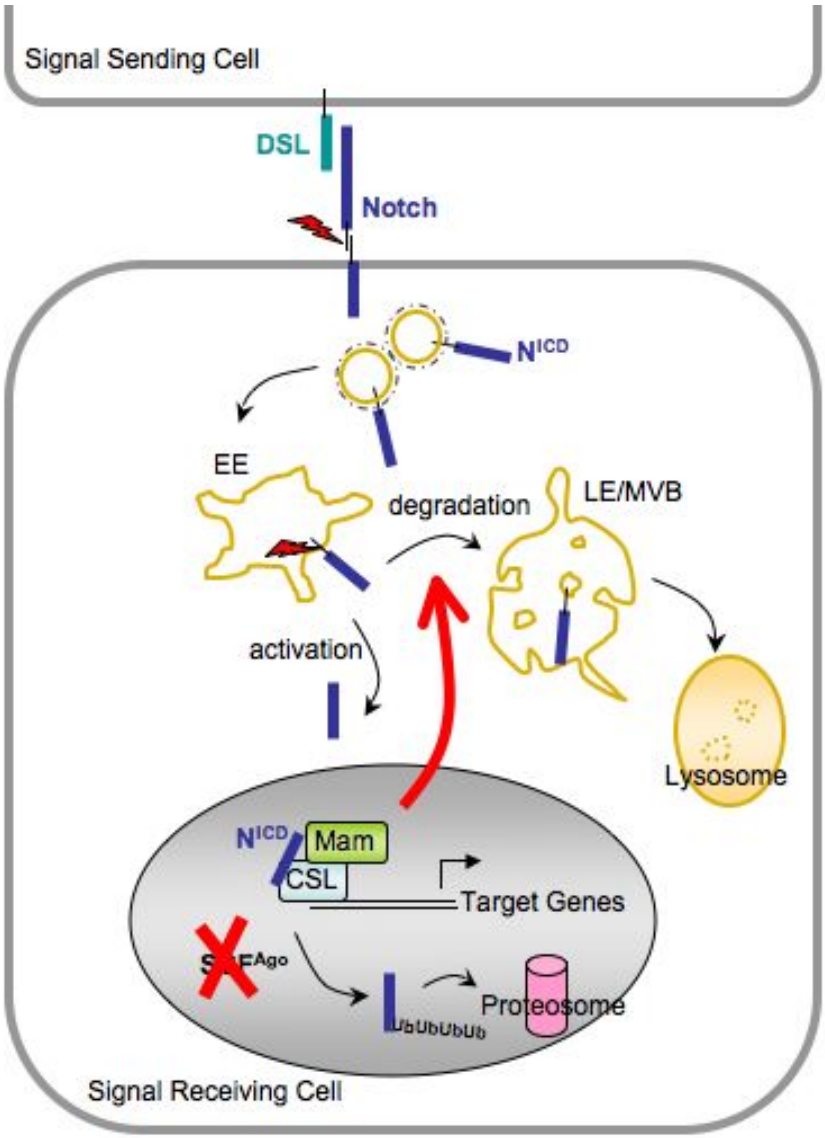

In Feedback Model 1, loss of *ago* and subsequent increase in Notch activity sends a feedback signal to up-regulate N^{ICD} lysosomal degradation.

Figure V.3. Feedback Model 2.

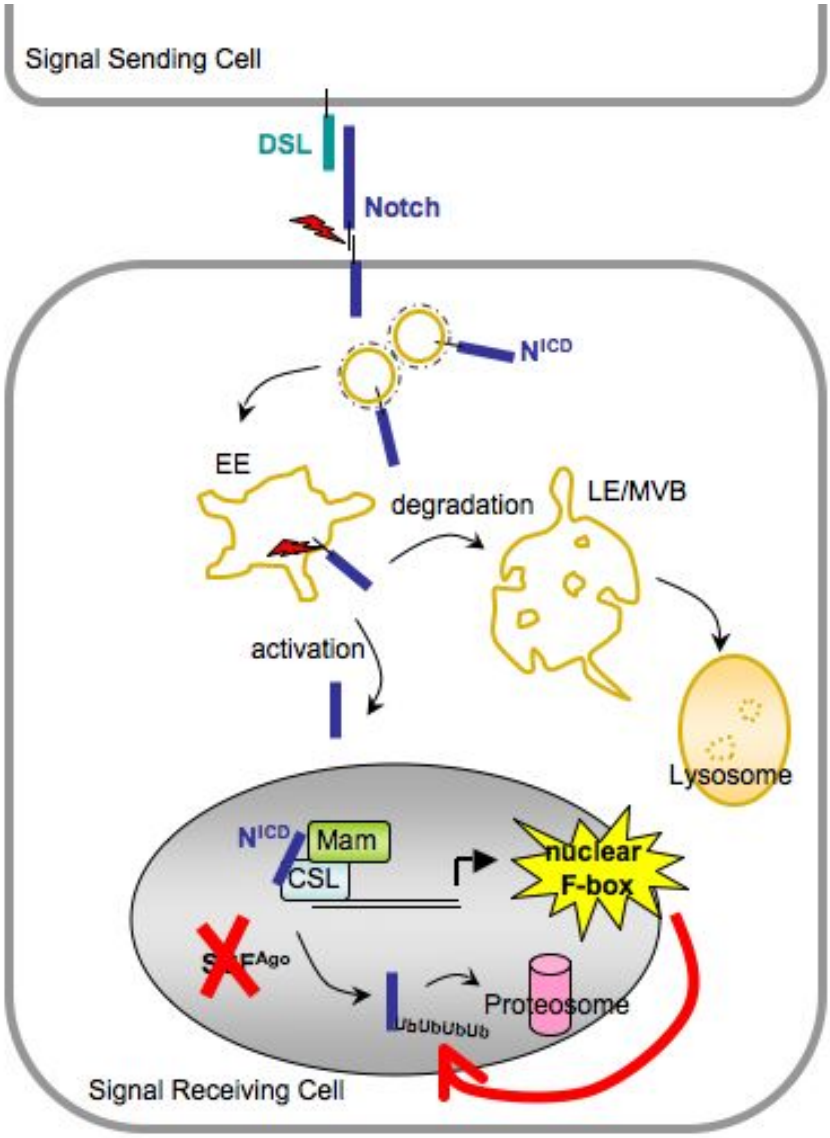

In Feedback Model 2, loss of *ago* promotes the transcriptional up-regulation of a related F-box that binds to and polyubiquitinates nuclear N^{ICD}.

V.B2. What is the role of Notch in *ago* growth and differentiation defects?

We have shown that Notch hyperactivity in *ago* mutant cells disrupts normal patterns of differentiation, and initial evidence suggests that this role is independent from its transcriptional regulation of *Cyclin D* (*CycD*). This led us to predict a bifurcation of Notch's effects on differentiation and growth (see Figure III.11). Although both thought to be pro-growth factors, Notch and CycD have anti-growth properties in the context of the *ago* mutant eye: reducing the dosage of either *Notch* or *cdk4* in the background of *ago* loss creates a larger eye. Immediate future directions discussed in Chapter III include the full characterization of Notch and its downstream effectors, such as *CycD*, in the *ago*-regulated apoptosis we observe in the pupal eye.

Following this initial characterization, long-term future directions include using the pupal eye system to better understand the effects of *Fbw7* mutational inactivation in cellular transformation. It is known that elevated Notch activity upon *Fbw7* loss is central to T-ALL development and that mutational inactivation of *Fbw7* plus suppression of p53-mediated apoptosis combine to promote transformation (reviewed in Demarest et al., 2008). Likewise, our data show that mutations in *ago* synergize with a reduction in p53 to promote cell survival in the early pupal eye. It would therefore be interesting to screen for collaborating mutations or small molecule inhibitors that specifically kill $ago^{-/-}$,*DNp53* cells or $ago^{-/-}$,$p53^{+/-}$ sensitized cells—cells known to be primed for cellular transformation in mammalian tissues. If either of these genetic combinations, $ago^{-/-}$,*DNp53* or $ago^{-/-}$,$p53^{+/-}$, indeed rescues the $ago^{-/-}$ small eye size, then a dominant modifier screen can be easily performed by screening for mutations that cause reversion back to the small eye phenotype. In a mouse model of Notch-induced T-ALL, inhibition of the

Notch transgene results in 100% tumor regression (Beverly et al., 2005). Indeed, pharmacologic inhibition of Notch activity with GSI (gamma-secretase inhibitors) is a mainstay of T-ALL treatment. However, identification of novel therapeutic strategies for T-ALL management is necessary because 20-25% of T-ALL patients have disease that is either refractory to initial GSI treatments or that relapses after a short remission period due to drug resistance. Therefore, modifiers of *ago* mutant, *p53*-compromised cells represent potential therapeutic targets for T-ALL treatment, especially in the setting of GSI-refractory or -resistant disease. In mice, activated Notch promotes leukemogenesis by decreasing ARF and thereby promoting the continuous Mdm2-induced proteolytic turnover of p53 (Beverly et al., 2005). Since flies do not have p19/ARF and Mdm2, it is the hope that modifiers of *ago*$^{-/-}$*,DNp53* cells represent components of other signaling networks previously unrecognized to contribute to T-ALL and can offer treatment strategies that complement GSI-mediated Notch inhibition.

V.C. FUTURE DIRECTIONS: *erupted*

Trafficking of the JAK-STAT receptor Domeless (Dome) is altered in *ept* mutant cells, and this correlates with Stat92E hyperactivity. Although we show that Dome is trapped in an Hrs-positive compartment (see Figure IV.6.A-A"), the main outstanding question remains: is Dome in fact routed through the ESCRT pathway? To test the involvement of endocytosis on Dome receptor signaling, a set of null mutations that disrupt representative core components of the endocytic machinery could be used to systematically evaluate effects on Dome localization and pathway activity at various stages of endocytosis (Figure V.4). This approach was used by Vaccari *et al*. to confirm that endosomal entry is required for Notch receptor activation *in vivo* (Vaccari et al., 2008). Performing a live trafficking assay, where an antibody to recognizing Dome is followed in eye discs that are individually mutant for a particular stage of endocytosis (Le Borgne and Schweisguth, 2003; Lu and Bilder, 2005; Vaccari and Bilder, 2005), will determine the effects of endocytosis on Dome localization. If Dome is trafficked through the endolysosomal pathway, then I would predict that in *DNshi*, *avl*, and *Rab5* mutants that block entry to the early endosome (EE), Dome would be localized to the cell surface; in *hrs* mutants Dome would be found in Avl- or Rab5-positive early endosomes; in the ESCRT mutants *ept*, *vps25*, and *vps20* that block entry into the late endosomal (LE) comparments, Dome would be found in an Hrs-positive compartment (as we have previously observed); and in *fab1* lysosomal mutants, Dome would be in the late endosome/multi-vesicular body (LE/MVB) and is therefore in a compartment that is neither Avl-postiive nor Hrs-positive. A similar analysis of endosomal mutants could be subsequently carried out to determine the effects of endocytosis on Dome activation by

assessing the accumulation of pY-Stat92E in each mutant eye disc. We already know that the JAK-STAT pathway is hyperactive in *ept* ESCRT-I mutants, but it would be interesting to see if pathway activation (i.e., Dome dimerization and Stat92E phosphorylation) occurs any later than at the cell surface—that is, if detection of pY-Stat92E is not detected in *DNshi*, *avl*, or *Rab5* mutants. Since the Dome ligand Upd is a secreted protein associated with the extracellular matrix that stimulates receptor dimerization and subsequent phosphorylation steps (Harrison et al., 1998), a delay in pathway activation until later in the endosomal pathway would challenge canonical models (reviewed in Li, 2008).

Figure V.4. Experiment to determine involvement of endocytosis on Domeless receptor signaling.

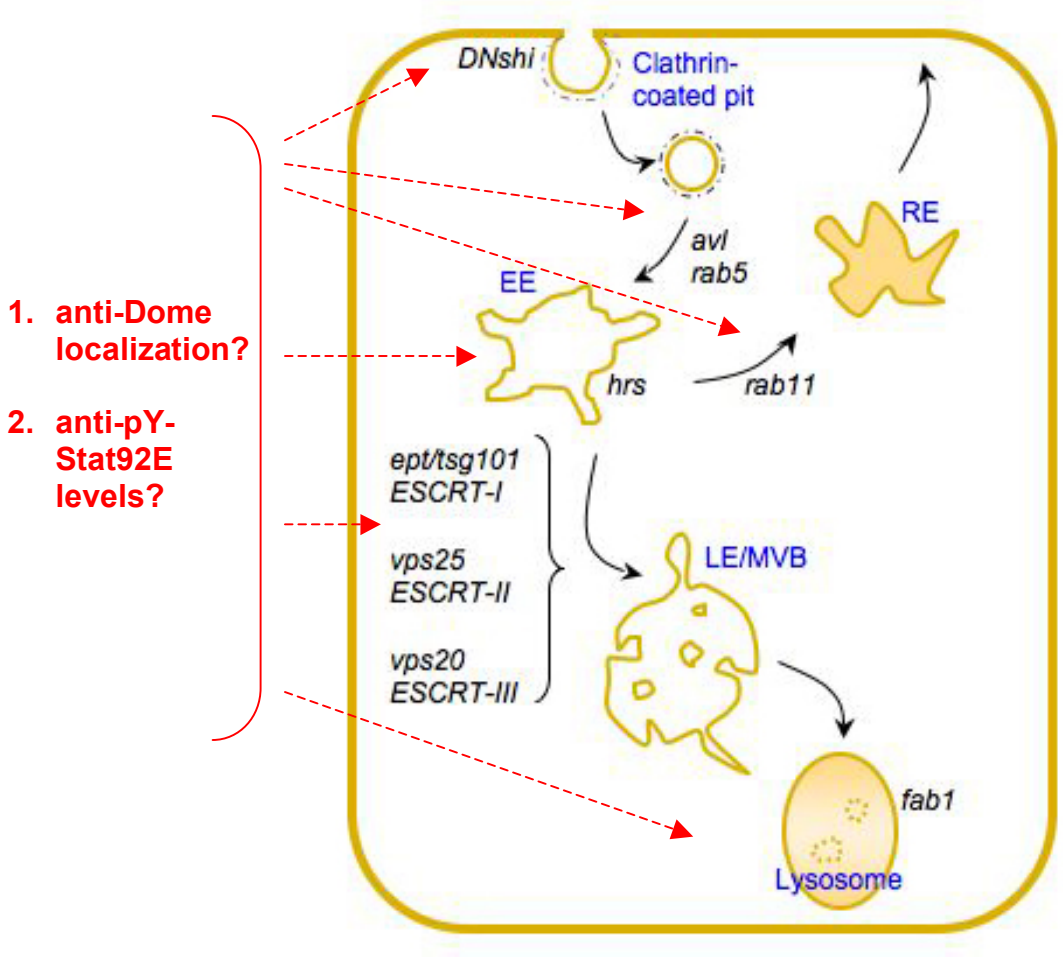

Diagram illustrates core components of the endolysosomal pathway. Endosomal compartments are labeled in blue; genes involved at each step of the pathway are indicated in black; and dashed red arrows indicate the various stages at which to detect Dome localization or JAK-STAT pathway activity in mutant imaginal discs. *DNshi*, dominant-negative shibire; *avl*, avalanche; *hrs*, hepatocyte growth factor regulated tyrosine kinase substrate; EE, early endosome; RE, recycline endosome; LE/MVB, late endosome/multi-vesicular body. (Adapted from Hariharan and Bilder, 2006; Vaccari et al., 2008)

V.D. CONCLUDING REMARKS

When the original *eyFLP/FRT* screen was conducted, it was the ideal hope that each unknown complemention group would represent alleles of conserved genes mutated in human cancers. And, as such, the screen would ultimately aid in the identification of novel human tumor suppressor genes. Three novel genes isolated in the screen, studied in our lab, and discussed here are *gfr*, *ago*, and *ept*. While *ago* indeed fit this perfect human-tumor-suppressor-gene scenario, the previous chapters have illustrated that even when roles for these genes in human disease are unknown or are controversal, studying alleles of overgrowth mutants like *gfr* and *ept* allows us to continue our goal of untangling the biological complexities of growth control and, ultimately, of human cancer.

V.E. REFERENCES

Beverly, L. J., Felsher, D. W. and Capobianco, A. J. (2005). Suppression of p53 by Notch in lymphomagenesis: implications for initiation and regression. *Cancer Res* **65**, 7159-68.

Bray, S. J. (2006). Notch signalling: a simple pathway becomes complex. *Nat Rev Mol Cell Biol* **7**, 678-89.

Demarest, R. M., Ratti, F. and Capobianco, A. J. (2008). It's T-ALL about Notch. *Oncogene* **27**, 5082-91.

Hariharan, I. K. and Bilder, D. (2006). Regulation of imaginal disc growth by tumor-suppressor genes in Drosophila. *Annu Rev Genet* **40**, 335-61.

Harrison, D. A., McCoon, P. E., Binari, R., Gilman, M. and Perrimon, N. (1998). Drosophila unpaired encodes a secreted protein that activates the JAK signaling pathway. *Genes Dev* **12**, 3252-63.

Ho, M. S., Chen, H., Chen, M., Jacques, C., Giangrande, A. and Chien, C. T. (2009). Gcm protein degradation suppresses proliferation of glial progenitors. *Proc Natl Acad Sci U S A* **106**, 6778-83.

Huang, J., Wu, S., Barrera, J., Matthews, K. and Pan, D. (2005). The Hippo signaling pathway coordinately regulates cell proliferation and apoptosis by inactivating Yorkie, the Drosophila Homolog of YAP. *Cell* **122**, 421-34.

Le Borgne, R. (2006). Regulation of Notch signalling by endocytosis and endosomal sorting. *Curr Opin Cell Biol* **18**, 213-22.

Le Borgne, R. and Schweisguth, F. (2003). Unequal segregation of Neuralized biases Notch activation during asymmetric cell division. *Dev Cell* **5**, 139-48.

Li, W. X. (2008). Canonical and non-canonical JAK-STAT signaling. *Trends Cell Biol* **18**, 545-51.

Lu, H. and Bilder, D. (2005). Endocytic control of epithelial polarity and proliferation in Drosophila. *Nat Cell Biol* **7**, 1132-9.

Moberg, K. H., Schelble, S., Burdick, S. K. and Hariharan, I. K. (2005). Mutations in erupted, the Drosophila ortholog of mammalian tumor susceptibility gene 101, elicit non-cell-autonomous overgrowth. *Dev Cell* **9**, 699-710.

Nagaraj, R. and Banerjee, U. (2009). Regulation of Notch and Wingless signalling by phyllopod, a transcriptional target of the EGFR pathway. *EMBO J* **28**, 337-46.

Peng, H. W., Slattery, M. and Mann, R. S. (2009). Transcription factor choice in the Hippo signaling pathway: homothorax and yorkie regulation of the microRNA bantam in the progenitor domain of the Drosophila eye imaginal disc. *Genes Dev* **23**, 2307-19.

Rizzon, C., Marais, G., Gouy, M. and Biemont, C. (2002). Recombination rate and the distribution of transposable elements in the Drosophila melanogaster genome. *Genome Res* **12**, 400-7.

Stofanko, M., Kwon, S. Y. and Badenhorst, P. (2008). A misexpression screen to identify regulators of Drosophila larval hemocyte development. *Genetics* **180**, 253-67.

Tien, A. C., Rajan, A. and Bellen, H. J. (2009). A Notch updated. *J Cell Biol* **184**, 621-9.

Vaccari, T. and Bilder, D. (2005). The Drosophila tumor suppressor vps25 prevents nonautonomous overproliferation by regulating notch trafficking. *Dev Cell* **9**, 687-98.

Vaccari, T., Lu, H., Kanwar, R., Fortini, M. E. and Bilder, D. (2008). Endosomal entry regulates Notch receptor activation in Drosophila melanogaster. *J Cell Biol* **180**, 755-62.

Zhai, R. G., Hiesinger, P. R., Koh, T. W., Verstreken, P., Schulze, K. L., Cao, Y., Jafar-Nejad, H., Norga, K. K., Pan, H., Bayat, V. et al. (2003). Mapping Drosophila mutations with molecularly defined P element insertions. *Proc Natl Acad Sci U S A* **100**, 10860-5.